Fault Location Estimation in Power Systems with Universal Intelligent Tuning

Dem Fachbereich 18
Elektrotechnik und Informationstechnik
Der Technischen Universität Darmstadt
zur Erlangung der Würde eines
Doktor-Ingenieurs (Dr.-Ing.)
genehmigte Dissertation

von

Tamer Amin Said Kawady, M. Sc.
geboren am 30. September 1972
in El.Menoufia, Egypt

Referent:	Prof. Dr.-Ing. J. Stenzel
Korreferent:	Prof. dr. hab. inż T. Łobos

Tag der Einreichung:	07-12-2004
Tag der mündlichen Prüfung:	04-02-2005

D 17
Darmstädter Dissertation

This work is gratefully dedicated to :

To the Soul of my Father, my dear Mother and my lovely Wife

Acknowledgements

Foremost, I would like to express my sincere gratitude and appreciation to my supervisor, Prof. Dr.-Ing. Jürgen Stenzel (TU-Darmstadt, Germany), for his support, patience and encouragement throughout my Ph.D. study.

I wish to express my deep gratitude to my co-referent, Prof. dr. hab. Inż. Tadeusz Łobos (Wroclaw University of Technology, Poland), for his valuable advice and suggestions that improved the whole dissertation.

Also, I wish to thank the staff of the Institute of electrical Power Systems for their support and cooperation during my study at TU-Darmstadt. Special thanks to Mrs. Stenzel and Mrs. Yang Jingfei for their kind help. Deep gratitude to all the people that I have met during my stay in Darmstadt for their sincere cooperation and support.

A special thank to all members in Minoufiya University (Egypt) and the Egyptian Ministry of Higher Education for giving me this opportunity to do my Ph.D. study in Germany.

Finally, I can not forget to express my deep thanks and sincere gratitude to my dear mother in Egypt and my lovely wife for their patience, strong encouragement and kind support.

Contents

1 Introduction

1.1 Motivation

Due to the increasing complexities of modern power system networks, improving the existent protection functions and developing new ones have got much attention recently. The goal is to enhance the overall power system performance. A few years ago, the supplementary protection equipment such as fault locators has got little consideration compared with the main protection ones. Nowadays, these ones have an increasing attention resulting in remarkable investments for these purposes. The essential factors behind these new strategies are due to the competitive markets and new deregulation policies, in which the terms such as the continuity, dependability and reliability play an important role.

For the purpose of fault location estimation, in particular, distance relays can be considered as the first attempt to realize this aim. However, these relays provide a fast and reliable indication of the faulted area rather than pinpointing the fault position accurately. They are, therefore, employed for initiating the protection reaction after the fault inception as soon as possible. On the other hand, fault location estimation requires more accurate and sophisticated computation routines. Thus, the need for particular fault location algorithms is obvious.

In spite of the developed research efforts in the literatures for fault location studies, providing a reliable and accurate fault location algorithm is still considered a challenge. This is mainly due to the varieties of the technical problems that can remarkably affect the behavior of the existing

algorithms. Thus, the research for fault location methodologies is an attractive area till present in order to have a better understanding of the problem essence and to develop advanced solutions.

1.2 Basic Problem Statement

Travelling wave phenomena was early employed for fault location purposes. However, these schemes suffered from different shortcomings associated with the propagation and economical problems. Then, the impedance-based fault locators were developed depending on the available measured quantities at the locator position. Later, the revolution of digital technologies and microprocessor applications were employed to develop these schemes into their digital forms. However, these digital versions are usually structured following almost the same basic functions that are used by the conventional schemes. Hence, these new versions in most cases suffered from the associated shortcomings with the function essence. On the other hand, real field tests and experimental investigations of the commercial fault location schemes raised higher errors than those ones from the simulation studies. As an example, real field tests concluded that a resulted estimation error up to 23% of the total line length have been recorded for some selected impedance-based commercial fault locators [1]. Different factors are responsible for these errors such as the simulation simplifications for the algorithm itself. Also, the operation characteristics including the source impedance, fault resistance, remote infeed, pre-fault loading and mutual coupling among the adjacent conductors have a basic role. Moreover, the non-deterministic interaction between these factors also has a remarkable effect. Hence, compensating these errors needs obviously more advanced computation tools rather than using conventional computational methods.

1.3 Overview of the Proposed Solutions

The aim of this thesis is to develop an accurate fault location scheme for overhead transmission lines depending only on the available information at the locator location. Although considering the available data at all line terminals may lead to a better performance, single end data architecture is practically preferable till present in real fields. This is mainly due to the extra complexities associated with two end algorithms including the communication and synchronization requirements between both line terminals. The proposed solution can be generally classified into the following two basic kinds.

1. Employing advanced mathematical tools may help to represent the formalization of the fault location function precisely. For this aim, the modal analysis may be a suitable candidate to formalize the objective problem in order to get a new fault location algorithm with an acceptable performance.

2. Artificial Intelligence (AI) techniques are expected to play a role to realize a better employment of the available information at the locator position. This depends on their extensive capabilities of information handling and decision making. Then, the collaboration of AI tools in conjunction with other mathematical algorithms is expected to introduce a precise overall fault location scheme.

As documented in the literatures, different AI tools were successfully employed for all power system purposes such as Expert Systems (ES), Artificial Neural Network (ANN), Fuzzy Logic (FL) and Genetic Algorithms (GA) realizing distinctive performances over the conventional ones. This was reviewed in [2, 3]. For protection purposes, in particular, [4, 5] provided coverage of the different applications of AI usage for these purposes. However, the development of these applications into their commercial figures is extremely limited, in which a few expert system applications were commercially developed for a wide usage [6, 7]. Different reasons are responsible for this situation. The lack of the universality essence is an essential factor. This results from developing these schemes for specific parameters in certain situations. Also, the reliability of AI-based tools is still questionable. Thus, developing a practical intelligent scheme having a wide availability and an acceptable reliability is still considered a challenge. For this reason, different AI tools with different architectures and training paradigms are tested to find out the optimum one. This aims finally to realize a universal AI scheme covering a wide range of system characteristics.

1.4 Thesis Organization Outline

The core of the thesis contribution can be divided into two basic phases. Firstly, a new fault location algorithm is introduced aiming to eliminate the fault location estimation error as possible. Then, AI tools are employed in order to compensate all errors that can not be eliminated by the conventional mathematical representation. The overall interaction between both phases is expected to introduce the aimed performance. The organization of the overall contribution of this work can be described into the following steps:

- Chapter 2 presents coverage of the basic concepts of the fault location procedure including the general aims, fault types and a general outline of the past contributions in the literatures for these purposes.
- All factors that can effectively influence the performance of fault location algorithms are evaluated in details employing ATP-EMTP simulation including mutual coupling, parameter distribution, etc. Also, the behavior of some selected fault location algorithms is evaluated under theses factors. These applied tests lead to establish a better understanding of the fault location problem and focus on the factors that can remarkably affect the accuracy of the fault location estimation process. This is covered in Chapter 3.
- The new mathematical fault location algorithm is then introduced in Chapter 4. It is based on modifying the apparent impedance approach using the modal transformation. Depending on the apparent impedance approach facilitates to compensate the effects of the remote infeed and the loading existence. Modal transformation, on the other hand, converts the coupled equations of the transmission line into decoupled ones. This perfectly eliminates the mutual coupling effects. It results in a new fault location algorithm which is able to deal with both single and double circuit lines with a remarkable performance.
- The performance of the aforementioned algorithm is evaluated and the resulting estimation error is compensated with AI-based tuning. Chapter 5 gives a comprehensive review for AI contributions in protection purposes and fault location. Chapter 6 illustrates the basic idea for tuning the fault location estimation error with AI tools. Then, Chapter 7 shows the overall AI scheme design.
- The overall scheme comprising of the mathematical fault location algorithm in conjunction with the AI-based tuner is then evaluated through some advanced test cases. These test cases include some examples that represent practical challenges for all fault locator algorithms such as the fault arc existence, multi-terminal lines and partially coupled lines as presented in Chapter 8.
- Chapter 9 finally summarizes the resulting contributions from this work as well as the suggested recommendations for future work in the area.

2 Basic Concepts of Fault Location Process

This chapter presents a summary of the basic concepts of fault location fundamentals in transmission systems. The history of the fault location process is firstly reviewed. Then, the faults in transmission nets are highlighted including their types, causes and occurrence rates. The fault location process is finally outlined including the process description, the aimed benefits and the classification of the various fault location algorithms.

2.1 Historical Background

A few years ago, most power companies elected to have little or no investment for improving fault location methods. This is mainly due to a belief that most of the faults are transient ones needing no information about their locations. Also, the weak or in accurate behavior of the earlier fault locators may have played a role in this belief. On the other hand, a huge amount of research contributions were presented for fault location purposes as reported in the literatures. However, these efforts received little consideration from these companies. These viewpoints are recently changed due to the new concepts of free marketing and de-regulation all over the world. These competitive markets force the companies to change their policies to save money and time as well as to provide a better service. This consequently leads to increasingly consider the benefits of fault location estimation methods. Nowadays, it is quite common for almost all modern versions of multi-function line protection units to include separate routines for fault location calculation.

Since the distance relay was not accurate enough to detect the fault distance precisely, research efforts were directed to develop dedicated fault location schemes by measuring the reactance from the sending end to the fault location. A brief coverage of the earliest methods for this purpose was presented in [8]. However these simple and approximated methods also suffered from the limited accuracy. Then the first generations of travelling wave-based fault locators were introduced in the field in the 50s of the last century [9]. The basic idea of these schemes was based on determining the time for the injected wave to travel between the injection point and the fault position. In spite of their remarkable performance as compared with reactance-based ones at that time, they were gradually abandoned due to the reliability and maintenance problems as well as to the economical factor [10]. Later, the great developments of injecting and capturing traveling wave signals as well as the modern algorithms support travelling wave-based fault locators to represent strong competitors to other fault location methods. A lot of papers were then published to employ this technique for fault location purposes. However travelling wave-based schemes still suffer from different shortcomings and disadvantages [11-13]. Another way has been introduced to capture and analyze the propagated transient waves into the voltages or currents during the fault [14].

The revolution of solid state relays and the later advancement in digital technologies attracted the researchers to develop modern impedance measurement-based fault locators. These schemes can optimally benefit from the mathematical handling abilities of microprocessors to develop modern digital fault location schemes. Each of them has its own advantages and disadvantages. These locators are basically distinctive with needing no further equipment as compared with travelling wave ones.

From the historical viewpoint, digital relaying was firstly initiated to implement all computational protection equipment in a substation during the late 1960s [15]. The first outline of a digital distance protection scheme was suggested in 1971 [16]. The first practical implementation of digital relay was introduced for line protection by Westinghouse and Pacific Gas & Electric company in USA in 1972 [17, 18]. The use of Fourier analysis to estimate the fundamental components of voltage and current phasors was proposed in 1975 for distance protection applications [19]. The moving window with Fourier Transform and the employment of Digital Fourier Transform (DFT) was introduced, implemented and tested in the early 1980s [20,21]. Then a huge amount of contributions were developed establishing the foundations of this art [22, 23]. These tools were successfully employed for developing impedance based fault

locator algorithms as well. The employment of these digital versions of protection equipment has numerous advantages such as reliability, flexibility adaptability, self monitoring and cost reduction. In spite of the promising performance and their remarkable performance, they still suffer from the associated shortcomings with the protection function itself. This is mainly due to a fact that the new digital versions of protection relays are, in most cases, modern replica for the old ones employing the new features of digital equipment. On the other hand, they are still suffering from those shortcomings related to the protection function essence. Thus their overall accuracy is sometimes questionable in certain circumstances. This requires further efforts to improve these approaches in order to realize the aimed performance.

2.2 Properties of Transmission Line Faults

Transmission lines are considered the most vital components in power systems connecting both generating and consumer areas with huge interconnected networks. They consist of a group of overhead conductors spreading in a wide area in different geographical and weather circumstances. These conductors are dispensed on a special metallic structure “towers”, in which the conductors are separated from the tower body with some insulating components and from each other with an adequate spacing to allow the air to serve as a sufficient insulation among them. Unfortunately these conductors are frequently subjected to a wide variety of fault types. Thus, providing proper protection functions for them is an attractive area for research specialists. Different types of faults can occur including phase faults among two or more different conductors or ground faults including one or more conductors to ground types. However, the dominant type of these faults is ground ones. Most of them occur temporarily as a result of a flashover on the insulation due to the environmental factors such as the lightning or humidity. Also, they may occur due to the insulation failures resulting from the deterioration of the insulating material itself. The current path for these faults includes the arc resistance, tower impedance and tower footing resistance. These factors can, therefore, impact the impedance ground returns and may consequently affect the related fault current.

Tower footing resistance (impedance between tower foundation and the earth) represents the basic factor that can remarkably affect the fault currents. This resistance is typically less than 10Ω for good transmission line lightning performance. Different factors can practically affect this value. The soil resistivity is considered a basic one as the tower footing resistance increases with increasing of the soil resistivity. The existence of overhead ground wires is another factor

as they help to reduce the effective footing resistance. This happens by allowing the flashover ground current to find a path to ground through several lines. Then the total footing resistance of several lines in parallel results in an overall reduction in the effective resistance value. However the application of ground wires is not common for all utilities. Thus footing resistance can vary from less than one Ohm to some hundreds of Ohms resulting in a wide range of the related fault resistance. As an example, some ground fault cases were actually measured from real field tests passing through a fault resistance as high as 800Ω [24]. Another type of temporary faults can happen when the path to ground is established due to growing trees in the gradient breakdown zone characterizing with a higher resistance path. Also ground faults may occur as a result of fallen conductors resulting in permanent single or double phases to ground faults. However, proper and continuous maintenance for overhead lines eliminates these faults greatly [25].

Temporary faults are normally characterized by the existence of non-linear arcs. Almost all known fault location algorithms were developed by assuming a linear fault arc with constant impedance. However, the simulation results showed that the non-linear physical behavior of the fault arc in air may remarkably influence the performance of all impedance measurement-based protection equipment such as distance relays and fault location equipment [26]. This is mainly due to the impedance nonlinearity resulting from the time varying parameters of the arcs during these faults. It is therefore more proper to consider the influence of these situations in order to realize the aimed accurate performance.

2.3 Fault Location Estimation Benefits

2.3.1 Time and effort saving

After the fault, the related relaying equipment enables the associated circuit breakers to deenergize the faulted sections. Once the fault is cleared and the participated faulted phase(s) are declared, the adopted fault locator is enabled to detect the fault position. Then, the maintenance crews can be informed of that location in order to fix the resultant damage. Later, the line can be reenergized again after finishing the maintenance task. Since transmission line networks spread for some hundreds of kilometers in different environmental and geographical circumstances, locating these faults based on the human experience and the available information about the status of all breakers in the faulted area is not efficient and time consuming. These efforts can therefore effectively help to sectionalize the fault (declare the faulted line section) rather than to

locate precisely the fault position. Thus the importance of employing dedicated fault location schemes is obvious.

2.3.2 Improving the system availability

There is no doubt that fast and effective maintenance processes directly lead to improve the power availability to the consumers. This consequently enhances the overall efficiency of the power nets. These concepts of (availability, efficiency, quality …. etc) have an increasingly importance nowadays due to the new marketing policies resulting from deregulation and liberalization of power and energy markets.

2.3.3 Assisting future maintenance plans

It is quite right that temporary faults (the most dominant fault on overhead lines) are self cleared and hence the system continuity is not permanently affected. However, analyzing the location of these faults can help to pinpoint the wake spots on the overall transmission nets effectively. This hopefully assists the future plans of maintenance schedules and consequently leads to avoid further problems in the future. These strategies of preventive maintenance enable to avoid those large problems such as blackouts and help to increase the efficiency of the overall power system.

2.3.4 Economic factor

All the mentioned benefits can be reviewed from the economical perspective. There is no doubt that time and effort saving, increasing the power availability and avoiding future accidents can be directly interpreted as a cost reduction or a profit increasing. This is an essential concept for competitive marketing. Thus the importance of proper fault location schemes for power system utilities is obvious.

2.4 Classification of Developed Fault Location Methods

Generally speaking, fault location methods can be classified into two basic groups, travelling wave-based schemes and impedance measurement-based ones as shown in Fig. 2.1. Travelling wave schemes can be used either with injecting a certain travelling wave from the locator position or with analyzing the generated transients due to the fault occurrence. Impedance measurement schemes are classified whether they depend on the data from one or both line

ends. Each category can be then classified according to the considered line model during the derivation method using either simpler (lumped) models or detailed (distributed parameters) ones.

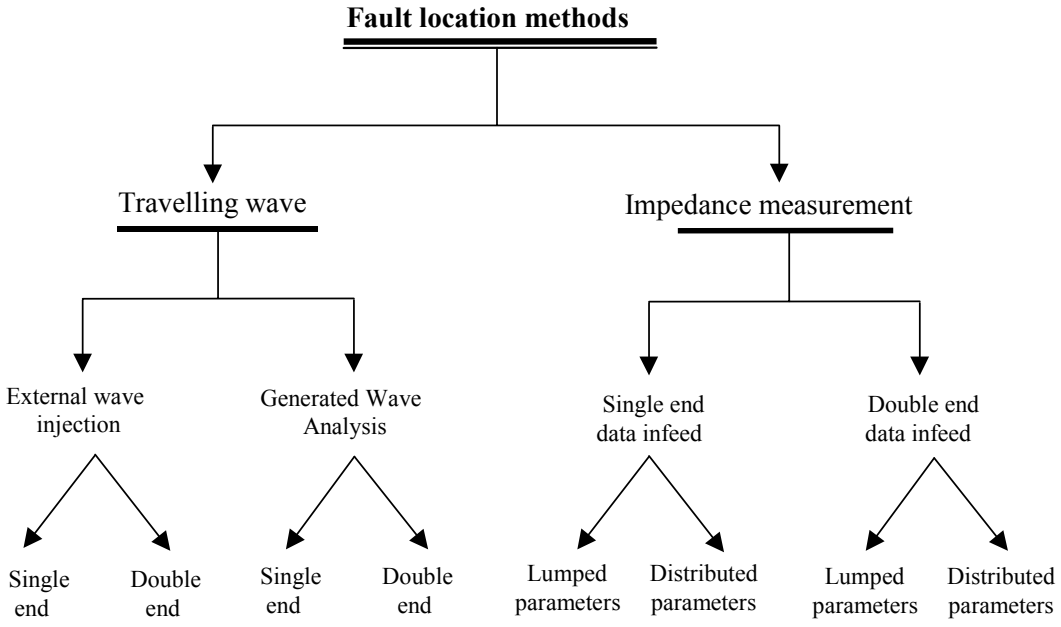

Fig. 2.1 Classification of fault location methods

2.4.1 Travelling wave-based fault locators

Employing travelling wave phenomena for fault location purposes for both underground cables and overhead lines was reported since 1931 [27]. In 1951, Lewis classified travelling wave-based schemes into different four types A, B, C and D according to their modes of operation using the traveling voltage waves [9]. Types A and D depend on analyzing the resulting transients from the fault itself needing no further pulse generating circuitry. Type A is a single end one capturing the transients only at one end. It relies on the generated transients from the arcing flashover during the fault. However the assumption of getting generated transients at the line end is not always satisfied. Moreover, the arc itself may extinguish rapidly. This makes the analysis of these transients to be almost impossible. Type D is a double end scheme depending on the difference in arrival times of the generated transients at both line ends. However, the communication and synchronized timing between both line ends are essentially important. Pulse generating circuitry is employed from a single line end (type C) or from both line ends (Type B). They rely on measuring the required time for the injected pulses to go and to be captured after reflection from the fault point. This time can be directly interpreted as a fault distance. A

new single end scheme (type E) was proposed in 1993 [12, 13]. Unlike the previous types, it employs the generated transients when the line is re-energized by the circuit breaker. Its field test records in various conditions show a promising performance, in which the maximum resulted estimation error does not exceed 2.7 %.

Travelling wave-based schemes, when they work properly, can provide very accurate results with estimation error near to 300 m. However, different factors may affect their performances remarkably. The propagation can be affected by the system parameters and the network configuration leading to a strong attenuation of the waves. Another difficulty arises for near faults to the busses or for those faults occurring at near zero voltage inception angles. Moreover, the reflected waves can be seriously affected by the line discontinuities such as branches, tapped loads and cable sections. The complexity of their simulation, especially when considering the frequency dependency of system parameters is also another difficulty [28]. Also, the economical factor is an essential disadvantage due to the extra required hardware for these schemes including wave sending and capturing instruments as well as the communication and timing synchronization tools for double end ones.

2.4.2 Impedance measurement-based fault locators

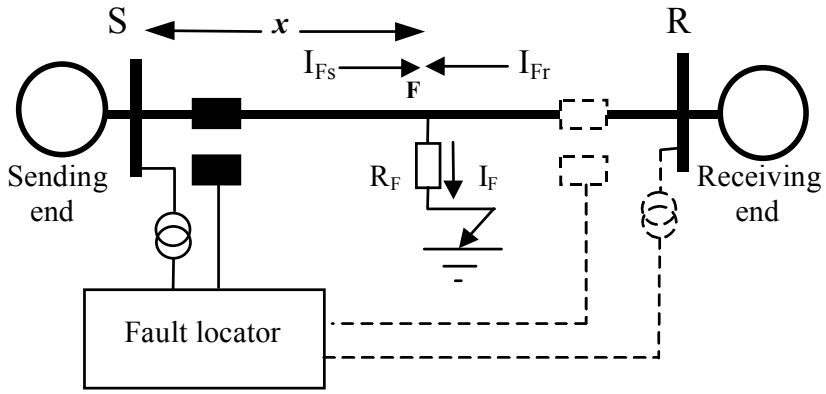

Fig. 2.2 One line diagram of a faulted transmission line

These schemes provide another alternative for the fault location estimation problem. Fig. 2.2 shows the one line diagram of a three phase double infeed faulted transmission line. A line to ground fault occurred on phase A at point F through a resistance R_F at a distance *x* from the locator position. The fault current I_F is comprised from two components I_{Fs} and I_{Fr} flowing from sending and receiving ends respectively. The essential task of the fault location algorithm is to estimate the fault distance *x* as a function of the total line impedance Z_L using the sending end

measurements (for single end algorithms) or both end measurements (for double end algorithms) with the most possible accuracy.

a) Double end algorithms

There is no doubt that the direct and most accurate way to calculate the fault distance is to depend on the measuring voltage and current quantities V_S, I_S and V_R, I_R at both sending and receiving ends for the faulted phase respectively. As shown in Fig. 2.2, the voltage of the fault point V_F can be described as functions of both sending and receiving end voltages as

$$V_F = V_S - I_{Fs}\, x\, Z_L \tag{2.1}$$

$$V_F = V_R - I_{Fr}\, (1 - x) Z_L \tag{2.2}$$

Equating both equations and rearranging yield,

$$x = \frac{\frac{V_S - V_R}{Z_L} + I_{Fr}}{I_{Fs} + I_{Fr}} \tag{2.3}$$

Then, the formulas for other fault types (double phase, double phase to ground and three phase faults) can be derived similarly [29]. In spite of the simple and direct derivation of the algorithm equations, its performance is remarkably questionable due to the simple line model (basic lumped resistance model) neglecting the capacitive currents and mutual coupling.

The same algorithm was reformed using the distributed parameter line model aiming to realize a more accurate performance [30]. For this purpose, equations (2.1) and (2.2) are modified using the line characteristic impedance Z_0 and line propagation constant γ as

$$V_F = \cosh(x\gamma)\, V_S - Z_0 \sin(x\gamma)\, I_{Fs} \tag{2.4}$$

$$V_F = \cosh((L - x)\gamma)\, V_R - Z_0 \sin((L - x)\gamma)\, I_{Fr} \tag{2.5}$$

The unknown fault distance x can be then written as

$$x = \frac{\tanh^{-1}\left(\frac{-B}{A}\right)}{\gamma} \tag{2.6}$$

Where

$$A = Z_0 \cosh(\gamma L) I_{Fr} - \sin(\gamma L) V_R + Z_0 I_{Fs} \quad (2.7)$$

and

$$B = \cosh(\gamma L) V_R - Z_0 \sin(\gamma L) I_{Fr} - V_S \quad (2.8)$$

On the other hand, the extra requirements for communication and accurate timing at both line ends are essential disadvantages of all double end algorithms. In order to overcome this disadvantage, non-synchronized double end algorithms were introduced [31, 32]. These algorithms fully utilized the advantages of modern digital technologies and the wide capabilities of signal processing to estimate the synchronizing difference between both ends using non-linear mathematical optimization. For this purpose equating equations (2.1) and (2.2) yields,

$$V_S - V_R + Z_L I_{Fr} = x Z_L (I_{Fr} + I_{Fs}) \quad (2.9)$$

Where $V_S = |V_S| e^{j(\alpha + \delta)}$ and $V_R = |V_R| e^{j\beta}$. The angles α and β are the own phase angles for sending and receiving end voltages to their own references respectively. The angle δ is the required angle to synchronize the sending end voltage as related to the receiving end one. Equation (2.9) can be rewritten as

$$V_S e^{j\delta} - V_R + Z_L I_{Fr} = x Z_L (I_{Fr} + I_{Fs} e^{j\delta}) \quad (2.10)$$

The two unknowns, the fault distance x and the complex number $e^{j\delta}$, can be estimated by least square optimization. Simulation tests have shown an accurate performance as compared with single end algorithms. However, the mathematical derivation is based on a simple lumped parameter line model. The existence of mutual coupling for double circuit lines and the charging currents for long lines are expected to affect their performances remarkably.

Another two ends algorithm was introduced utilizing the Global Positioning System (GPS) in conjunction with the Phase Measurement Unit (PMU) for fault location purposes [33, 34]. Employing the GPS enables to ensure the accurate timing between both of the line ends, whereas the PMU is employed for phasor estimation purposes as described in Fig. 2.3. The algorithm core is basically similar to the main double end algorithm equations by equating the fault point voltage from both line ends using a distributed parameter line modeling. All

evaluation tests of its performance revealed its higher accuracy as reported in their relevant references. However, the economical factor arises here as a basic disadvantage due to the required cost for the GPS synchronization systems as well as for the communication requirements.

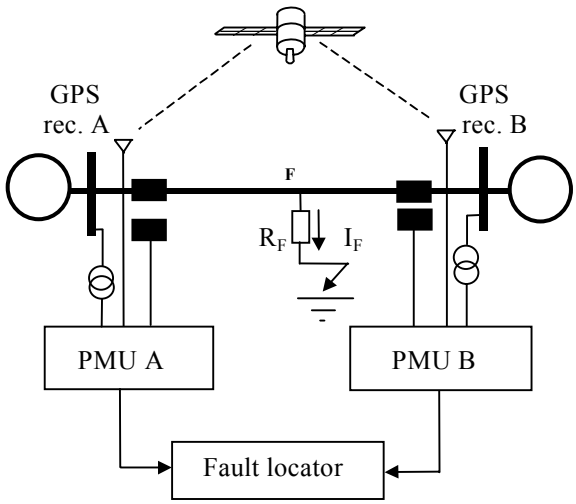

Fig. 2.3 PMU-based fault location schematic

Two different methods were introduced by measuring the seen impedance from each line end [35, 36]. However, both algorithms depend on a simple line modeling suffering from the same shortcomings as well.

b) Single end algorithms

Due to the extra costs for double end algorithms, single end ones attract an increasing attention and consequently they have the superiority from the commercial viewpoint. From Fig. 2.2, equation (2.1) can be rewritten as

$$V_S = xZ_L I_{Fs} + R_F I_F \tag{2.11}$$

The unknown fault distance x can be directly found by equating the imaginary parts of both equation sides as follows:

$$x = \frac{\mathrm{Im}\{V_S - R_F I_F\}}{\mathrm{Im}\{Z_L I_{Fs}\}} = \frac{\mathrm{Im}\{\frac{V_S}{I_{Fs}}\} - \mathrm{Im}\{R_F(\frac{I_F}{I_{Fs}})\}}{\mathrm{Im}\{Z_L\}} \tag{2.12}$$

In order to solve the above equation, the unknown R_F should be excluded considering here some proper simplifying assumptions. If both sending end and fault currents (I_{Fs} and I_F) are considered

to be in phase, the term containing R_F vanishes as its imaginary part equal to zero. This yields the final form for fault distance *x* as [37]

$$x = \frac{\mathrm{Im}\{\frac{V_S}{I_{Fs}}\}}{\mathrm{Im}\{Z_L\}} \tag{2.13}$$

This derivation summarizes the basic feature of single end algorithms, in which the lower amount of available data (as compared with other two end ones) leads to simplify the fault location equations with some assumptions. It consequently affects the overall accuracy of the calculation process remarkably. The research efforts aim therefore to improve these algorithms in order to get the possible highest accuracy.

One of the earliest and practical algorithms was introduced depending on decomposing the faulted system network into a pre-fault network and a pure-fault one as shown in fig. 2.4 [38, 39].

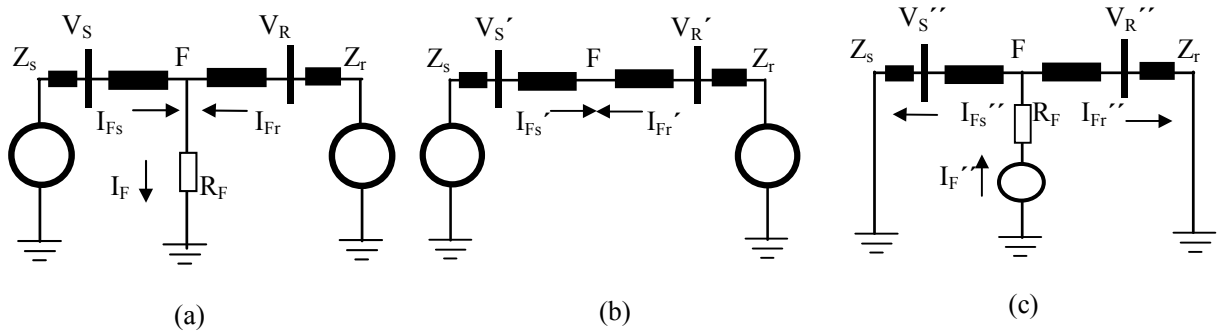

Fig. 2.4 Faulted network analysis decomposition

(a) Faulted network (b) Pre-fault network (c) pure-fault network

The fault point voltage V_F can be described as

$$V_F = R_F I_F = -R_F (I_{Fs}^{''} + I_{Fr}^{''}) \tag{2.14}$$

$$= -R_F I_{Fs}^{''} (1 + k(x)) \,,\; k(x) = \frac{I_{Fr}}{I_{Fs}} \tag{2.15}$$

Where k(*x*) is the current distribution factor defined as a function of the fault distance *x*. I_{Fs} and I_{Fr} correspond to the total fault current parts contributing from both line ends respectively. $I_{Fs}^{'}$ and $I_{Fr}^{'}$ are the loading current contributions towards the fault point from both line ends. $I_{Fs}^{''}$ and

I''_{Fr} are the fault currents at the point F flowing to the sending and receiving ends respectively. V_F and I_{Fs} can be expressed as functions of the sending end quantities as

$$V_F = \cosh(x\gamma)\, V_S - Z_0 \sinh(x\gamma)\, I_S \tag{2.16}$$

$$I''_{Fs} = \frac{\sinh(x\gamma)}{Z_0} V''_S - \cosh(x\gamma)\, I''_S \tag{2.17}$$

Substituting with equations (2.16) and (2.17) into equation (2.15) and rearranging yields,

$$R_F(1+k(x)) = -\frac{\cosh(x\gamma)\, V_S - Z_0 \sinh(x\gamma)\, I_S}{\frac{\sinh(x\gamma)}{Z_0} V''_S - \cosh(x\gamma)\, I''_S} \tag{2.18}$$

If both sending and receiving end currents are assumed to have a common phase angle, then k(x) is a real number yielding,

$$\mathrm{Im}\{\frac{\cosh(x\gamma)\, V_S - Z_0 \sinh(x\gamma)\, I_S}{\frac{\sinh(x\gamma)}{Z_0} V''_S - \cosh(x\gamma)\, I''_S}\} = 0 \tag{2.19}$$

Equation (2.19) can be solved numerically to find out the fault distance x.

The above algorithm was modified later using the same fault network decomposition as well [40]. Then, the estimated fault distance x was found as

$$x = \frac{\mathrm{Im}\{V_S\ I''^*_S\}}{\mathrm{Im}\{Z_L\ I_S\ I''^*_S\}} \tag{2.20}$$

Two other fault location algorithms were proposed considering a real current correction factor with a simple lumped line model depending on analyzing the phasor diagram for impedance phasors [41, 42].

The apparent impedance approach (the seen impedance from the locator location) was employed in conjunction with current compensation for fault location purposes. This approach is similar to the distance relay phenomena, while utilizing a suitable current compensation for the occurring fault (after detecting and classifying the fault type). Starting from Fig. 2.2 the apparent voltage V_{app}, seen by the locator, can be expressed similarly with equation (2.11). Then, the unknown

equation part of $I_F R_F$ can be replaced by $I_{Fs} R_{Fs}$, in which R_{Fs} is the apparent part of fault impedance seen form the relay location. The relation between the total and the apparent fault resistances can be expressed as

$$R_{Fs} = R_F C(x) \tag{2.21}$$

Where the correction factor $C(x)$ depends on the fault current contribution from both ends and can be therefore an imaginary value. Equation (2.11) can be rewritten by dividing by I_{Fs} as

$$\frac{V_{app}}{I_{Fs}} = Z_{app} = xZ_L + R_{Fs} \tag{2.22}$$

Equation (2.22) can be considered as the main equation to find out the seen apparent impedance (Z_{app}) from the locator location. In order to get the unknown fault distance x, the equation should be simplified by considering only a real correction factor. The above equation can be solved by equating the real and imaginary parts in both equation sides [43, 44].

2.4.3 Non-conventional fault locators

Instead of the normal mathematical derivation, non-conventional fault location algorithms were introduced depending on other processing platforms such as Wavelet Transform (WT), ANN or GA. These methods have their own problems that result from the line modeling accuracy, data availability and the method essences.

ANN provides a promising tool for classification and non-linear mapping problems. For power system purposes, many successful applications have been proposed for different purposes such as load forecasting, security assessment, control ...etc. This is well covered in the published literatures. For protection purposes, different applications were developed covering a wide range of protection purposes such as faulted area estimation, fault direction discrimination, generator protection, transformer protection ...etc. However, almost all of these applications mainly use the ANN as a simple discriminator having only the outputs of 1 or 0 using voltage and current samples directly. This simple topological use of ANN may reach the aimed accuracy with the proper training. However, employing ANN for fault location purposes requires the ANN to perform more advanced calculations in order to predict the fault impedance seen from the locator location. The training sets should be prepared properly covering all situations that can

happen in the real situations. Thus, the ANN efficiency essentially depends on the properly selected network design as well as the sufficient amounts of training data. Some successful applications employing the ANN for fault location purposes were published as seen in [45, 46, 47].

WT provides an advanced tool for signal analysis purposes. Unlike the conventional signal processing tools such as Fourier analysis, the wavelets are not only localized in frequency domain but also in time domain as well. This localization enables to detect the occurrence times of even fast disturbances such as fault transients. These transients are generated by the fault and travel continuously between the fault point and the line terminals until the post fault steady state is reached. Thus, processing these signals with WT reveals their travel times between the fault point and the locator position. These times can directly refer to the unknown fault distance [48, 49, 50].

The fault location problems can be interpreted as an optimization problem, in which the seen impedance from the relay location can be described as the objective function of this problem. Then, it can be mathematically optimized in order to find out the function unknowns including the fault distance as well as the fault resistance. For this purpose, GA can be employed successfully [51, 52].

In spite of the accepted performance of these non-conventional applications with simulation testing, their reliability and dependability are still questionable. Therefore, almost none of these proposed applications are commercially developed till present. However, the wide capabilities of these modern tools may motivate to improve the employment of these tools so that they will fit the practical requirements for real usage.

2.5 Requirements for Fault Location Process

Fig. 2.5 presents a general explanation of the essential requirements for fault locators. Generally speaking, fault locator works in off-line mode after performing the relaying action. Once the fault is detected and the faulty phase(s) are successfully classified, the fault locator is enabled to find out the estimated fault distance. The recorded data by the Digital Fault Recorder (DFR) is passed through the locator input manipulator to the fault locator. A few seconds or minutes (according to the locator speed) later, the fault distance is estimated and then the maintenance crews can be sent to the fault position [53, 54]. For those locators that use double terminal

information, an extra data communication link is fitted between both line ends. Also, travelling wave-based locators require extra hardware for generating and capturing the resulting waves. Practical fault locators may be stand alone devices in the sub-stations or included as parts of the modern multi-function protection equipment for overhead lines, which is the most economical and common protection tools for transmission networks recently.

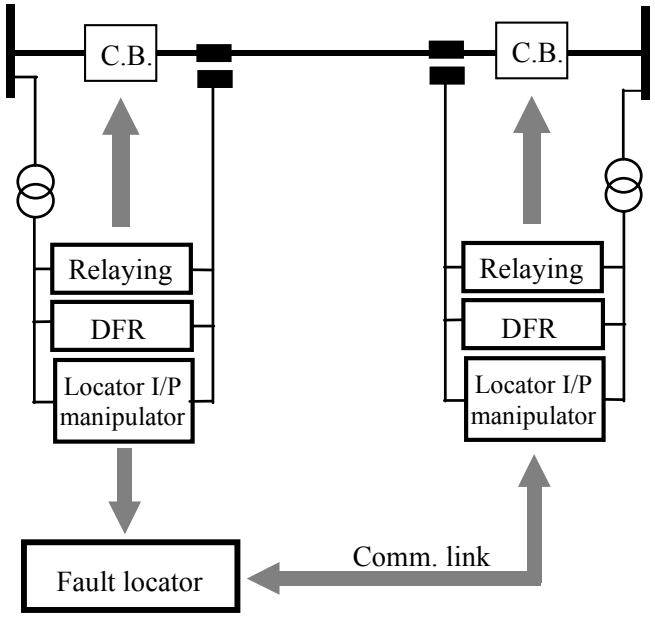

Fig. 2.5 General requirements for fault location schemes

3 Conventional Fault Location Algorithms: An Extended Comparative Study

The aim of this chapter is to give a comprehensive investigation of some selected fault location algorithms employing a sophisticated transmission line simulation with ATP-EMTP software. These investigations emphasize on the main characteristics of the fault location process. They also pinpoint the factors that can affect the accuracy of the estimated fault distance such as mutual coupling, parameter distribution, line configuration, parameter variations, and fault resistance. The results can therefore supervise the next efforts in order to realize the aimed accurate fault location computation.

3.1 Selected Fault Location Algorithms

As the aim of this thesis is to develop an accurate fault location approach using the impedance measurement methods, this chapter concerns only with the related algorithms to this category. The selected group of these algorithms should cover both single and double end ones including different calculation concepts. For this purpose, 12 fault location algorithms are selected as summarized in Table 3.1. The first six algorithms are for single end methods including A1 to A6 ones, whereas the other six algorithms are examples for double end methods including B1 to B6 ones. On the other hand, these algorithms can be classified according to their basic mathematical concepts. This is mainly in order to generalize comparable results so that the resulting conclusions are still applicable for other algorithms with similar concepts. The earliest concept for single end algorithms depended on approximated analyzing of lumped model phasor diagrams realizing simple fault location formulas. Both A1 and A2 algorithms are selected as examples of this category. Another concept is based on approximating the complex current

distribution factors between the sending and receiving end currents into real values. Then, the fault distance can be estimated using single end data (A3 and A4 algorithms). The third concept calculates the apparent impedance seen from the locator location as presented by the algorithms of A5 and A6 respectively.

Double end algorithms can be classified according to their mathematical concepts as well. A direct and easy concept is to equalize the voltage of fault point from both line ends. B1 and B2 are examples of this category using lumped parameters and distributed parameters line modeling respectively. The second category concerns with enhancing the last concept with computing the phase difference between both line ends iteratively as proposed with the algorithm B3. This requires no further synchronization between both line ends. The next concept employs the PMU with GPS synchronization as in B4. Finally, the seen impedance from each line end is used to calculate the required fault distance as used by the algorithms B5 and B6 respectively.

Table 3.1 Selected fault location algorithms

Algorithm no.	Algorithm authors	Solution method	Refs.
A1	Sant, Tech and Paithankar	Non-iterative	42
A2	Wiszensiki	Non-iterative	41
A3	Takagi, Yamakoshi, Baba, Uemura and Sakaguchi	Iterative	38, 39
A4	Takagi, Yamakoshi, Yamaura, Kondow and Matsushima	Non-iterative	40
A5	Eriksson, Saha, Rockefeller	Non-iterative	43
A6	Girgis, Makram	Non-iterative	44
B1	Jeyasurha & Rahmen	Non-iterative	29
B2	A.T. Johns, Jamali	Non-iterative	30
B3	Novosel, Hart, Urden and Garitty	Iterative	31
B4	Jiang, Lin, Yang, Too and Liu	Non-iterative	33, 34
B5	Cook	Non-iterative	35
B6	Sachdev and Agarwal	Non-iterative	36

3.2 Testing Strategy and Modeling Aspects

Fig. 3.1 shows the proposed structure of the simulation process. The testing process has two stages. Firstly, the required test cases were prepared covering all different situations and network circumstances using the ATP-EMTP software [55]. For each test case, the samples of voltage and current waveforms at each line end were extracted, prepared and saved to be fed into the second stage. The second stage concerns with estimating the fault distance with each

selected fault location algorithm. For this purpose, the required codes for signal processing as well as the associated code for each algorithm were implemented into MATLAB environment [56]. MATLAB is considered as one of the most powerful and dependable packages for modeling and mathematical formalization purposes.

A sampling rate of 32 samples per cycle was chosen which is sufficient for signal processing requirements. The required voltage and current phasors were estimated with the recursive DFT routine. Appendix A presents a brief description of the mathematical basis of the DFT routine.

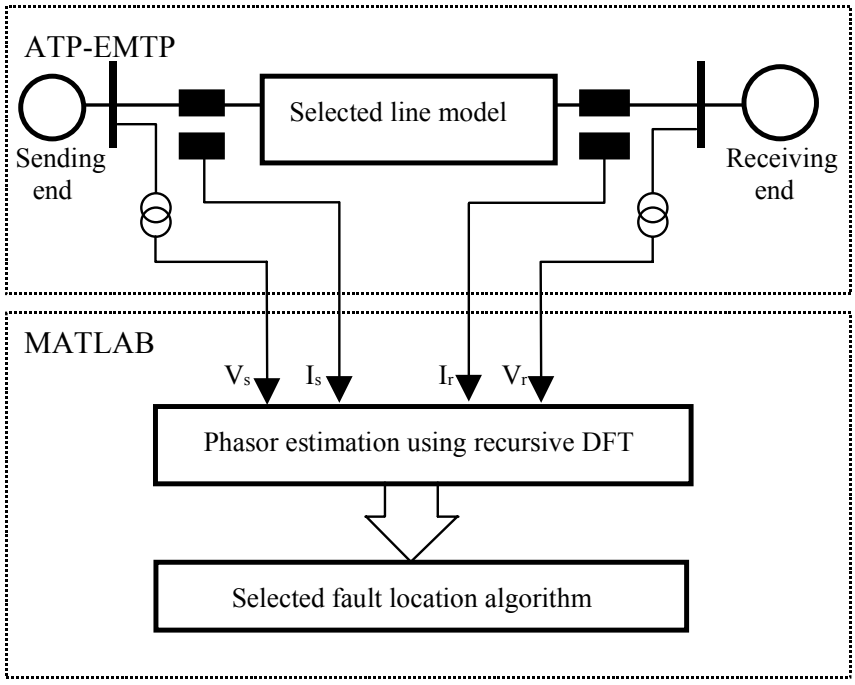

Fig. 3.1 Simulation process schematic

More than 1200 simulation cases were performed via the EMTP-ATP covering the entire range of the line length as well as the following varieties of the line configurations and system conditions.

- Line model [lumped parameters (coupled/uncoupled), distributed parameters line model]
- Line imbalance [transposed / untransposed line model]
- Fault types [line-ground, double line, double line-ground, three phase faults]
- System infeed [single infeed / double infeed]
- Line loading [no-loading / full loading]
- Fault resistance [from solid faults up to 10 kΩ]

A double circuit transmission system of 220 kV and 200 km was selected as a test system. The system configuration, parameters and dimensions for this transmission system are given in the Appendix B.

For each test case, the algorithms were examined individually to find out its associated estimation error during this test case. This error was characterized by the deviation of the estimated fault distance (L_E) from the actual fault distance (L_A) for the test case. This estimation error can be interpreted as the accuracy of this algorithm. As far as this distance deviation increases, the algorithm accuracy decreases. Three different accuracy definitions are defined. The individual accuracy A_I for a certain fault position is defined as the percentage of the maximum estimation error for all possible fault types to the actual fault distance at this fault position as

$$A_I = \frac{L_E - L_A}{L_A} \times 100 \tag{3.1}$$

The local accuracy A_L for a fault location algorithm can be defined as the maximum individual accuracy along the entire range of the line length. It can be found out by computing and comparing the individual accuracies for the whole line length. Finally, the overall accuracy, A_O, can be expressed by the maximum resulting estimation error along the entire range of the line length as well as for all possibilities of fault types as a percentage of the total line length L_L as

$$A_O = \frac{L_E - L_A}{L_L} \times 100 \tag{3.2}$$

As seen in the literatures, A_O is the most common used accuracy definition. All these definitions are required in order to generalize valuable and comparable results to compare the performance of different fault location algorithms. The overall accuracy enables to compare the performance of the algorithms even with different concepts such as comparing both single and double end ones. On the other hand, the individual and local accuracy terms help to get a better understanding of the performance of each algorithm individually. It shows the variations of the algorithm performance along the line length. They facilitate to find out the weak spots for a certain fault location algorithm by detecting the maximum error areas on the line. These weak spots may be in the “close-in”, “line-middle” or “line-end” areas of the whole line. It is, therefore, more helpful to investigate all of the selected algorithms considering all of these accuracy terms aiming to get more meaningful comparison results.

3.3 Power System Network Impact

As the line is embedded into a large interconnected network, the network circumstances including loading, configuration and network parameters vary by time. On the other hand, all fault location algorithms are commonly derived based on some simplification assumptions. They sometimes neglect the impact of the overall network such as the loading and remote infeed. Therefore, it is expected that the practical use of all fault location algorithms will encounter different problems during these situations.

3.3.1 System infeed and line loading

Single end algorithms depend only on the data available at the locator position. Then, the influences of the remote infeed and the pre-fault load flow are eliminated by regarding some certain assumptions. They are expected to be remarkably affected by the existence of these factors. Also, double end ones are expected to have a better performance in these situations. However, some of these algorithms may be also affected by these situations depending on their mathematical concepts in conjunction with their considered assumptions. It is, therefore, more convenient to evaluate all selected algorithms under these conditions.

For this purpose, the performance of each algorithm was evaluated regarding four situations including single infeed (with and without loading) and double infeed (with and without loading) using the pre-prepared test cases. The considered line model was a lumped parameter line model without mutual coupling and solidly ground faults. The goal is to investigate the algorithm concepts independently disregarding other effects that can share the resulted accuracy.

For each situation, every test case was checked with the selected algorithms individually to find out their individual accuracy. Comparing the resulting individual accuracy for each algorithm yields its local accuracy for each situation as summarized in Table 3.2. The results conclude the general superiority of double end algorithms as compared with other single end ones. Moreover, most of the single end algorithms are seriously affected by close-in faults. However, the algorithms with approximated current distribution factors (A3 and A4) are more stable during close-in fault cases. Double end algorithms that consider equating the fault point voltage from both line ends (B1, B2, B3 and B4) have generally their weak area in the middle of the line. Other double end algorithms (B5 and B6) are surprisingly affected through those close-in fault cases.

Table 3.2 System infeed and loading evaluation considering local accuracy A_L

Algorithm no.	Local accuracy A_L, %							
	Single infeed with no load		Single infeed with load		Double infeed with no load		Double infeed with load	
	A_L	Location	A_L	Location	A_L	Location	A_L	Location
A1	18.67	close-in	20.12	close-in	19.88	close-in	22.76	close-in
A2	23.17	close-in	24.85	close-in	24.92	close-in	26.63	close-in
A3	3.25	line end	4.13	line end	5.64	line end	7.23	line end
A4	2.48	line end	3.85	line end	4.66	line end	6.82	line end
A5	6.24	close-in	6.97	close-in	7.10	close-in	7.65	close-in
A6	5.32	close-in	5.84	close-in	5.98	close-in	6.23	close-in
B1	1.90	middle	2.02	middle	1.90	middle	2.14	middle
B2	1.32	middle	1.37	middle	1.44	middle	1.51	middle
B3	9.59	close-in	9.62	close-in	9.61	close- in	9.73	close-in
B4	1.31	middle	1.32	middle	1.37	middle	1.40	middle
B5	7.64	close-in	8.12	close-in	7.98	close-in	8.26	close-in
B6	6.23	close-in	6.42	middle	6.26	close-in	6.64	middle

Finally, the overall accuracy for each algorithm was computed as presented in Table 3.3. Although double end algorithms generally present a better performance than other single end ones, the algorithms considering the apparent impedance approach with compensation (A5 and A6) have a distinctive performance as well. The results reveal the efficiency of employing compensation features for single end fault location methods as compared with the efficiency of double end ones. However, both algorithms are significantly affected during close-in faults similar to other single end ones as well.

Table 3.3 System infeed and loading evaluation considering overall accuracy

Algorithm no.	Overall accuracy A_O, %			
	Single infeed with no load	Single infeed with load	Double infeed with no load	Double infeed with load
A1	1.462	1.882	2.214	2.689
A2	1.647	2.120	3.471	4.221
A3	3.256	4.126	5.641	7.225
A4	2.482	3.841	4.655	6.812
A5	2.164	2.811	3.092	3.251
A6	1.722	1.763	2.482	2.602
B1	0.946	1.011	0.923	1.064
B2	0.661	0.662	0.713	0.751
B3	1.583	1.647	1.594	1.649
B4	0.651	0.651	0.653	0.701
B5	2.889	3.011	3.141	3.223
B6	2.115	2.156	2.416	2.491

3.3.2 Selected line model and accuracy

Most of fault location algorithms are derived with simple line model equations in addition to their own simplification assumptions. These approximations may be sufficient to be used with short lines with an acceptable efficiency. This is mainly due to the relatively low amounts of charging currents in short lines. However, this may be no longer sufficient for long lines as the charging currents considerably affect the performance of all protection equipment. Hence, the performances of those fault locators working with long lines are significantly perturbed. Thus, analyzing the behavior of the selected algorithms considering different modeling aspects presents a better understanding of the fault location process as well as pinpoints the impact of the considered assumptions on their performances. For this aim, the behavior of each algorithm was checked with the selected transmission line (220 kV, 200 km) considering only a single circuit line. The line is considered to be fed from both ends and fully loaded. Both local and overall accuracy of each algorithm were evaluated as summarized in Table 3.4. As concluded from the results, all the algorithms with lumped parameter models are obviously affected. Where other distributed parameter algorithms were less affected in this test (A4, B2 and B4). This reveals the need for such sophisticated line models for evaluating fault location algorithms in order to get more reasonable and accurate investigations close to the circumstances in real field operation.

Table 3.4 Line model effect on algorithm accuracies

Algorithm no.	Local and overall accuracy investigation					
	Lumped parameter line model at full load and double infeed			Distributed parameter line model at full load and double infeed		
	A_L	Location	A_O	A_L	Location	A_O
A1	22.76	close-in	2.689	29.64	close-in	8.972
A2	26.63	close-in	4.221	22.29	close-in	9.415
A3	7.23	line end	7.225	9.37	line end	7.437
A4	6.82	line end	6.812	7.56	line end	6.951
A5	7.65	close-in	3.251	10.41	close-in	5.682
A6	6.23	close-in	2.602	9.95	close-in	5.473
B1	2.14	middle	1.064	6.86	middle	3.431
B2	1.51	middle	0.751	1.62	middle	0.768
B3	9.73	close-in	1.649	13.18	close- in	3.872
B4	1.40	middle	0.701	1.37	middle	0.714
B5	8.26	close-in	3.223	17.67	close-in	6.594
B6	6.64	close-in	2.491	13.82	close-in	6.863

3.3.3 Mutual coupling impact

Among the most effective problems for all fault locators, the existence of mutual coupling is a serious one. The mutual coupling among the adjacent conductors is effectively measurable in all multi-phase systems. However, it is more effective and measurable in multi-circuit lines. Owing to its existence, the total line impedance significantly changes resulting from the mutually reflected impedances from the other phases. The actual line parameters significantly deviate from those parameters that are adjusted by the off-line relay setting. Moreover, the problem of mutual coupling is not really constant and strongly depends on different interacting factors such as conductors' spacing and voltage levels. For the purpose of fault location, in particular, these effects remarkably increase the error levels in the estimated distance and affect the locator accuracy seriously. For this purpose, each algorithm is examined via the prepared test cases covering the entire range of line length and all possible fault types using a distributed parameter line model and considering both transposed and untransposed cases. Table 3.5 summarizes the results of these tests showing the resulted overall accuracy of all algorithms. The results reveal the increasing errors resulting from the mutual coupling existence. Also, the effect of line imbalance on the resulting accuracy is obvious. However, double end algorithms generally have a better performance than other single end ones, specially those algorithms depending on equating fault point voltages from both line ends (B1, B2 and B4). Those single end algorithms that used the compensation features (A5 and A6) are characterized with a better performance than other single end ones.

Table 3.5 Line model variation evaluation

Algorithm no.	Overall accuracy A_O	
	Distributed line model (transposed case)	Distributed line model (untransposed case)
A1	20.221	20.982
A2	16.113	16.920
A3	19.662	20.412
A4	17.293	17.972
A5	11.316	12.064
A6	9.347	10.127
B1	6.830	7.171
B2	4.115	4.551
B3	7.936	8.363
B4	5.388	5.768
B5	9.868	10.160
B6	8.456	8.826

3.4 Fault Resistance Impact

Involving a resistance in the fault loop during phase and double phase to ground faults is a typical fault condition for overhead lines. This resistance is not only caused by the arc resistance between the fault point and the ground, but also by some other reasons such as the resistance of any path to ground or errors in the ground resistivity modeling [57]. The existence of this resistance during the fault has a remarkable impact on all algorithms. However, this impact differs from one algorithm to another with the considering assumptions for each one. Generally, all those algorithms that are based on lumped parameters are thought to be seriously affected by higher resistance values due to the considerable charging currents as compared with fault currents in these situations. On the other hand, double end algorithms are theoretically not affected by the fault resistance, especially those algorithms that are based on equating fault point voltage from both line ends. However, high resistance values may be still effective due to the charging current modeling inaccuracy. Also, the performance of single end ones depends mainly on the considered assumptions for each algorithm. It is worth to investigate these situations thoroughly. In order to evaluate the performances of the algorithms during these situations, a group of testing cases was prepared covering the entire range of the line length as well as a wide range of the added fault resistances up to 10 kΩ. The overall accuracy of each algorithm was plotted for single and double end algorithms in Fig. 3.2(a) and (b) respectively. A single circuit, double infeed and loaded line with untransposed distributed parameter line model was considered here.

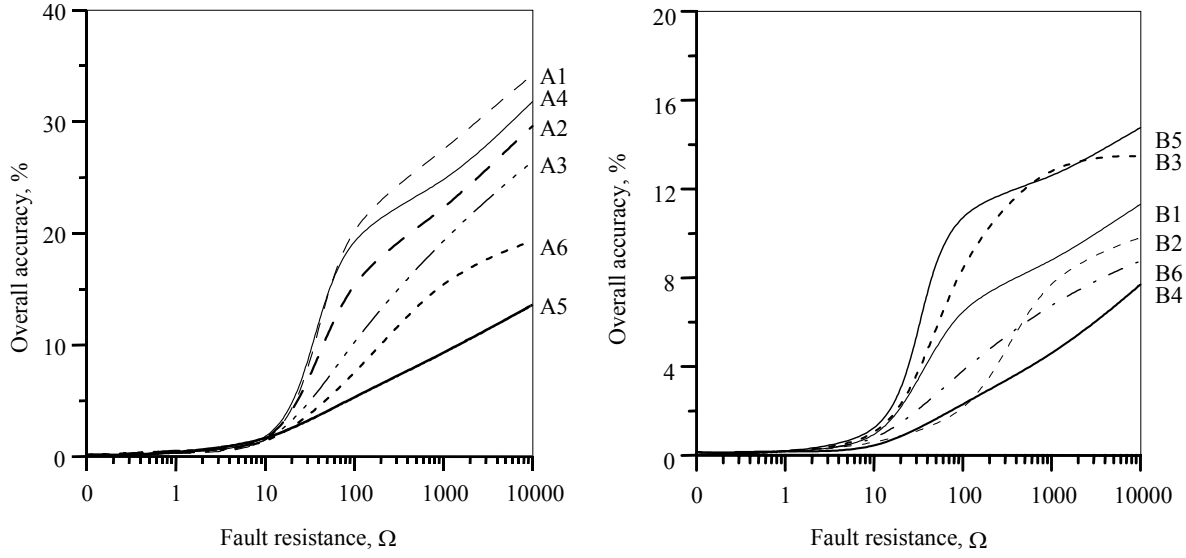

Fig. 3.2 Fault resistance effects on selected algorithms
(a) One terminal data algorithms, A1-A6 (b) Two terminals data algorithms, B1-B6

The line is supposed here to be untransposed considering full loading and double infeed for investigating the worst case for the fault types to find out the lowest accuracy for each algorithm. The results reveal the significant influence of the added fault resistance on the performance of fault location algorithms, especially with large resistance values. It has also been found that one terminal data algorithms A5, A6 have relatively lower errors as compared with other single end ones. This reveals the remarkable improvement with the compensation employment for fault location estimation. However, the superiority of double end algorithms as compared with single end ones considering the existence of fault resistance is obvious.

3.5 Industrial Usage of Fault Location Algorithms

Due to the extra hardware requirements for double end algorithms including synchronization and communication tools between both line ends, single end ones have the superiority from the commercial and the industrial viewpoints till present. Generally, those algorithms with real current distribution factors represent the main platform of most commercial locators [37]. A dedicated fault location scheme was earlier developed in Japan in the early 1980s [38, 39, 40]. With the development of the modern multi-function digital relays, fault location algorithms are included as a sub-function in the relaying unit [58, 59]. The apparent impedance approach was also employed aiming to develop an accurate single end fault location estimation routines [60]. Also, the dedicated communication equipment and accurate timing with GPS units were tested recently for a double end algorithm with distributed parameter model [3, 34]. However, the usage of those double end algorithms is still commercially limited in spite of their promising performances. On the other hand the rapid development of communication and timing equipment may lead to develop cheaper, more compact and more reliable units. This is expected to facilitate the usage of double end methods to be a real competitor for the single end ones.

4 Modal Transformation-Based Fault Location Algorithm

This chapter proposes a new fault location algorithm aiming to overcome the basic factors that can affect the accuracy of fault location calculation methods. The decoupling feature of modal transformation in conjunction with the apparent impedance approach collaborate together to realize this goal.

4.1 General Recommendations

The presented comparative study in the last chapter pinpointed the essential factors that can remarkably affect the fault location accuracy. These factors mainly result from the considered simplifications assumptions for each algorithm. The results show that the mutual coupling and high fault impedance are the most effective factors that can affect all fault location algorithms. Also, both remote infeeding and pre-fault loading arise as critical issues for all single end algorithms. Moreover, all of the aforementioned factors have more effects with the existence of line imbalance situations. Another point of view arises when considering the commercial recommendation and technical limitations. Till present, single end fault locators have the commercial superiority due to the extra requirements for two end ones. It is, therefore, recommended for the aimed fault location algorithm to be a single end one in order to fit all transmission system types.

The different basic concepts for single end fault locators are described in the last chapter; including simple phasor diagram analyzing, approximated real current distribution factors and

the apparent impedance approach. The results show the efficiency of the apparent impedance approach as compared with the other ones. However, its accuracy is still generally lower than the double end algorithms. Thus, the proposed fault locator considers the apparent impedance approach in order to eliminate the effects of the remote infeed and pre-fault loading. Also, the modal transformation is employed to eliminate the effects of the mutual coupling. The problem of high impedance faults will be considered with AI tuning as seen in the next chapters..

4.2 Mathematical Fundamentals

4.2.1 Apparent impedance approach

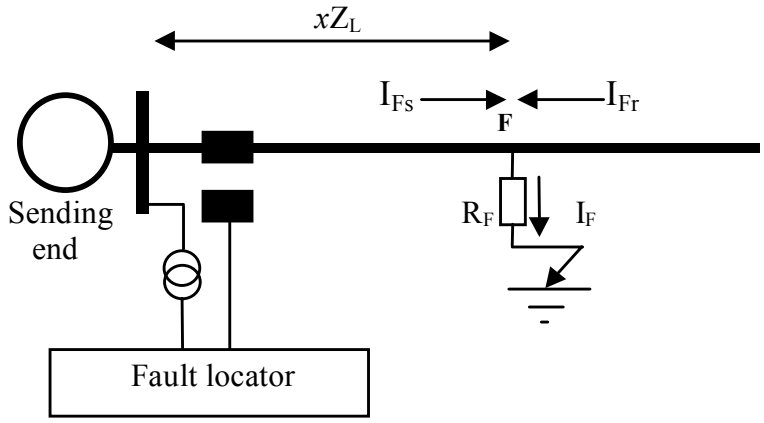

Fig. 4.1 One line diagram of a three phase transmission line

Fig. 4.1 shows the one-line diagram of a double infeed transmission line, in which the fault locator is equipped at the sending end. A line to ground fault occurs on a phase A through a resistance R_F at a distance x from the sending end. The fault current I_F comprises from two components I_{Fs} and I_{Fr} flowing from the sending and receiving ends respectively. The apparent impedance Z_{aap}, seen from the locator position, is equal to the ratio of the selected apparent voltage V_{sel} to the selected apparent current I_{sel} as

$$Z_{app} = \frac{V_{sel}}{I_{sel}} \tag{4.1}$$

These selected apparent voltage and current quantities are based on the fault type as well as the associated faulty phases. For the occurring phase to ground fault in particular, the selected voltage V_{sel} can be written as a function of the selected current I_{sel} as

$$V_{sel} = xZ_L I_{sel} + I_F R_F$$

$$= x\, Z_L I_{sel} + (I_{Fs} + I_{Fr}) R_F \tag{4.2}$$

However, neither the current I_F nor the current I_{Fr} is available for single end algorithms. Hence, the algorithm should depend only on the available data at the sending end. The part $R_F\, I_F$ can be replaced by $R_{Fs}\, I_{Fs}$, where R_{Fs} is the apparent fault resistance value as seen from the sending end as follows:

$$R_{Fs} I_{Fs} = R_F (I_{Fs} + I_{Fr}) \tag{4.3}$$

In which the resistance R_{Fs} can be rewritten as

$$R_{Fs} = R_F \left(1 + \frac{I_{Fr}}{I_{Fs}} \right) \tag{4.4}$$

In order to get a real value for the assigned R_{Fs} resistor, it is assumed that the resistance has only a resistive component. Both I_{Fs} and I_{Fr} are then in phase. To fulfil this assumption, the system is assumed to be a homogeneous one. Substituting from equation (4.4) and (4.3) in equation (4.2) and rearranging yield the general seen apparent impedance form as

$$Z_{app} = \frac{V_{sel}}{I_{sel}} = x\, Z_L + R_{Fs} \frac{I_{comp}}{I_{sel}} \tag{4.5}$$

Owing to the fault type and the associated faulty phases, the selected voltage and current quantities, V_{sel} and I_{sel}, as well as the compensation current quantity, I_{comp}, are computed. Then equation (4.5) can be directly solved for the unknown fault distance x. As clear from the above equation, the approach can effectively compensate the effects of remote infeed. Also, considering the pre-fault loading current is possible. This results in a successful single end fault location estimation method [34, 44].

4.2.2 Benefits of modal transformation

Modal transformation is essentially characterized with the ability to decompose a certain group of coupled equations into decoupled ones excluding the mutual parts among these equations. This can be typically applied to the impedance matrices for coupled conductors. As shown Fig.

4.2, the terms of mutual impedance Z_m disappeared from the transformed impedance matrix; in which the modal impedance quantities Z_{m1}, Z_{m2} and Z_{m3} only appear and the other off-diagonal elements are equal to zero. This decoupling is remarkably important as the required complex mathematical manipulation for those applications can be efficiently performed without further complexity or approximations. This successfully enhances the overall efficiency of their applications. An example for these applications is the modal transformation-based distance protection schemes [61, 62, 63, 64].

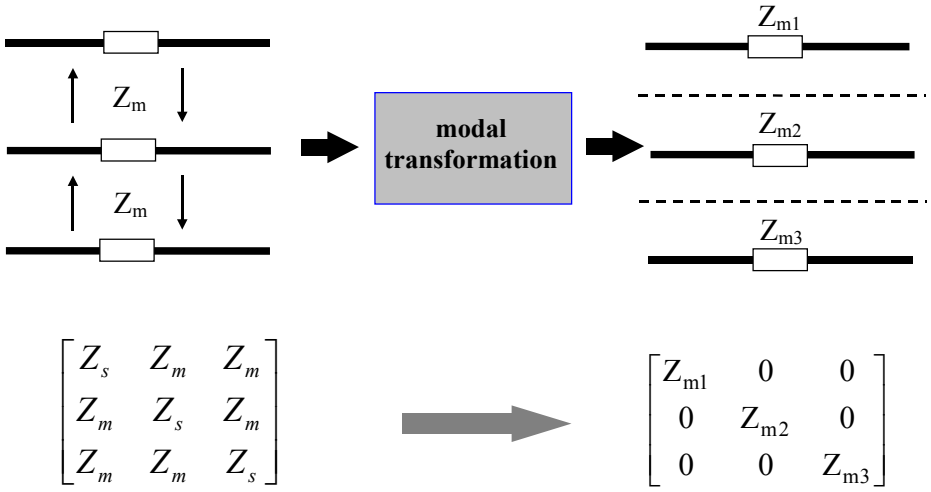

Fig. 4.2 Modal transformation decoupling

For power system applications, the measured voltages and currents can be transformed into their modal quantities as

$$\mathbf{V}_m = \mathbf{T}_v^{-1} * \mathbf{V}_p \tag{4.6}$$

$$\mathbf{I}_m = \mathbf{T}_i^{-1} * \mathbf{I}_p \tag{4.7}$$

Where the indices m and p are related to modal and phase quantities, respectively. $\mathbf{T}_v$ and $\mathbf{T}_i$ are the corresponding voltage and current transformation matrices. Appendix C presents a sufficient explanation for its mathematical basis. For balanced (equally transposed) multi-phase lines both $\mathbf{T}_v$ and $\mathbf{T}_i$ matrices can be easily chosen to Clarke transformation as [65]

$$\mathbf{T}_V = \mathbf{T}_i = \mathbf{T} = \frac{1}{\sqrt{3}} \begin{pmatrix} 1 & \sqrt{2} & 0 \\ 1 & \frac{-1}{\sqrt{2}} & \frac{\sqrt{3}}{\sqrt{2}} \\ 1 & \frac{-1}{\sqrt{2}} & \frac{-\sqrt{3}}{\sqrt{2}} \end{pmatrix} \tag{4.8}$$

Then, the modal impedance and admittance matrices $\mathbf{Z}_m$ and $\mathbf{Y}_m$ can be found respectively as

$$\mathbf{Z}_m = \mathbf{T}_v^{-1} * \mathbf{Z} * \mathbf{T}_v \quad (4.9)$$

$$\mathbf{Y}_m = \mathbf{T}_i^{-1} * \mathbf{Y} * \mathbf{T}_i \quad (4.10)$$

4.3 Fault Location Algorithm Mathematical Basis

The structure of the proposed fault location algorithm is generally based on two essential concepts. Firstly, the modal transformation is employed in order to transform all measured voltage and current quantities into their modal values. The aim is to eliminate the mutual effects perfectly. Then, the apparent impedance approach is employed using the resulting modal quantities to benefit from the compensation features of the approach to eliminate the influence of remote infeed and pre-fault loading. This combination is expected to result in a powerful fault location algorithm dealing with both single and multi-circuit lines using single end data.

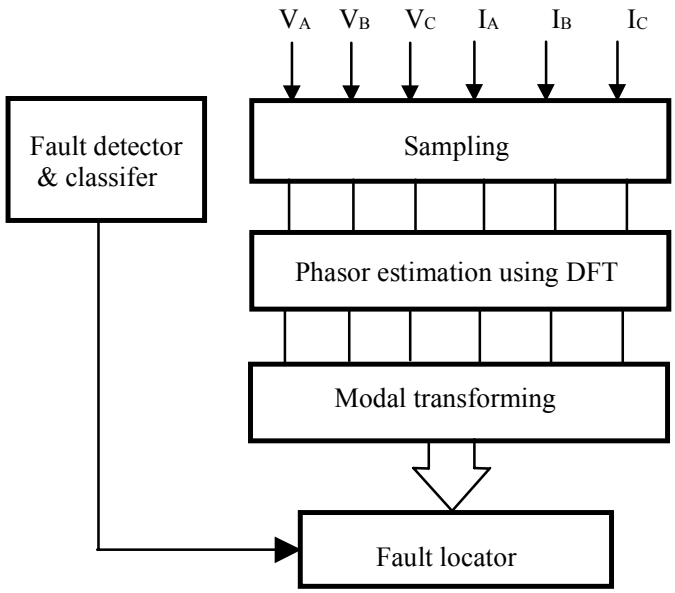

Fig. 4.3 Schematic of the proposed fault location algorithm

A general description of the proposed algorithm is given in Fig. 4.3. Currents and voltages of all phases are extracted and sampled with a sampling rate of 32 samples per cycle. This sampling rate is currently common for modern digital relay requirements and enough for all required phasor estimation purposes. These quantities are designated as V_A, V_B, V_C, I_A, I_B and I_C respectively. These sampled inputs are fed to the locator via DFT filtering stage as well as modal transformation stage. All extracted voltage and current phasor quantities are transformed

into their modal forms with the main transformation equations (4.6) and (4.7). Once the disturbance occurs, the fault detector & classifier enables the locator to start the estimation process. The resulting modal quantities are processed according to the classified fault type as well as the associated faulty phases.

4.3.1 Phase to ground fault

As shown in Fig. 4.4, a line to ground fault is assumed to occur on phase A through a certain fault resistance R_F. The fault occurred at a distance *x* percentage of the total line length L. First the fault is assumed to be solidly earthed to explain the algorithm essence.

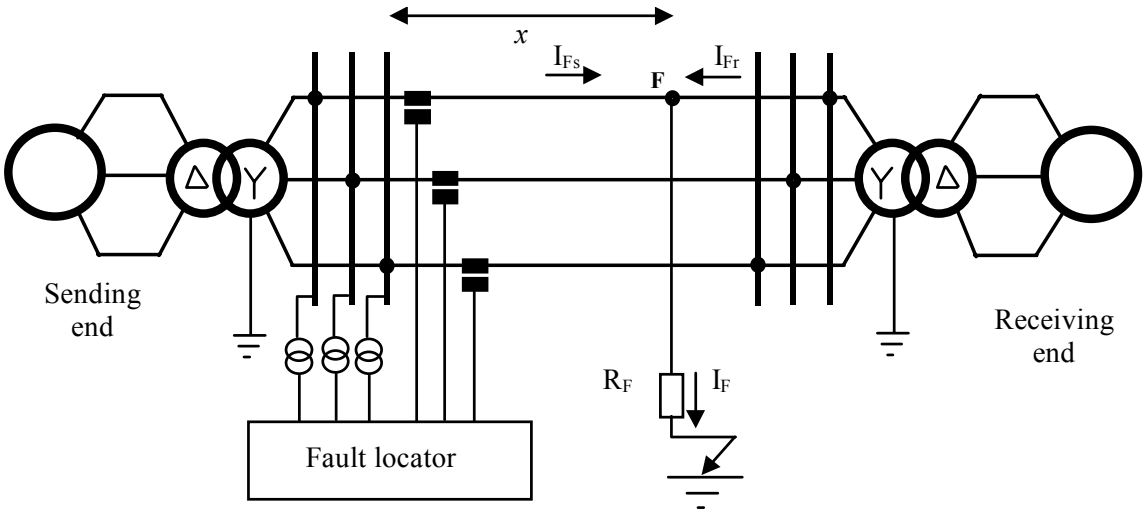

Fig. 4.4 Phase to ground fault

Considering R_F to be zero, the describing equation for this fault type can be then written as

$$V_{AF} = 0 \tag{4.11}$$

where V_{AF} is the measured voltage for phase A at the fault point F. The faulted network can be expressed by a three uncoupled circuits using modal transformation as seen in Fig. 4.5. Then equation (4.11) can be rewritten as follows:

$$V_{AF} = T_{1,1}V_{Fm1} + T_{1,2}V_{Fm2} + T_{1,3}V_{Fm3}$$

$$= \sum_{J=1}^{3} T_{1,j}(V_{Fmj}) \tag{4.12}$$

Where V_{Fm1}, V_{Fm2} and V_{Fm3} are the modal voltages at the point F.

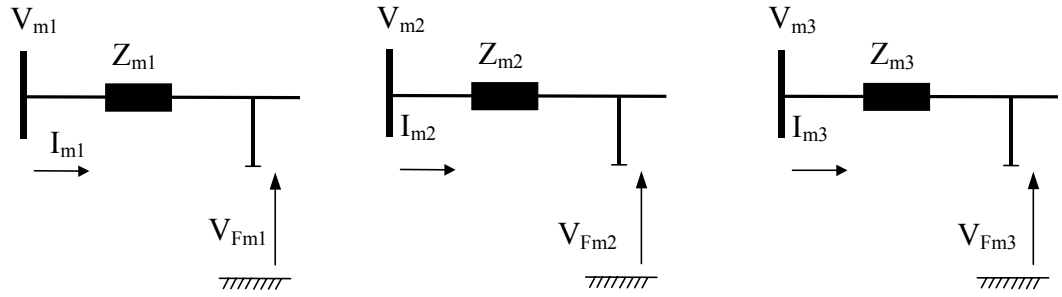

Fig. 4.5 Faulted network modal circuits

Owing to these uncoupled modal circuits, substituting with fault point modal voltages as function of their related modal quantities at the sending end in equation (4.12) yields,

$$V_{AF} = \sum_{J=1}^{3} T_{1,j}(V_{mj} - xZ_{mj}I_{mj}) \tag{4.13}$$

Where j is the number of modes (3 for balanced lines). From equations (4.11) and (4.12), the apparent impedance $Z_{aap,\ AG}$ seen from the relay location can be expressed according to the apparent impedance approach as

$$Z_{app,\ AG} = x\,Z_{ml} = \frac{T_{1,1}V_{m1} + T_{1,2}V_{m2} + T_{1,3}V_{m3}}{T_{1,1}I_{ml} + T_{1,2}I_{m2}\dfrac{Z_{m2}}{Z_{ml}} + T_{1,3}V_{m3}\dfrac{Z_{m3}}{Z_{ml}}} \tag{4.14}$$

$Z_{app,\ AG}$ is expressed as a percentage of the modal impedance Z_{m1}. The equation can be then directly solved for the unknown fault distance x according to the apparent impedance approach using equation (4.5) with the following selected voltages and currents:

$$V_{sel,\ AG} = T_{1,1}V_{m1} + T_{1,2}V_{m2} + T_{1,3}V_{m3} \tag{4.15}$$

$$I_{sel,\ AG} = T_{1,1}I_{m1} + T_{1,2}I_{m2}\frac{Z_{m2}}{Z_{m1}} + T_{1,3}I_{m3}\frac{Z_{m3}}{Z_{m1}} \tag{4.16}$$

The procedure is repeated considering the existence of the fault resistance R_F in which the fault current I_F is supplied with both the sending and receiving end currents as

$$I_F = I_{Fs} + I_{Fr} \tag{4.17}$$

The new describing equation considering a non-zero fault point voltage is written as follows:

$$V_{AF} = R_F I_F \tag{4.18}$$

By replacing the part $R_F \times I_F$ with $R_{Fs} \times I_{Fs}$ as explained before with equation (4.3) and (4.4) equation (4.18) can be rewritten as

$$V_{AF} = R_{Fs} I_{Fs} \tag{4.19}$$

Expressing this equation using modal quantities similarly to the solid fault case procedure using equation (4.13) and the new describing equation (4.19) yields,

$$Z_{app,\,AG} = \frac{V_{sel,\,AG}}{I_{sel,\,AG}} = x\, Z_{m1} + R_{Fs} \frac{I_{Fs}}{I_{sel,\,AG}} \tag{4.20}$$

Where the compensation current for this case, I_{Fs}, is calculated as follows:

$$I_{Fs} = \sum_{j=1}^{3} T_{1,j} I_{mj} + \sum_{j=1}^{3} T_{2,j} I_{mj} + \sum_{j=1}^{3} T_{3,j} I_{mj} \tag{4.21}$$

In order to compensate the effect of pre-fault currents, these currents should be subtracted from the compensation current in equation (4.20). The pre-fault current matrix I_L can be written for each circuit as

$$\mathbf{I}_L = [\, I_{LA} \;\; I_{LB} \;\; I_{LC} \,]^t \tag{4.22}$$

Where I_{LA} , I_{LB} and I_{LC} are designated for pre-fault currents for phases A, B and C respectively. The equivalent modal quantity matrix I_{LM} is then found as

$$\mathbf{I}_{LM} = \mathbf{T}_i^{-1} * \mathbf{I}_L = [\, I_{L1} \; I_{L2} \; I_{L3} \,]^t \tag{4.23}$$

Similar derivation are performed for other phase to ground faults on phase B or C as well.

4.3.2 Double phase fault

As shown in Fig. 4.6, a phase to phase fault is assumed to occur between phases A and B at a distance *x* from the sending end. The new constraint for this fault condition is described as

$$V_{AF} = V_{AB} \tag{4.24}$$

Where V_{AF} and V_{AB} are the phase voltages at the fault points FA and FB for both faulted phases A and B respectively.

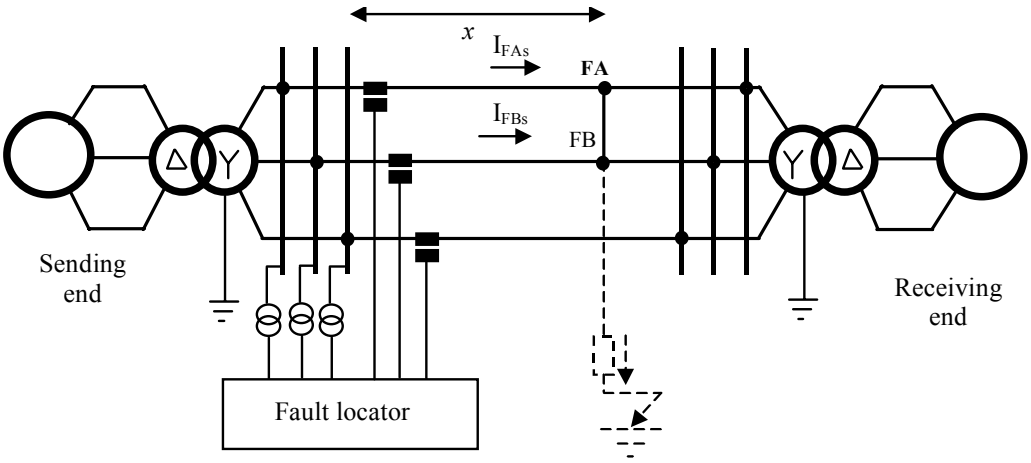

Fig. 4.6 Double phase fault

Using modal quantities equation (4.23) can be rewritten as follows:

$$\sum_{j=1}^{3} T_{1,j}(V_{FAmj}) = \sum_{j=1}^{3} T_{1,j}(V_{FBmj}) \tag{4.25}$$

Then, substituting in equation (4.25) using decoupled modal networks yields,

$$\sum_{j=1}^{3} T_{1,j}(V_{Amj} - xZ_{mj}I_{Amj}) = \sum_{j=1}^{3} T_{1,j}(V_{Bmj} - xZ_{mj}I_{Bmj}) \tag{4.26}$$

Rearranging equation (4.26) to get the apparent impedance $Z_{app,\,AB}$ finally yields the $Z_{app,\,AB}$ as

$$Z_{app,\,AB} = \frac{V_{sel,\,AB}}{I_{sel,\,AB}} = x\,Z_{m1}$$

$$= \frac{\sum_{j=1}^{3} T_{1,j}V_{mj} - \sum_{j=1}^{3} T_{2,j}V_{mj}}{\sum_{j=1}^{3} T_{1,j}I_{mj}\frac{Z_{mj}}{Z_{m1}} - \sum_{j=1}^{3} T_{2,j}I_{mj}\frac{Z_{mj}}{Z_{m1}}} \tag{4.27}$$

When the fault occurs through the ground with a certain impedance R_F, the new boundary condition for this case can be described as,

$$V_{FA} = V_{FB} = I_F\,R_F = I_{FS}\,R_{Fs} \tag{4.28}$$

Then, equating the first two terms of the equation (4.28) yields a similar relation as by equation (4.27) in addition to the compensation current part I_{comp}. The compensation current can be

described as a function of sending end modal currents and the pre-fault modal currents as seen bellow as:

$$I_{comp} = \sum_{j=1}^{3} T_{1,j} I_{mj} - \sum_{j=1}^{3} T_{2,j} I_{mj} - \left(\sum_{j=1}^{3} T_{1,j} I_{Lj} - \sum_{j=1}^{3} T_{2,j} I_{Lj} \right) \quad (4.29)$$

4.3.3 Three phase fault

A three phase fault occurs at the points FA, FB and FC at a distance *x* from the sending end as shown in Fig. 4.7. The describing equation for this fault case can be described as

$$V_{FA} = V_{FB} = V_{FC} = 0 \quad (4.30)$$

Hence, this fault can be considered by the same equations of double phase fault (considering $V_{FA} = V_{FB}$ as in double phase faults), or with single phase to ground fault (considering $V_{FA} = 0$ as in case of line to ground faults).

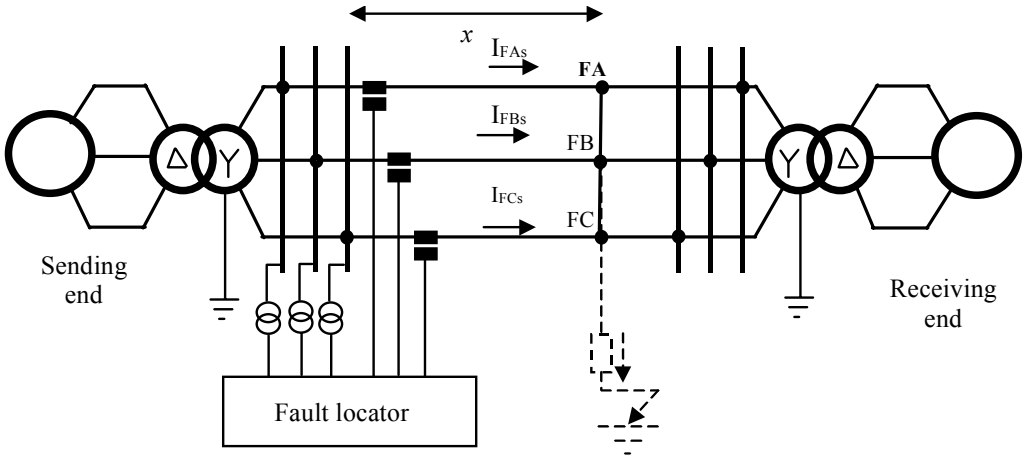

Fig. 4.7 Three phase fault

4.3.4 Generalization of the fault location equations

As seen in the last subsection, a special formula has been derived for each fault type. However, it is more convenient to rewrite the proposed algorithm in a general form for all fault types. This is more practical and helpful especially for implementation purposes. Equation (4.5) is the main apparent impedance formula. Where the coefficients V_{sel}, I_{sel} and I_{comp} are calculated according to the fault type as expressed in the following equations:

$$V_{sel} = a_1 \sum_{j=1}^{3} T_{1,j} V_{mj} + a_2 \sum_{j=1}^{3} T_{2,j} V_{mj} + a_3 \sum_{j=1}^{3} T_{3,j} V_{mj} \quad (4.31)$$

$$I_{sel}=a_1\sum_{j=1}^{3}T_{1,j}I_{mj}\frac{Z_{mj}}{Z_{m1}}+a_2\sum_{j=1}^{3}T_{2,j}I_{mj}\frac{Z_{mj}}{Z_{m1}}+a_3\sum_{j=1}^{3}T_{3,j}I_{mj}\frac{Z_{mj}}{Z_{m1}} \tag{4.32}$$

$$I_{comp}=\left(b_1\sum_{j=1}^{3}T_{1,j}I_{mj}+b_2\sum_{j=1}^{3}T_{2,j}I_{mj}+b_3\sum_{j=1}^{3}T_{3,j}I_{mj}\right)-I_{LC} \tag{4.33}$$

Where I_{LC} is the subtracted current part due to pre-fault currents and can be calculated as

$$I_{LC}=b_1\sum_{j=1}^{3}T_{1,j}I_{Lj}+b_2\sum_{j=1}^{3}T_{2,j}I_{Lj}+b_3\sum_{j=1}^{3}T_{3,j}I_{Lj} \tag{4.34}$$

These equations represent the general equations of the proposed locator. They are available for all fault types, where the associated constants are selected depending on the fault type. A key of the related values for these constants is given in Table 4.1.

Table 4.1 Key table for equation constants

Fault type	a_1	a_2	a_3	b_1	b_2	b_3
A-G	1	0	0	1	1	1
B-G	0	1	0	1	1	1
C-G	0	0	1	1	1	1
A-B/A-B to G	1	-1	0	1	-1	0
A-C/A-C to G	1	0	-1	1	0	-1
B-C/B-C to G	0	1	-1	0	1	-1
A-B-C	1	0	0	1	1	1

4.3.5 Correction of charging currents

Since the derivation of the fault location algorithm is based on the simple lumped parameter line model, charging currents arise as an essential source of the estimation error. Several tests have been carried out in order to investigate the contribution of these currents into the overall estimation error. The results concluded that these currents introduce a significant error contribution particularly with high resistance fault cases. This is due to the relatively low currents during these faults. Thus, the compensation of their effects improves the overall performance. Fig. 4.8 shows the current contribution from both self and mutual capacitance parts, lumped at locator location, which are designated as C_s and C_m. To illustrate the mathematical description for this compensation. A line to ground fault on phase A is considered as an example as shown in the figure. In order to get more accurate fault distance estimation, the locator should depend on the contributed current in the fault, I_A', rather than the current I_A seen

by the locator at its location. Thus, the resulted self and mutual capacitance currents I_{Cs} and I_{Cm} are subtracted respectively as follows:

$$I_A' = I_A - I_{Cs} - I_{Cm} \tag{4.35}$$

Where the associated values for both I_{Cs} and I_{Cm} are calculated as

$$I_{Cs} = C_s \frac{dV_A}{dt} \tag{4.36}$$

$$I_{Cm} = C_m \frac{d(V_A - V_B)}{dt} + C_m \frac{d(V_A - V_C)}{dt} \tag{4.37}$$

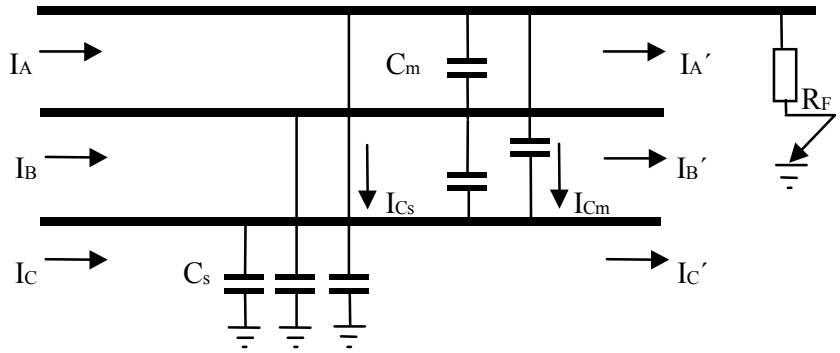

Fig. 4.8 Contribution of capacitance currents at the relay location

Similarly I_B' and I_C' are calculated, then the three line current values are updated before the fault location calculation routine is executed.

4.4 Algorithm Performance Evaluation

The evaluation of the proposed fault location algorithm was performed using the constructed testing mechanism that was described in the last chapter using both ATP-EMTP and MATLAB. A group of test cases were prepared with the EMTP-ATP covering the entire range of the line length and a wide range of the fault resistance. At each fault location, all possible fault types (phase to ground, double phase, double phase to ground, and three phase fault cases) were tested to find out the individual accuracy at this location. Also, the overall accuracy was computed by comparing the resulting estimation errors along the entire range of the line length according to both equations (3.1) and (3.2) respectively. The selected test cases were prepared covering the

different situations that may significantly affect the algorithm accuracy such as line loading, double infeed, fault resistance and line imbalance using the same 220 kV, 200 km line. The system parameters as well as conductor configuration are listed in Appendix B.

4.4.1 Pre-fault line loading impact

In order to investigate the effects of pre-fault line load before the occurrence of disturbance, a certain group of different test cases were prepared with faults occurring under both no load and full load conditions. The line was assumed to be single circuit line fed from only one line end. Also, all ground faults occurred solidly and the line was assumed to be only with transposed parameters. The aim is to investigate the pre-fault load effects regardless of other sources of estimation error. The resulting estimation error of combination of these error sources simultaneously will be covered later. Firstly, the individual accuracy was evaluated in order to investigate the fault position effect on the scheme accuracy. Fig. 4.9 shows the variation of the individual accuracy (A_I) along the entire range of the line length for both no load and full load situations. The shown results reveal the relatively higher estimation error for close-in faults as a common feature of most single end algorithms. Also, the figure shows that the local accuracy A_L for the proposed algorithm for both loading conditions does not exceed 3 %.

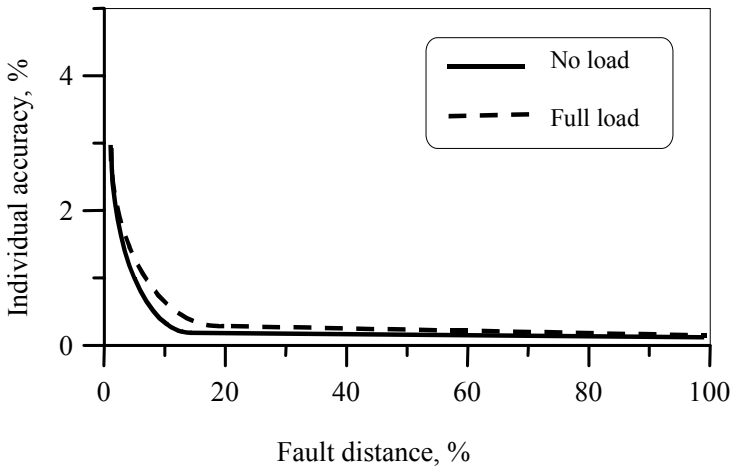

Fig. 4.9 Individual accuracy along the entire range of the line length

Then, the overall accuracy, A_O, was investigated as a percentage of the occurring maximum estimation error to the total line length. For this purpose the maximum resulting estimation error for each fault position is plotted against the fault distance for both no load and full load situations as shown in Fig. 4.10. As revealed from the shown results, the overall accuracy does not exceed 0.3 % and 0.5 % of the total line length for both situations respectively.

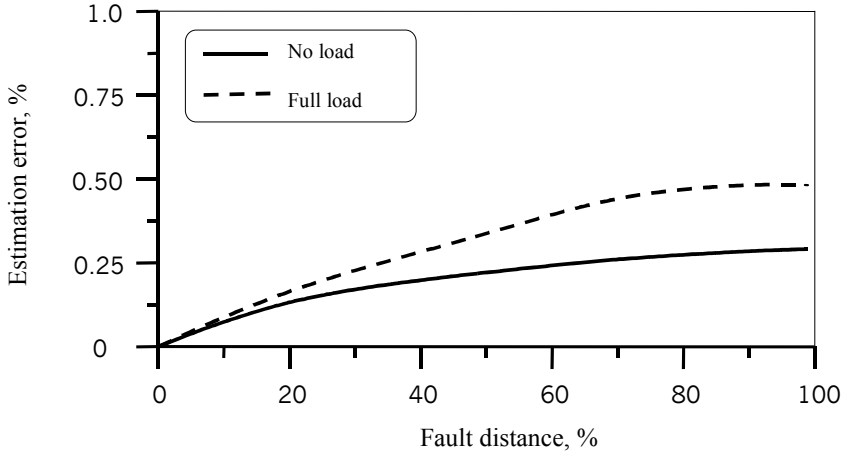

Fig. 4.10 Overall accuracy evaluation for both no load and full load cases

4.4.2 Remote infeed impact

As the proposed algorithm depends only on the data available at the relay location, the need to evaluate the impact of the remote infeed on the algorithm accuracy is obvious. This problem is a considerable error factor for all single end relaying algorithms. However, the apparent impedance approach is expected to present an acceptable performance considering this situation. In order to investigate the influence of remote infeed existence, some test cases were prepared with all fault type possibilities considering single circuit line with no pre-fault loading. For all these test cases, the line was assumed to be single circuit line and fed from both line ends. Also all ground faults occurred solidly and the line was assumed to be with transposed parameters. Fig. 4.11 plots the maximum resulting estimation error against the fault position for both cases. The shown results reveal the algorithm efficacy in both single and double infeed situations.

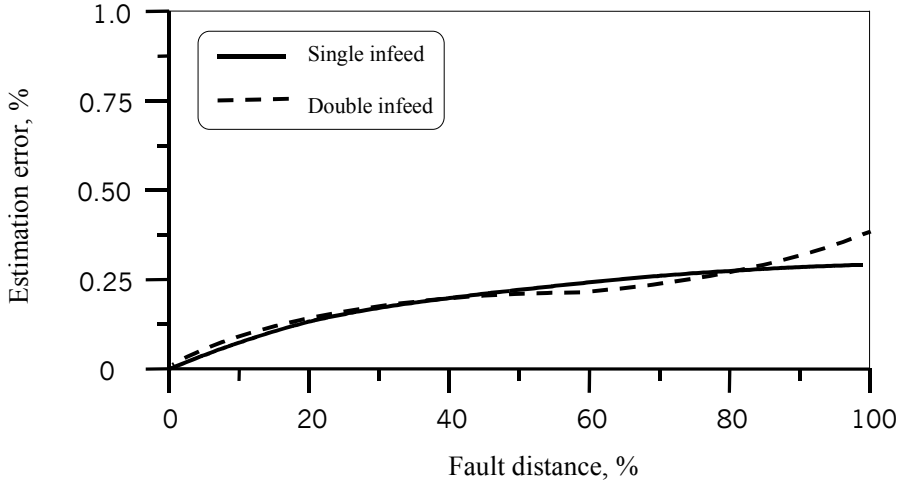

Fig. 4.11 Evaluation of double infeed line situations

4.4.3 Fault resistance impact

Involving a resistance in the fault loop during phase and double phase to ground faults is a practical situation in typical fault conditions. This resistance is not only caused by the arc resistance between the fault point and the ground, but also by some other reasons like the resistance of any path to ground or errors in the ground resistivity modeling. Thus, it is a basic challenge for all fault locators. Ideally, the proposed algorithm is immune to the existence of fault resistance. This is clear from the derivation of the algorithm as shown in section 4.3, in which the formula for the estimated fault location x is independent of the apparent fault resistance R_{Fs}. Also, the charging currents are compensated as seen in section 4.3.5.

Since the algorithm derivation considers only a lumped parameter line model, the parameter distribution is strongly expected to have a remarkable influence on the algorithm performance. It is, therefore, more worth to investigate the performance of the proposed algorithms during these situations. For this purpose, some test cases were prepared with the added fault resistance for both single phase and double phase to ground faults. For these test cases, the line was assumed to be single circuit line and fed from only one line end with no pre-fault load with transposed line parameters. These test cases covered a wide range of the added fault resistance up to 1kΩ. At each fault resistance value the response of the proposed approach is checked to find out the overall accuracy of the proposed algorithm. Fig. 4.12 shows the results for both single phase and double phase to ground faults using solid and dashed lines respectively. As revealed, the algorithm is still showing an acceptable overall accuracy for both fault cases along the selected range of the fault resistance.

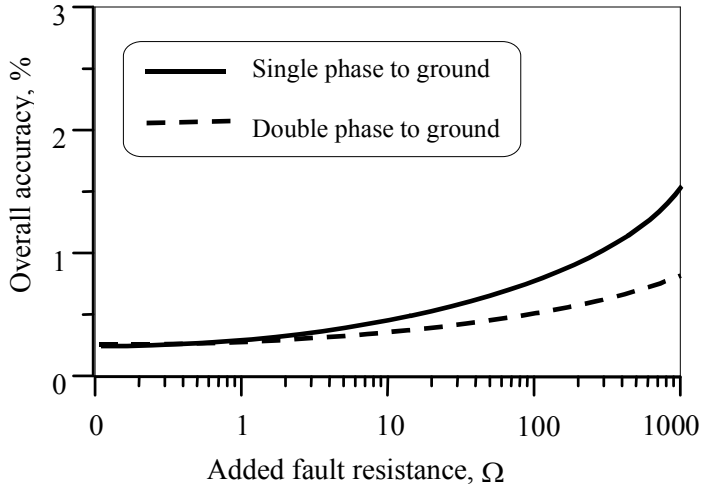

Fig. 4.12 Fault resistance impact evaluation

4.4.4 Line imbalance impact

During the algorithm derivation, the line is considered to be homogeneous with balanced (transposed) parameters along the whole line length. This assumption is essential in order to formalize the required algorithm using the apparent impedance approach. Also, the balanced line parameters facilitate to exclude the unknown apparent fault resistance value perfectly to get the unknown fault distance x as seen in section 4.3. This assumption is quite acceptable for transposed line cases. This is mainly due to the efficient compensation features owing to the apparent impedance approach. However, for untransposed line cases, the line parameters are no longer equally distributed along the whole line. Also, the allocation of the considered lumped capacitance for compensating the charging currents differs from the actual distributing capacitance along the line. Both line imbalance and capacitance allocation effect collaborate together to enlarge the resulting estimation error. Thus, the algorithm performance is expected to be affected remarkably in these situations. Moreover, the resulting error may increase considerably due to the existence of non-solid ground faults and doubly fed lines. It is therefore more convenient to investigate these situations.

Firstly, the collaboration of the line imbalance case with the remote infeed is considered under no-loading operation. Fig. 4.13 shows the variation of the resulting estimation error against the line length for both transposed and untransposed line cases. The algorithm encountered a higher level of error during the untransposed one. The overall accuracy can be then found for both situations with the maximum estimation error as 1.1% for untransposed parameters and 0.3% for the transposed case.

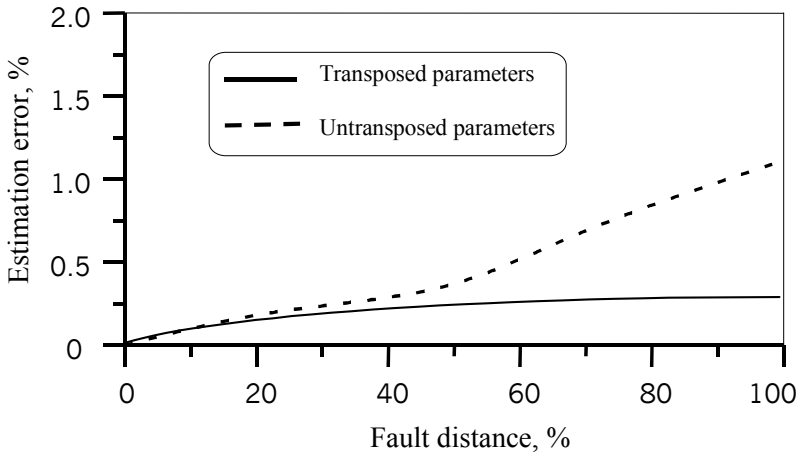

Fig. 4.13 Remote infeed impact investigation with line imbalance

For the case of fault resistance existence, Fig. 4.14 shows the resulting overall accuracy against the added fault resistance for both single phase and double phase to ground fault conditions. The line was fed from only one end with no pre-fault loading. These results reveal the remarkable impact of line imbalance on the algorithm performance.

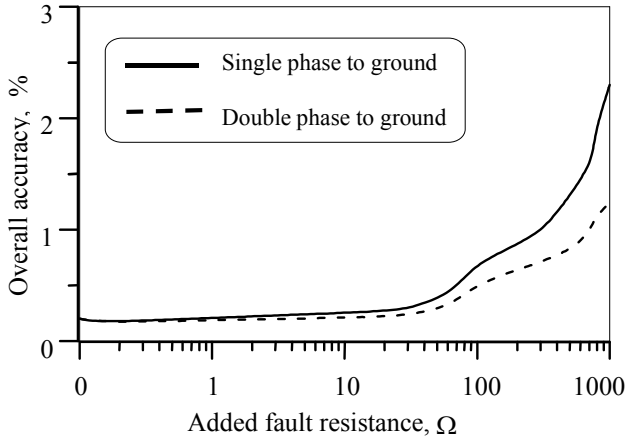

Fig. 4.14 Fault resistance impact considering untransposed line

4.4.5 Mutual coupling impact

Owing to the decoupling feature of modal transformation, the proposed algorithm is expected to have a high immunity to those problems that result from the mutual effects. In order to evaluate the algorithm performance during these situations, the applied tests were repeated for double circuit transmission line case as shown in Fig. 4.15. The results compare the algorithm behavior for both single and double circuit lines with different infeed situations and different loading conditions considering the line imbalance and the existence of fault resistance. As revealed from the results, the algorithm has a perfect immunity to the resulting mutual coupling from the adjacent multi-circuit lines. It, therefore, provides a powerful fault location scheme for both single and multi circuit lines.

4.4.6 Cumulative total error

All of the applied tests reveal the superior performance of the proposed approach for the selected situations. However, these situations consider the factors that may affect the overall performance of the proposed algorithm individually. It is expected that the contribution of the simultaneous existence of some of the aforementioned factors may result in a higher estimation error. It is, therefore, more convenient to develop a general estimation of the total error considering the existence of these factors simultaneously.

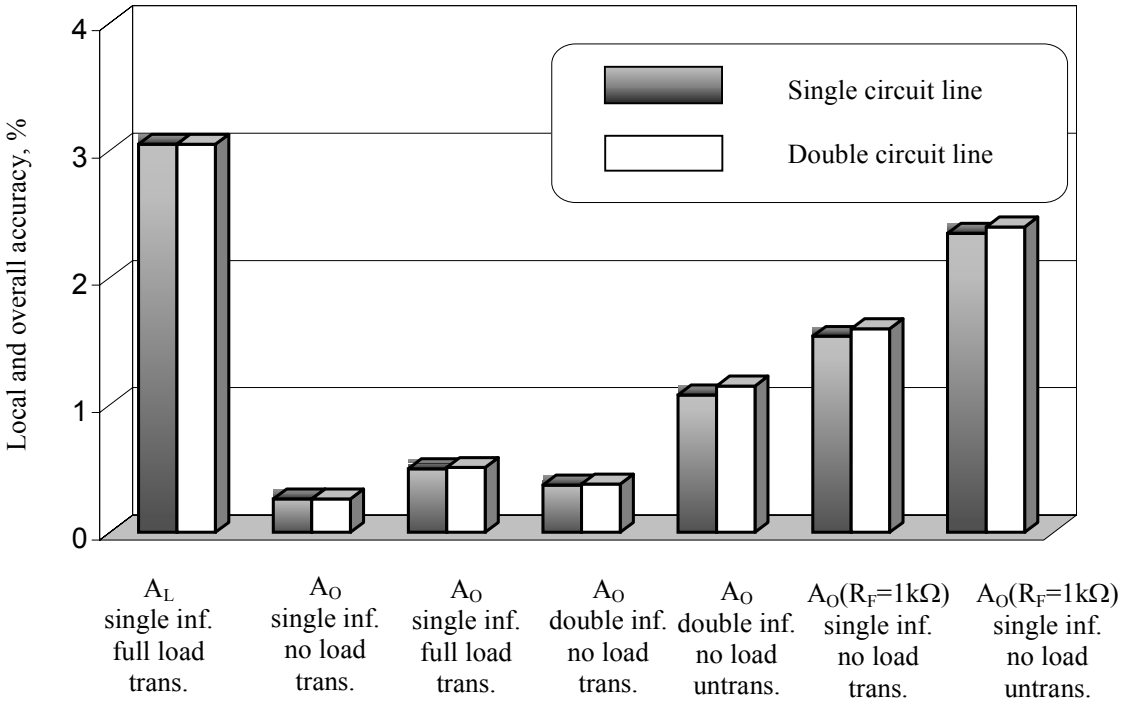

Fig. 4.15 Algorithm performance during single and double circuit lines

For this purpose, different test cases were prepared covering the entire range of the line length considering the aforementioned individual circumstances simultaneously. These test cases dealt with a double circuit untransposed line, assuming full loading, double infeed and different values of fault resistance. Both single and double phase to ground faults were examined using a wide range of the added fault resistance. Thus the total error for this situation primarily depends on the value of the added fault resistance in conjunction with the fault point position along the line. Fig. 4.16 (a) and (b) plot the total error versus the fault point position and the added fault resistance. The results show that the proposed approach is characterized by a maximum total estimation error of 4.4% and 2.0% for single and double phase to ground faults respectively.

4.5 General Concluding Remarks

Through the mathematical handling for the approach derivation, the full transposing of the line is assumed. This assumption resulted in considering constant transformation matrices into modal form and can be easily achieved using the Clarke transformation matrix for both currents and voltages as explained before. For unbalanced (untransposed) lines, two different treatments are valid. The first one is achieved by neglecting the untransposing effects and using the same equations of the transposed one, and hence every circuit (for a double circuit line) is considered

individually using three modes for each one. The same equations are applied for the faulty circuit. The other treatment is achieved by depending on the associated untransposed line parameters. Hence, the related equations must be rewritten using the new resultant transformation matrices. The associated equations can be easily adopted to be suitable for the untransposed situation by changing the number of modes (equal to 3 in a transposed one) to be equal to the number of phases (6 for a double circuit line). However, the related transformation matrices differ from one line to another depending on the conductor configurations and line parameters. This represents a practical difficulty due to the need to calculate the individual matrices for each line. Different test cases were accomplished to investigate both situations. It has been concluded that using constant transformation matrices (neglecting untransposition) is sufficiently accurate for all configurations. This is also clear in the presented tests in the last section.

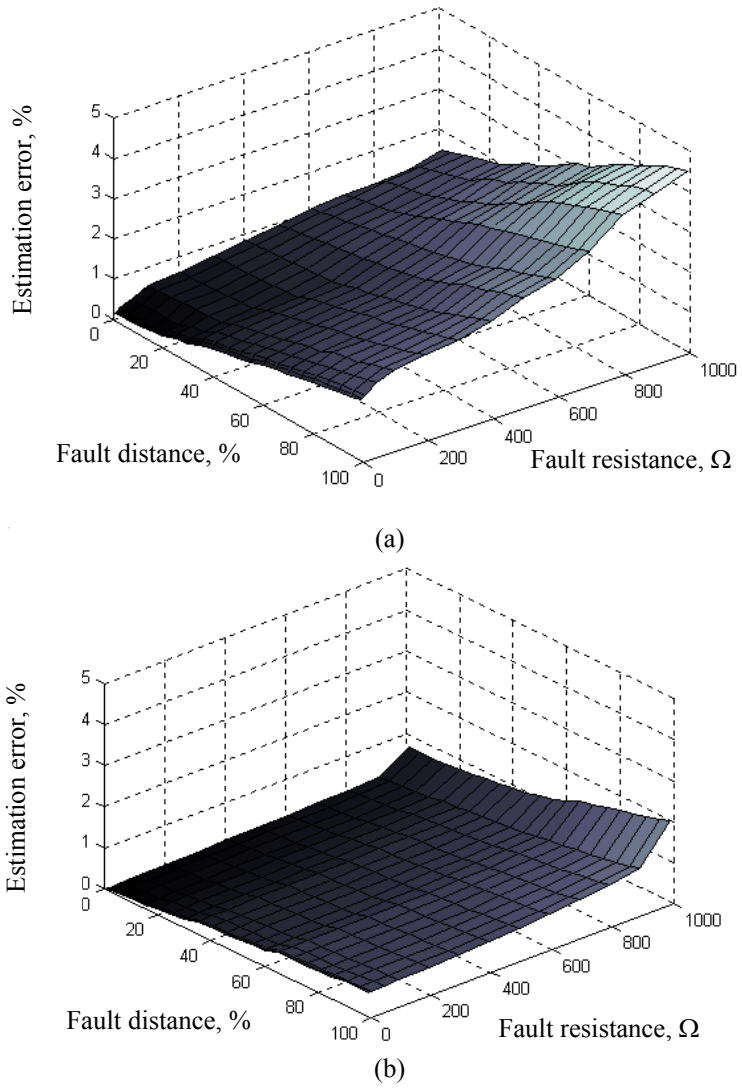

Fig. 14.16 Percentage of total error limit for cumulative error factors

(a) Single phase to ground fault (b) double phase to ground fault

As revealed in the presented tests, the proposed algorithm is characterized by a high performance during all loading and infeeding conditions. Also, the algorithm is able to eliminate perfectly the mutual coupling effects on the algorithm accuracy. This leads to provide a practical fault location algorithm suitable for both single and multi-circuit lines even with the line imbalance. However, the algorithm performance during those fault cases with high fault resistance values is still questionable. Different factors participated into this response including the charging currents inaccuracies and simplification assumptions. The nature of these factors and their interaction has a non-deterministic behavior so that eliminating them using normal mathematical compensation is quite difficult. Thus, the need for some modern processing tools is obvious. The Artificial Intelligence (AI) tools are therefore expected to provide a solution for this problem as described in the following chapters.

5 Assessment of AI Tools for Protection Purposes and Fault Location

The goal of this chapter is to review the employment of Artificial Intelligence (AI) tools for power system protection purposes including the applications, the used tools and the provided improvements. Also, employing these tools for fault location purposes are here highlighted for the later usage of these tools. Next chapters explain in detail how AI methods can significantly improve the performance of the proposed fault location algorithm with the proper intelligent tool to compensate the resulting estimation error and consequently improve its fault location estimation accuracy.

5.1 AI Techniques: Tools, History and Abilities

The basic feature of the human sense is the ability of approximated reasoning dealing with subjective knowledge, ambiguity and uncertainties. On the other hand, conventional mathematical basis deals only with those deterministic and well defined data. These wide capabilities of human intelligence inspired the researchers to attempt to emulate the human thinking with artificial approaches. They mainly aim to make use of these intelligent abilities for solving the complex problems that are extremely difficult (or impossible) to be accessed with conventional methods. There are several categories of AI tools; whereas, each of them has certain characteristics and employs different intelligent processes. Those tools have been employed for a wide variety of applications. For protection applications in particular, Artificial Neural Network (ANN), Expert Systems (ES), Fuzzy Logic (FL) and Genetic algorithms (GA) are successfully employed as seen in the literatures.

One of the first attempts to emulate the human thinking is the ANN, which tries to simulate the activities of human biological neuronal-system. The work in this field has started from the 1940s. However, since the late of 1980s the significant contributions for ANN have really begun by developing practical and efficient training algorithms in order to optimize the arbitrary designed network structures [66]. The essential feature of the ANNs is the ability to be trained so that the structure of the designed ANN can be optimized in order to get the highest performance through the real operation. The power of neural networks is manifested in complex classification problems or in modeling of highly non-linear systems whose behavior can not be directly expressed by conventional mathematical forms. This can be achieved through a wide variety of ANN construction models and different powerful training paradigms. Each of these models has its own advantages and disadvantages as explained intensively in the literatures.

ES arises as a typical AI powerful tool designed to mimic the basic aspects of human intelligent thinking including knowledge handling and reasoning. It is commonly developed by inputting the collected experience from the human experts into certain rules in a pre-defined rule base. For practical use in the real field, the defined input information vector is processed via a suitable search mechanism providing the resulting final decisions. The first ES, “DENDRAL”, was introduced in 1965 to assist chemists by determining the molecular structure of complex organic compounds. A few years later, another system, “MYCIN”, appeared for similar chemical purposes. Starting from the 1980s, ES applications were provided for industrial purposes as well [67]. For power system purposes, some successful applications were developed covering a wide variety of purposes as highlighted in the literatures. In spite of the good information handling of ESs, the learning inability, the doubtful performance through the uncertainties and non-linearity handling are basic disadvantages.

FL systems provide a robust and rich methodology for solving non-conventional problems that have defined by terms such as ambiguity, vagueness, uncertainty and conflicting knowledge. Similarly to ESs, FL systems describe the considered task into pre-defined rules. However, their response is much faster depending on a direct and simple inference mechanism. The mathematical basis of fuzzy set theory was first suggested by L. Zadeh in 1965 to describe those problems that are difficult (or impossible) to be described using deterministic variables. The first practical FL-based application was the “Automatic Train Operator” by Sendai subway, Japan, in 1987. Then, FL systems got much attention resulting in a huge amount of contributions by different authorities all over the world [68]. FL is considered to be a powerful tool for non-linear

mapping as well. Thus, it can be used optimally for complex classification and non-linear simulation problems. Also, FL systems are more distinctive with understandable configuration in forms of linguistic rules of knowledge than ANN ones. Moreover, recent training methods support FL strongly to be an optimal AI tool.

GA is considered a mathematical representation of the natural theory of evolution that happens in living beings. These concepts of the biological process to select the fittest elements can be translated into a certain mathematical algorithm to search for the best solutions for a specific problem using different operators similar to those natural ones. For the considered problem, a fraction of the good solutions is selected among all possible solutions, while the others are rejected (survival of the fittest). Then, the selected solutions undergo the processes of reproduction, crossover, and mutation to produce a new generation of possible solutions. This process is repeated until an acceptable conversion within a generation is got. The basic benefit of this technique is that it performs the search in an intelligent manner starting from a broad spectrum of possible solutions; rather than restricting the search into a narrow domain, in which the results would be initially expected [69]. Thus, the GA is expected to be an optimal tool for optimization purposes providing a fast and robust convergence.

Generally speaking, AI tools provide a powerful solution method by performing non-conventional mathematical operations aiming to emulate the human intelligence. It mainly can be employed for those problems that can not be manipulated by conventional methods due to their unknown characteristics, non-linearity, ambiguity or uncertainties. However, developing a proper solution depends essentially on the own characteristics of each AI tool as well as the own characteristics of the considered task.

5.2 AI and Protection

The basic technologies for fundamental components in power systems like generators, lines and transformers change slowly. On contrast, the power system industry seeks for the ways that can improve the reliability and the efficiency of power delivery rapidly. Hence, those supplementary tools such as protection and control equipment have an increasing attention. Thus, employing the AI tools has a continuous interesting for research efforts for all power system purposes. For protection purposes, in particular, many successful contributions were introduced as seen in the literatures. This is mainly due to the promising performance and the expected efficacy of these

tools. The rapid development of modern communication and computer engineering is also another important support by providing the basic platform for developing these AI-based applications.

5.2.1 AI protection applications overview

The usage of AI tools was firstly initiated to perform the ancillary functions relating to the relaying processes rather than the relaying functions themselves such as relay setting, equipment coordination and fuse selections. This was achieved basically by employing ESs depending on the human expertise starting from 1980s as seen in [70, 71, 72, 73]. By providing the practical and efficient training algorithms for ANNs, a huge amount of applications covering all protection purposes were developed hereinafter. A literature survey of the published AI-based contributions for protection application according to the percentage of application sharing of each tool and the considered protection functions was recently introduced in [4]. This is shown in Fig. 5.1(a) and (b) respectively. The results help generally to order the amount of applications for each tool rather than to present the accurate percentage of sharing. This is mainly due to the huge and fast growing of AI-based protection tools.

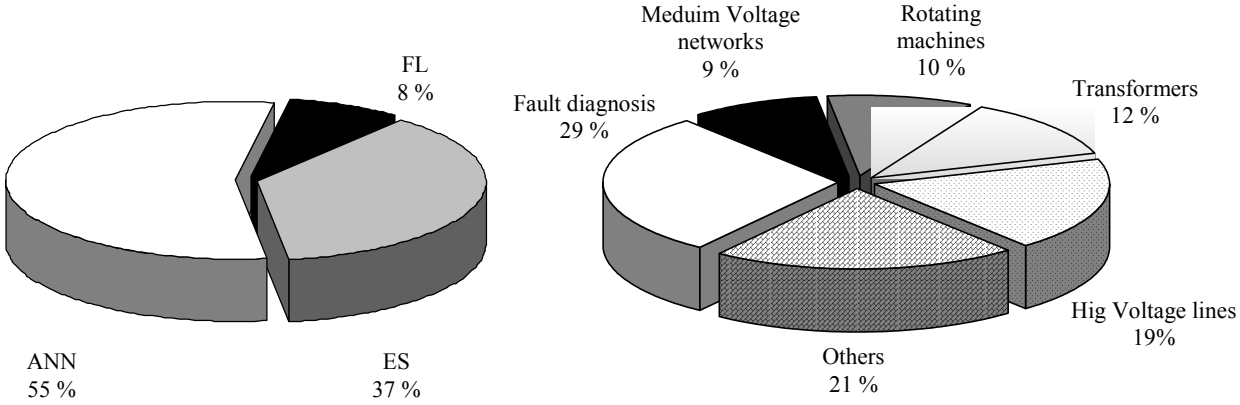

Fig. 5.1 Classification of protection applications using AI tools

(a) tools (b) Functions

As revealed from Fig. 5.1(a), ANNs have the dominant part of sharing (55 %) due to their direct designing methods, fast response and their optimum suitability for on-line operation. Due to the relatively long and well established experience of ESs, they became the second with sharing percentage of 37 %. In spite of the high capabilities of FL systems, they became the third after the ANN and ES ones. This is partially due to the relatively later employment of FL systems for protection applications. Also, the difficulty in optimizing the FL network parameters was

another factor. Nowadays, the recent methods for optimizing the designed FL networks promisingly lead to an increasing employment of FL systems efficiently. As concluded from Fig. 5.1(b), fault diagnosis is the largest field of AI-based applications for protection purposes. This is mainly due to its wide coverage of all network elements. Then, line protection is the next field of applications. It mainly results from the wide variety of protection applications of transmission networks and their suitability to be handled with AI tools including fault detection, arcing fault detection, fault location, adaptive line relaying, autoreclosure operation, direction elements .... etc. Transformer and rotating machinery came in the next two categories. Finally Medium voltage networks have the lowest sharing of applications.

5.2.2 AI tools and overhead line fault location

Locating the occurring faults on overhead lines usually encounters a variety of technical problems resulting from different circumstances as explained in Chapters 2 and 3. These problems oppose to get an accurate estimation of the aimed fault distance. Thus, it arises as one of the most favorable areas for AI research studies. A dedicated ES was earlier employed in 1989 to select the proper fault location algorithm among different ones according to the fault type, the available information and the network circumstances [74]. The fault location routine came as a part of an integrated ES-based scheme for fault detection, sectionalizing and location. However, selecting a fault location algorithm is a straightforward task depending on the available data at the locator position as well as the network configuration. This may be required to be performed once during the fabrication and installation of the fault location unit in the field. Thus no further advantages may be gained by employing ES for selecting the fault location algorithm in on-line mode.

With the great developments of ANN training and designing methods, a trail of contributions have been introduced to estimate the fault distance of the faulted line. This is mainly accomplished by those ANN types that use supervised training to map the hidden relations among the available data and the unknown fault distance through the collected training data [45, 46, 47]. The Multilayers Feedforward (MLF) ANN is considered the basic platform for these applications.

Unfortunately, FL systems have no solid contributions for fault location purposes till present. The essential reason behind this situation is the difficulty in optimizing the constructed FL

network parameters. However, the recent training methods for optimizing the parameters for FL networks are strongly expected to enable to employ FL tools for these purposes successfully.

Other applications have been introduced employing GA for fault location purposes as well. The common idea for these applications is to express the fault location formula as an optimization problem and seek for the optimum solution for the unknown fault distance [51, 52].

As revealed from the above explanation, the fault location problem is considered to be a highly suitable problem to be dealt with AI-based solutions. This can be achieved by adopting the considered AI tool to formalize the fault location estimation process in the right manner. However, the efficacy of the overall performance is highly characterized by the capabilities of each AI method as well as the accuracy of the problem formalization itself.

5.2.3 AI employment: a practical viewpoint

In spite of the huge amount of published contributions employing all known AI tools for all industrial purposes for power systems, a few of them were actually implemented and already used commercially. As reported in the literatures, ES has the majority of these real applications [2-6]. Other successful applications were developed using FL for control purposes, in particular, such as the FL-based subway control in the Japanese Sendai subway company. The developed system has managed to reduce more than 70 % of those errors that may happen with human operators.

Employing AI tools for protection purposes, in particular, is unfortunately limited. Some applications were developed using ES for those off-line purposes such as relay initial setting and coordination [75, 76, 77, 78]. A recent intelligent application was developed by employing both pattern recognition and expert system to detect the fault [79]. The proposed scheme has the ability to recognize downed conductors, persistent arcing faults and temporary arcing faults for distribution networks. However, neither of FL-based nor ANN-based schemes is employed commercially for protection purposes till present. Different factors participate into this situation. Most of these AI-based relaying schemes were introduced to replace the conventional ones completely depending on full AI-based protection functions. Also, most of these applications utilized the AI tools as a new fashion realizing no or little further technical enhancements. Moreover, the dependability and the reliability of these proposed schemes have not been emphasized. The economic viewpoint plays a basic role as well. Therefore, the industrial

acceptability to replace the well known technologies with the AI-based modern ones is still limited.

5.2.4 Proposed AI tools employment outline

The aforementioned analysis of the AI application realization may characterize the AI tools with a false impression about their abilities and efficacy. These tools have, however, great capabilities and superior performances as compared with other conventional ones. The optimal employment of AI tools can be practically realized with dedicating these tools for those tasks that have no or inefficient conventional solutions. It is more preferable and convenient to employ these tools to improve the performance of the existing conventional methods rather than to replace them completely. Then, AI is proposed here to enhance the resultant overall fault location accuracy. This is achieved by adapting the presented modal transformation-based fault location algorithm by compensating the total resulting estimation error. This collaboration between the mathematical fault location algorithm and the intelligent adaptation is expected to present a superior performance eliminating all expected fault location estimation errors. The required performance adaptation is carried out by training the constructed intelligent networks properly via well prepared input-output pairs from a proper simulation tool. This can be accomplished by either ANN or FL networks; in which the most suitable tool should be realized. Both AI tools are briefly reviewed in the following two sections, whereas the proposed fault location adaptation is covered in the next chapters.

5.3 ANN Basics

5.3.1 ANN basic structure

A neural network is a collection of neurons (or simply nodes) that are connected in a certain configuration to allow the communication among these nodes. Each node receives the weighted sum of the received signals coming from either the general inputs to the network or from other nodes and propagates the weighted outputs to other nodes as shown in Fig. 5.2. The node core simply consists of two parts. Firstly, the weighted inputs to the node are integrated with a summing function. Then, the resulting sum is aggregated with a dedicated activation function resulting in the output of the node. Many activation functions are available. The most common ones include the linear, the step change, the ramp, the sigmoid function and the Gaussian

functions. These non-linear functions can introduce the non-linearity in the network dynamics by bounding the output values in a fixed range.

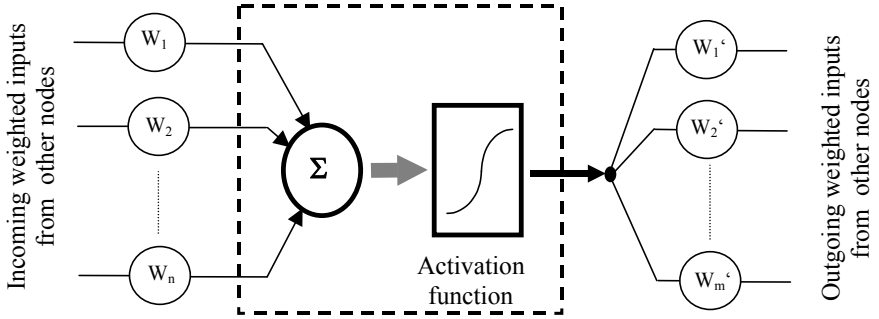

Fig. 5.2 A single node basic construction

The node output is transmitted to other nodes through the pre-defined selected weights. These weights are basically determined via the training process depending on sufficient collected training patterns with regard to the considered task [66]. The ANN nodes can be connected in different ways according to the selected ANN architecture. Each of them is described with certain characteristics. It is consequently applicable for certain applications. One of the most common ANN structures is realized by adjusting the nodes into sequential layers. Each layer includes a certain number of nodes. The first layer is the input layer and it is usually a passive one corroborating no further processing. It just distributes the inputs to the next layer. The last layer is the output one containing sufficient nodes according to the aimed outputs for the considered application. The hidden layers are inserted between both input and output ones containing a sufficient number of hidden nodes. Practically one or two hidden layers are sufficient for almost all applications. The wiring of connectivity and its direction among the different layers detect the type of the network and refer consequently to the suitable training paradigm. Among the available network architectures; MLF, Radial Basis Functions (RBF) and Elman networks arise as examples of the most known and common ANN architectures. MLF network is the most common type with its easy development, efficient training and direct implementation. For MLF networks, the signals are distributed from the input layers towards the outputs in one direction. Thus, it does not exhibit any memory actions or network dynamics. It is, therefore, more popular and considered a basic platform for the majority of applications using ANNs.

RBF network can be considered as a special feedforward network utilizing basis functions in its hidden layer rather than using the sigmoid activation as in normal MLF networks. Each of these

hidden neurons has a symmetrical response around its selected center vector. Each of the output nodes accumulates the weighted sum of all hidden neurons. Thus, the hidden neurons just map nonlinearly the inputs from the input space into a new space with a fixed parameter transformation. The output layer combines linearly the content in this new space, where the weights connecting both layers are adjusted through the training process using the Least Square optimization. This simple topological structure and fast training paradigm provide a powerful tool for various applications including function approximation and classification purposes [80, 81].

Recurrent networks, on the other hand, employ one or more feedback from a certain layer to the foregoing one(s). Unlike the normal MLF networks, recurrent ones can distinguish the temporal patterns due to the memory action of the context inputs. A popular example for this category is the Elman network. The special feature of this network is that one or more feedbacks are extracted from the hidden neurons and fed to the input layers "Context Units" [82, 83]. Fig. 5.3 shows simplified graphs of the these ANN types, whereas the training of these networks is considered in the next subsection.

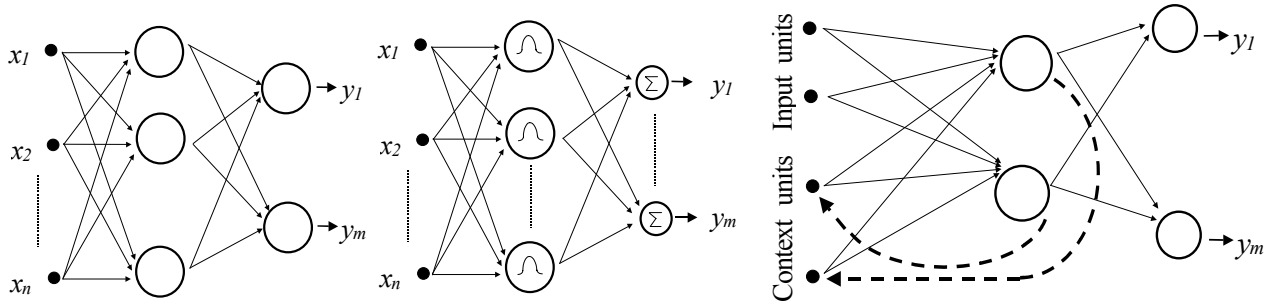

a) (b) (c)

Fig. 5.3 Selected ANN architectures
(a) MLF-network (b) RBF-network (c) Elman network

5.3.2 ANN designing

a) Feature extraction

The aim of this step is to find out the more relevant variables that can be nominated as the selected inputs to the desired network. Those variables should have a distinguishable configuration for the required task along the entire range of the dimensional space so that they can help to perform the required convergence through training. This set of inputs should be

selected carefully in order realize the minimum sufficient number of inputs, since these redundant inputs may burden the optimization procedure resulting in a weak or non-stable ANN. Also, the outputs are selected according to the required task and its aimed decisions.

b) ANN primary construction

The preliminary configuration of the aimed ANN is arbitrary initiated with a pre-defined set of inputs and outputs. The characteristics of each ANN type and the essence of the regarded problem may help to realize the optimum network type. However, the most critical problem in constructing the ANN is to choose the number of hidden neurons. Using too few hidden neurons may prevent the training process to converge, while using too many hidden neurons may extend the training time and cause overfitting. Thus, it is convenient to start the training with a small set of hidden units. The number of hidden neurons can be slightly increased and the network is retrained. This process is repeated until the lowest acceptable training error is reached.

c) Data preparation and training process

Training the ANN can be generally described as a certain mathematical optimization process that serves to find out the optimum set of network parameters that can represent the required task. Different training paradigms are available according to the selected ANN type. In order to perform this stage a sufficient amount of training cases should be collected covering the entire range of the dimensional space of the required task. The majority of ANN-based applications use the supervised training methods, in which the outputs of the collected training patterns are employed to regulate the conversion through the training process. The “Delta Rule” was introduced in 1960 as the first practical attempt for training the ANN Perceptron (simple ANN structure without hidden layers). However the Perceptron has limited capabilities dealing only with those linearly separable problems. In 1986, the Backprobagation (BP) training was introduced for MLF networks. This algorithm is nominated as the first practical and most common training method for separable or non-separable applications [84, 85].

The basic BP training algorithm was then enhanced with different mathematical improvements. Firstly, the momentum term was added during the convergence process. The momentum allows to perturb the weight changes resulting from the normal BP calculations to avoid falling into a local minimum. Also, considering adaptive learning rates can accelerate the training process. Other figures of training paradigms were developed as well depending on different mathematical criteria such as the Conjugate Gradient (CG) and the Levenberg Marquardt (LM).

Both algorithms employed the numerical optimization techniques in order to optimize the initial set of network parameters. Elman network, as a special MLF network, can be trained similarly with aforementioned training paradigms. For RBF networks, the Orthogonal Least Square (OLS) learning was employed in order to get a compact network structure. MATLAB software represents the basic platform to perform the training procedure [86]. Appendix D presents a brief description of these training paradigms.

d) Testing of the trained ANN

The final step in the design process is to evaluate the resulting networks thoroughly via a well prepared group of test cases. These test cases should differ from those used cases in the training stage. Also the test cases should cover all circumstances that may affect the system performance covering the entire range of the dimensional space.

5.4 FL System Fundamentals

FL can efficiently formalize all those problems that can be described by subjective knowledge. These types of knowledge are represented by linguistic information that is usually impossible to be described using conventional mathematics. In conventional mathematics, the subjective knowledge is usually disregarded at the front end of the design processes depending normally on the objective knowledge using ordinary mathematical formulas. Thus, it is quite right to expect that utilizing both knowledge types through the designing procedures will present an optimal tool dealing with all complicated and unsolved problems. This integration between both types of knowledge can be directly performed with FL systems [87]. FL systems can be generally defined as non-linear systems capable of inferring complex non-linear relationships between certain input and output variables. Over the conventional methods, FL is characterized with several advantages:

- FL is based on the natural language using the same basis that is used for human communications. It is, therefore, more conceptual and easy to be understood.
- FL has simple mathematical concepts and clear construction. It is highly flexible and suitable to all kinds of applications.
- FL is tolerant of imprecise data and able to handle ambiguity.

- FL systems are built based on the experience, in which the experts translate it into understood simple rules and memberships.
- FL is flexible and hence its applications can be implemented into real systems easily.

Thus, it can be considered as an ideal candidate for non-linear mapping and modeling purposes covering a wide variety of applications.

5.4.1 FL system construction

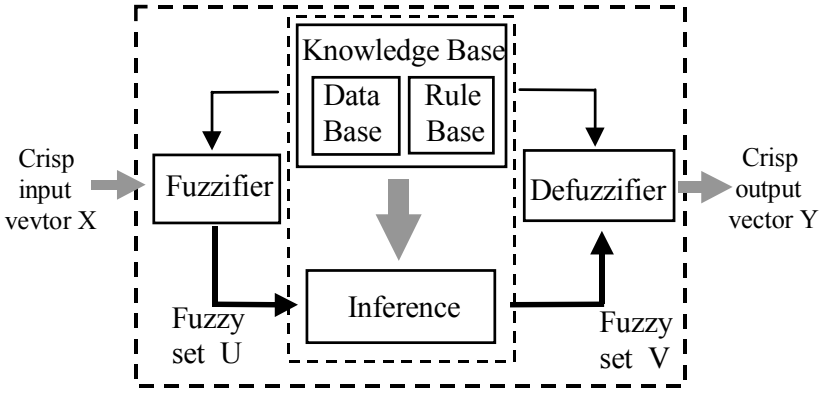

Fig. 5.4 FLS schematic diagram

Fig. 5.4 shows a general scheme of a FL system. The constructed FL system maps the crisp input vector X into the crisp output vector Y. The Fuzzifier maps the crisp input vector X into the fuzzy input space U. The Knowledge Base contains all network parameters and the set of properly defined meaningful linguistic IF-THEN rules. All fuzzified inputs are then inferred to produce the considered nonlinear mapping from the input space $U = U_1 \times U_2 ..... \times U_n$ to the output space V. Finally the Defuzzifier maps the fuzzy outputs from the output space V produced by the inference stage into the crisp output vector Y.

Unlike crisp values, being fuzzy means that there is no definite boundary distinguishing between the end of one value and the start of another one. The mapping from this crisp value into its fuzzy value is represented by a fuzzy membership function. A membership function exists for each linguistic variable, in which the degree of this membership is a measure of the strength of association that a measured value has with some linguistic value. Fig. 5.5 illustrates this concept for an example crisp value x_1. The corresponding fuzzy value of x_1 can be described belonging to either the linguistic value A or B. The notation $\mu_A(x_1)$ is used to denote the belonging degree

of the value x_1 to the linguistic value A. Similarly, the notation $\mu_B(x_1)$ is used to denote the belonging degree of the value x_1 to the linguistic value B. The different values of memberships for the same crisp point enable to be inferred through different rules during the inference process. This wide range of inference applicability points out the richness of FL obviously by providing enormous numbers of possibilities and consequently leads to a flexible and efficient mapping. There are different shapes of membership functions, where the most common ones are the triangular, trapezoidal, piecewise linear, Gaussian distribution, sigmoid and bill membership function shapes.

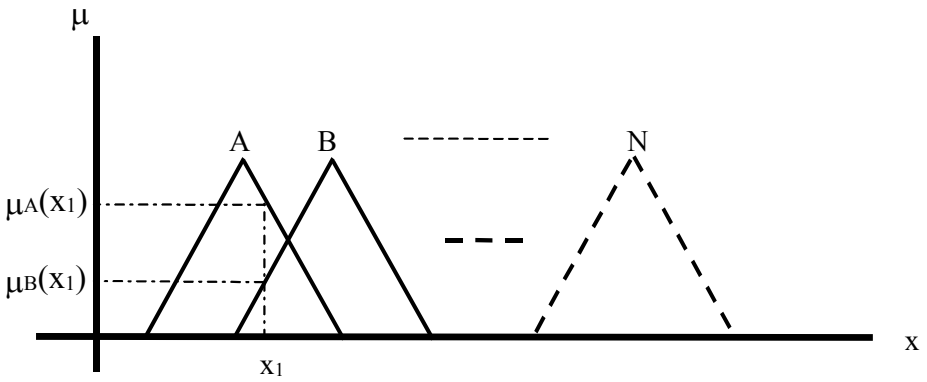

Fig. 5.5 Illustration of fuzzy membership function notation

The Knowledge Base is the basic core of a FL system containing the collected rules in the Rule Base as well as the total set of the numerical characteristics and boundaries and in the data base. These rules are obtained either from sufficient simulations or from familiar experts with the considered problem. Collecting these rules should be performed carefully in order to realize the aimed performance for the considered task. For a set of fuzzy inputs (u_1, u_2, ...u_n) and a set of fuzzy outputs (v_1, v_2, ...v_m), the k^{th} rule can be described as,

$$\text{IF } u_1 \text{ is } f_1^k \,\&\, u_2 \text{ is } f_2^k \,....\, \&\, u_n \text{ is } f_n^k \text{ THEN } v_1 \text{ is } g_1^k \,\&\, v_2 \text{ is } g_2^k \,....\, \&\, v_n \text{ is } g_m^k \qquad (5.1)$$

Where f_1^k, f_2^k, ... $f_n^k \subset U$ are the corresponding antecedent membership functions for the k^{th} rule inputs and g_1^k, g_2^k, ... $g_m^k \subset V$ are the corresponding consequent membership functions for the outputs for the same rule.

Each of the fuzzy inputs activates each rule in the Rule Base producing different outputs according to its own memberships. All these outputs are aggregated to produce the total output set. These linguistic fuzzy outputs are not suitable to be employed in the actual process domain

which normally deals with specific crisp data. Thus, the conversion of these fuzzy output quantities into their equivalent crisp forms is obligatory. This is achieved through the defuzzification stage. The basic function of the Defuzzifier is to map the fuzzy outputs from the resulted output space vector V from the inference stage into the crisp output vector Y. As reported in the literature, several deffuzification methods are available with different mathematical basis and different degrees of complexity. The most common methods for defuzzification include the Max-membership, the centroid method, the weighted average and the center of sums.

5.4.2 FL system design

Designing a FL system can be described as a process for approximating a non-linear function or fitting a complex surface in a properly high dimensional space [88]. This was achieved through a similar process to the ANN designing using the FL Toolbox in the MATLAB software as well. Firstly, the most suitable inputs should be selected. Then, the preliminary design of the FL network was adopted considering the arbitrary initial rules and membership functions. Finally, the related parameter of these networks should be optimized through a pre-prepared set of input-output pairs via a proper simulation. Building meaningful rules is an essential step in order to develop a successful fuzzy system. These rules are developed based on the available knowledge about the required task and its relation to the selected inputs. Thus, the importance of the successful selection of these input features among all of the available ones is obvious.

The set of inputs should be selected carefully in order to realize the minimum sufficient number of inputs. Extra or redundant inputs do not contribute significantly to the required process. Moreover, they can burden the later optimization procedure resulting in a weak or non-stable FL system. The initial configuration of the aimed FL system is arbitrary initiated and optimized later employing the selected training process. For each of the selected input variables, an arbitrary set of membership functions is adopted. Each of these sets is initialized with a grid of equally spaced overlapping memberships. All the available membership shapes in the MATLAB should be considered individually. Then, the training process realizes the optimum shape of membership functions for the required task. The corresponding set of rules is then constructed depending on the available experience as well as the variations of the selected inputs along the dimensional space. The initial design of the aimed FL system is optimized by off-line training in a supervised manner through different input-output training pairs covering all possible modes of operation.

5.4.3 Optimizing constructed FL systems with ANFIS

Different training paradigms can be employed using different methods such as Least Squares, GA-based or BP training. The training efficiency mainly depends on the characteristics of the training method, the amount of training data and the complexity of the required task. Among the different available methods for fuzzy logic system training, the Adaptive Network Fuzzy Inference System (ANFIS) routine arises as a direct and powerful tool [89, 90, 91]. It is, therefore, included in the fuzzy logic toolbox in MATLAB. However, it is characterized by a few limitations. The available version of ANFIS supports only first or zero order Sugeno-type fuzzy systems with multi-inputs and one output network. In Sugeno-based fuzzy systems all inputs are described by a set of selected overlapping membership functions, while the outputs are described as a linear function of the inputs.

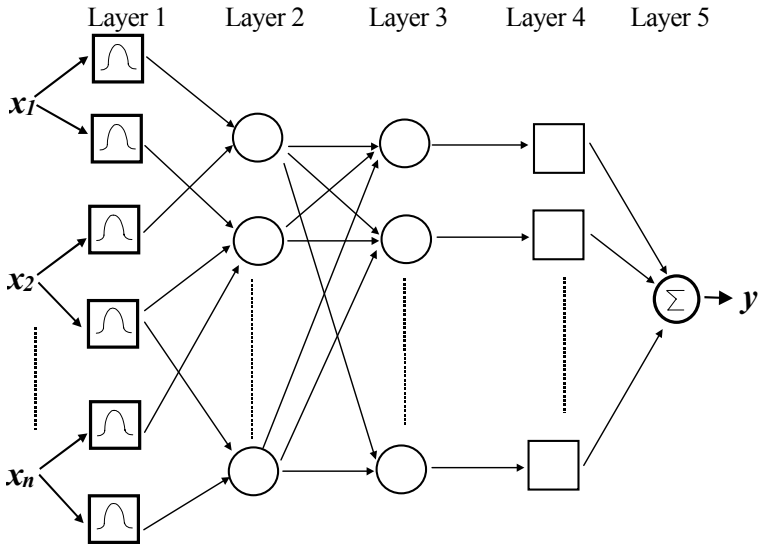

Fig. 5.6 ANFIS network structure

As shown in Fig. 5.6, the ANFIS model of a fuzzy system has a special five layers feedforward architecture with n-inputs (x_1, x_2, ...x_n) and one output y. The first layer represents the selected memberships for each input, whereas the next three layers represent the relations between the network inputs and the required output via the constructed fuzzy rules. The network can be trained similarly to ANN training. This is accomplished in MATLAB by either a Back-propagation algorithm, or a combination of both Least Square and Back-propagation algorithms (Hybrid learning). Hybrid learning updates the consequent parameters in the forward path using the Least Squares optimization and updates the antecedent parameters in the backward path with the gradient-based method. This combination of both learning methods converges much faster,

since it reduces the searching space of the original back-propagation method. Further details of the ANFIS training algorithm for FL systems are introduced in Appendix E.

6 AI-Based Fault Location Tuning

As explained in the last chapter, it is more beneficial to employ the AI tools in such a way that they support the existing schemes rather than to replace them. This chapter describes a new method to employ these tools in order to compensate the resultant total error in the fault location estimation process basing on the normal measurements at the locator position. Both ANN and FL based schemes are examined to realize the most suitable tool. Later, the full tuning scheme will be described in the next chapter.

6.1 Proposed Tuning Function Definition

Fig. 6.1 simply explains the elementary operation of the proposed tuning process. The essential aim of the proposed tuner is to compensate the resulting total error of the basic protection function in order to realize the aimed accurate performance. This is accomplished into two steps. Firstly, the tuning calculation stage is employed to map the relation between the total error and the basic protection function behavior in order to generate the required proper compensation manner. This step should be realized regarding the own characteristics of the protection function and its operation circumstances depending only on the available information at the relaying scheme location. Then, the resulting tuning action is simultaneously integrated with the basic protection function output in the processing stage in order to produce the final tuning decision. This decision can be finally employed either for adapting off-line those supplementary protection functions such as fault location or for adapting on-line the basic protection function itself.

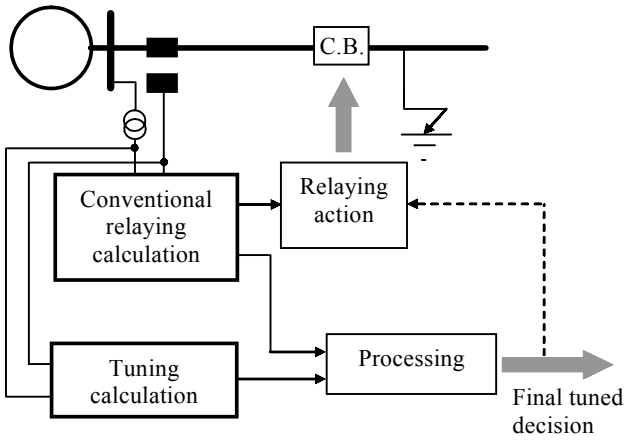

Fig. 6.1 Tuning Concept explanation

Theoretically, the basic protection function should be formalized carefully so that it is characterized with sufficient accuracy. This is, however, changed remarkably during the practical operation in the real field producing a significant deviation from the desired behavior. Different factors lead to these situations including the considered simplification assumptions, the inaccuracies of the system data and the existence of uncertainties. Thus, mapping the relation between the resulting estimation error and the performance of the basic protection functions is more complex to be directly handled by normal mathematical formalization. Hence, the need for advanced tools such as AI ones is clear.

6.2 Intelligent Location Tuning Formalization

As revealed before in Chapter 4, the modal transformation-based fault location algorithm was generally characterized with an accepted performance. The algorithm eliminates perfectly the mutual coupling effects providing an accurate tool for both single and multi-circuit lines. However, the algorithm accuracy is significantly influenced by those fault cases that are involved with the existence of higher fault resistance values. An extra tuning routine is, therefore, required to integrate with the proposed fault location algorithm providing a precise fault location scheme for all possible fault types. Fig. 6.2 shows a general schematic of the proposed overall fault location scheme. The Intelligent Location Tuner, ILT, is generally employed to find out the required correction factor C_f to compensate the accumulated errors in the estimated fault distance L_E from the modal transformation-based fault location algorithm. Then, the final fault distance L_F can be found as,

$$L_F = C_f * L_E \tag{6.1}$$

As shown in Fig. 6.2 the overall scheme is comprised of two basic phases. In the first phase, the basic fault distance L_E is estimated using the modal transformation-based fault location algorithm. The algorithm details were previously covered in Chapter 4. In the second phase, the ILT is employed to generate the required correction factor C_f. Finally the outputs of both phases are aggregated according to Equation (6.1) to find out the final estimated fault distance L_F.

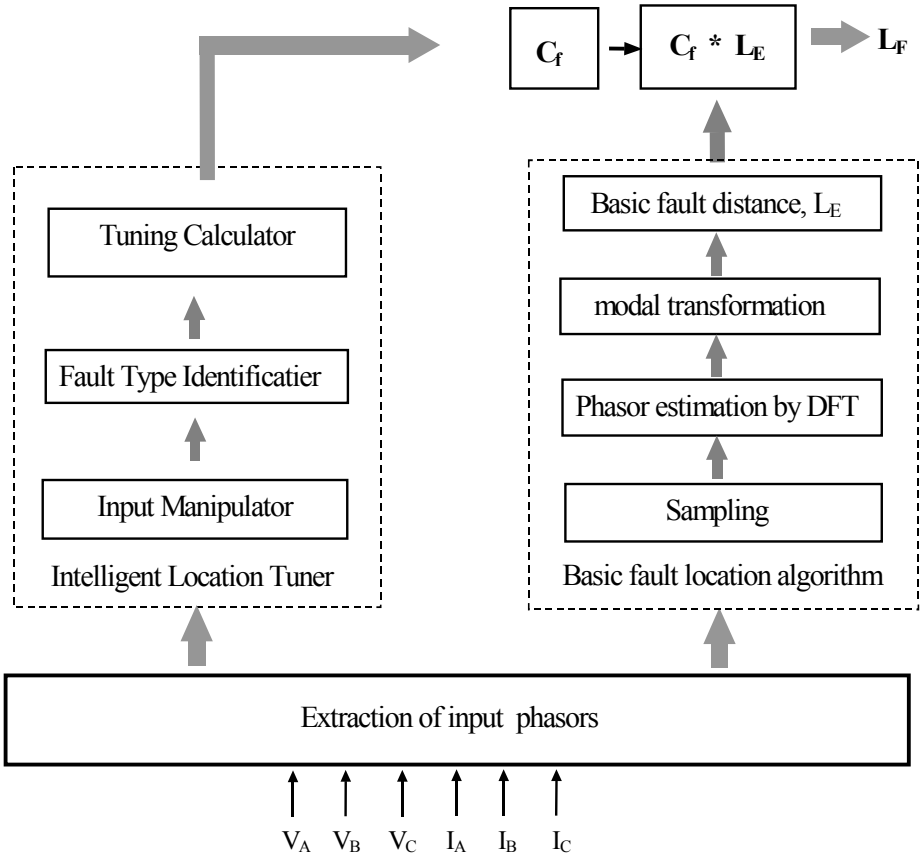

Fig. 6.2 Schematic diagram of the proposed overall location scheme

The ILT should depend on the normal available information at the locator position including the three phase voltages and currents. These quantities are processed through the Input Manipulator (IM) in order to prepare the required input features that are suitable for the tuning process. According to the occurring fault type (single phase or double phase to ground fault) as well as the associated faulty phases, the Fault Type Identifier (FTI) feeds the prepared input features to the Tuning Calculator (TC) in which the corresponding correction factor is finally produced.

Both FL and ANN tools were examined to perform the required tuning. Then, the performances of both intelligent tools were comparatively evaluated in order to find out the most suitable AI tool for the tuning purpose. Since the basic aim of this part of the work is to assess the tuning abilities for improving the fault location process, it is quite sufficient in this stage to consider

only the case of single phase to ground faults on phase A. Then, the tuning function will be expanded to cover all fault types and all operation conditions later.

6.3 ILT Development

According to the designing steps of FL and ANN systems described in Chapter 5, both ANN-based and adopted FL-based tuners were designed. The designed procedure will be described below.

6.3.1 Input features selection

The aim of this step is to find out the more relevant inputs that have a distinguishable configuration for the required task along with the entire range of the dimensional space. This effectively reduces the selected input features depending on the most useful information. It reduces the network structure, which consequently enhance the training efficacy. In order to accomplish this step efficiently the available information at the locator location should be checked along the entire range of the line length and the selected fault resistance. For this goal, many checks including the spectral contents of the three phase voltages and currents have been evaluated using either the DFT-based or modal-based phasor quantities. It has been concluded that all the available phasor contents do not have the capability to perform the mapping task distinguishably due to the wide considered range for the fault resistance (up to 1 kΩ). Different tests were applied in order to deduce further quantities combining one or more phasors from the available information at the locator location. For the phase A to ground fault, the following conclusions have been got:

- The direct seen impedance for the first modal quantity at the locator location (calculated as a percentage of the first modal voltage to the first modal current) increases proportionally as the fault distance increases.

- The direct seen impedance for the second modal quantity at the locator location (calculated as a percentage of the second modal voltage to the second modal current) increases proportionally as the fault resistance increases.

- The percentage of the second modal voltage to the first modal voltage increases proportionally as the fault distance or the fault resistance increases.

The three quantities are shown in Fig. 6.3 depending on the fault position and the added fault resistance. The distinguishable manner of these quantities benefits the training convergence of both ANN and FL to realize the optimum configuration. Therefore, they can be effectively employed for the required mapping task considering these three quantities as the input vector to the ILT.

6.3.2 Data preparation

Both FL-based and ANN-based algorithms share the same training and testing data sets. For each training data case, the required inputs (prepared in their selected form) and the desired output (the pre-calculated correction factor) were prepared. The correction factor was assigned for each test case as the percentage of the actual fault distance to the calculated fault distance resulting from the conventional algorithm. Then, the whole training and testing files were created. In order to develop these cases, the ATP-EMTP electromagnetic transient simulation software was employed considering the selected 220 kV 200 km, double circuit double infeed line. The line parameters as well as the configuration of the line conductors are given in the appendix B.

Different 6 loading conditions were considered (0, 20, 40 ..... 100) % of the full load current. For each loading condition, a group of 483 fault cases were collected. These cases covered the entire range of the line length of (1, 5, 10, 15 ..... 100) %, as well as the selected range of the added fault resistance of (1, 5, 10, 50, 100, 150 ..... 1000)Ω. The upper limit of the fault resistance was selected to be adequate with the possible recorded fault resistance values as experimentally measured from the real field [24]. While the testing cases were adopted to differ from the used ones in the training stage.

6.3.3 ANN-based tuner design

The ANN Toolbox in the MATLAB software has been selected as a basic platform for developing, training and testing all required ANN-based tuner. In order to realize the optimal ANN tuner construction, different network structures and different training paradigms were considered for designing the ANN-based tuner. Three types of ANN structures were considered including the MLF, RBF and Elman networks. Then, the performance of each constructed ANN architecture was investigated through the collected test cases collaborating with the modal transformation-based fault location algorithm.

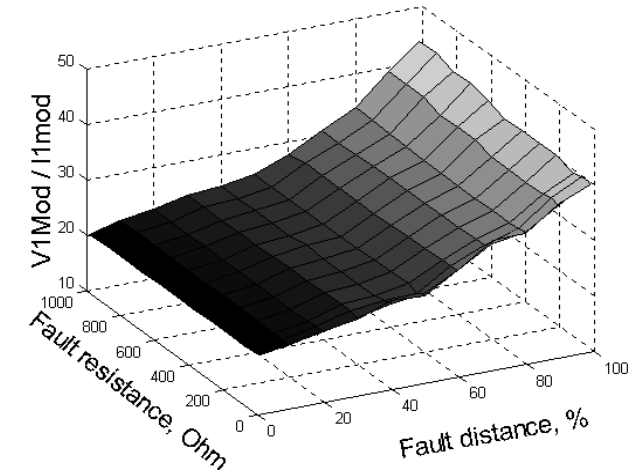

(a)

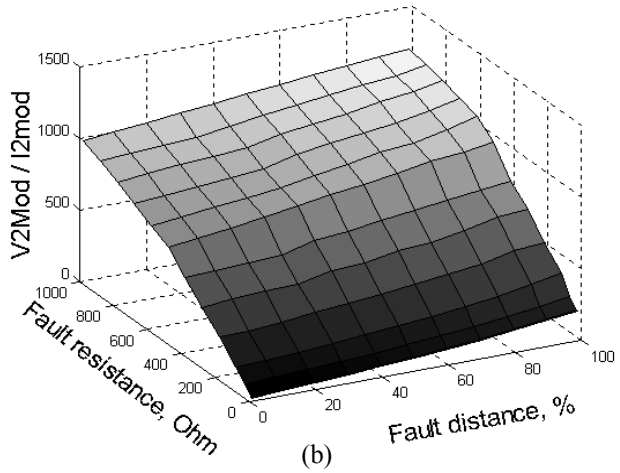

(b)

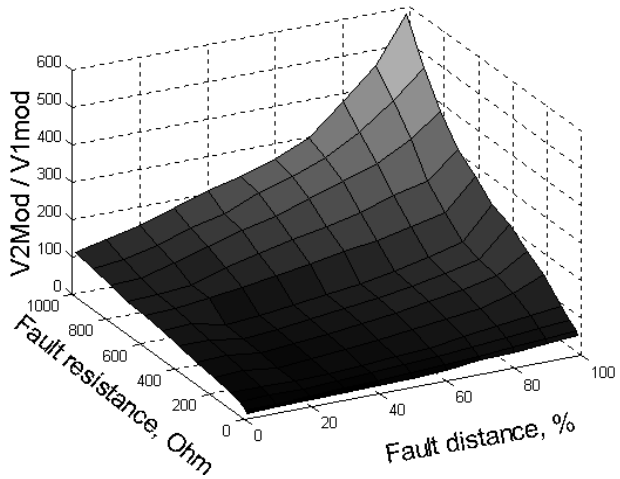

(c)

Fig. 6.3 Selected feature variable variation in dependence of fault distance and fault resistance
(a) First quantity (b) Second quantity (c) Third quantity

The training process has been carried out as described in the last chapter. For the MLF-based network, the gradient descent Backprobagation training with Momentum (BP&M), the BP training with adaptive learning rate (ABP), the Conjugate Gradient (CG) and the Levenberg Marquardt (LM) training algorithms were employed individually to perform the training. The RBF network was trained using the OLS training. The Elman network was trained through the same selected training algorithms for MLF networks. Each of the three different ANN types was trained with the same collected training data having three inputs and one output.

6.3.4 FL-based tuner design

The initial design of the FL system was constructed with two steps. First an arbitrary set of membership functions should be adopted for each of the three input variables. Each of these sets is initialized with a grid of equally spaced overlapped memberships. Different membership shapes are available in fuzzy logic Toolbox in MATALAB including (Triangular, Trapezoidal, Gaussian ...). These memberships were tested intensively to find out the optimal membership configuration. Then, the required set of rules in the Rule Base was prepared according to the variation of the selected inputs along the entire ranges of the fault distance and the added fault resistance. Finally, the initialized FL system was optimized through the training paradigm to find out the optimal FL system configuration. As concluded from the training process, five bell-shape memberships are sufficient for each of the three inputs to perform the required mapping efficiently.

6.4 Training Performance Evaluation

6.4.1 Simplified single loading training set

In this test phase, only the full-loading (483 cases) condition was considered. The training was implemented using the MATALB toolbox for both FL and ANN depending on a common CPU of 1.7 GHz Processor with 256 MB-RAM. The training performance is evaluated via three different factors: the final training error, the number of repeated epochs and the exhausted training time. MLF network was considered first using the selected four training algorithms. As the number of hidden neurons is arbitrary, the training process was repeated until the optimum number of hidden neurons was reached. It has been found that seven hidden neurons were sufficient to present the required convergence.

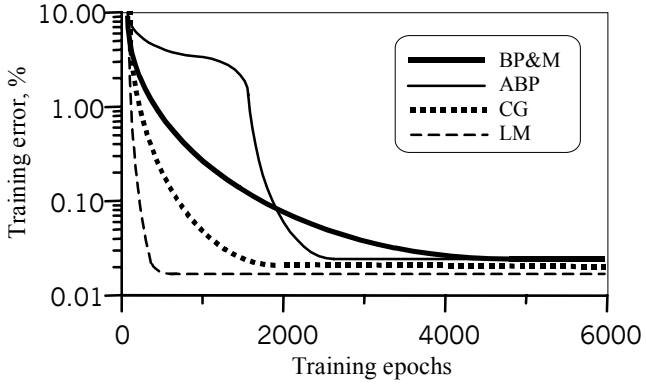

Fig. 6.4 Training convergence for MLF networks

Fig. 6.4 shows the convergence of the generalized training error for the selected algorithms against the number of training epochs for MLF tuner. The exhausted training time for each algorithm is listed in Table 6.1. The results show that the LM algorithm reached a better convergence (0.0185 %) through 500 epochs in 3.5 Minutes.

Table 6.1 MLF network training times

Training algorithm	BP&M	ABP	CG	LM
Training time (Min.)	18.0	10.5	6.0	3.5

Surprisingly, the training of the tuner considering RBF network reached an error of 1.8% with 112 hidden neurons during 42 Minutes. This is mainly due to the considerable large training set so that the required centers and consequently the associated hidden neurons are extensively large. On the other hand, the main advantage of the RBF network is the ability to perform the required approximation through a reduced training set. Thus, the constructed training set is reduced by enlarging the adopted step size in fault location as well as the added fault resistance covering the entire range of the selected space. 75, 50, 25 % reduced training sets were prepared and the corresponding trained respectively. The resulted training for these networks is presented in Table 6.2 showing the training error, exhausted time, repeated epochs and the adopted number of hidden neurons.

Table 6.2 Variable training set for RBF networks

Training set reduction (%)	**No. of h. units**	**Training time (Min)**	**Training epochs**	**Training error (%)**
100 %	112	42.0	500	1.8
75 %	86	23.0	324	0.82
50 %	64	7.0	180	0.24
25 %	38	2.5	68	0.017

The results reveal that the required training time was enormously decreased by reducing the collected training set.

TABLE 6.3 Elman network training times

Training algorithm	BP&M	ABP	CG	LM
Training error (%)	0.0221	0.0211	0.0192	0.0181
Training (epochs)	2200	1440	600	240
Training time (Min)	14.0	7.0	4.0	2.0

The Elman network, as a special MLF network with an extra feedback path from the hidden layer, was trained similarly through the selected four training algorithms. Table 6.3 shows its training results. The LM training converged to an error of 0.0181% within only 2 minutes. Thus, the influence of the feedback loop for accelerating the training is revealed.

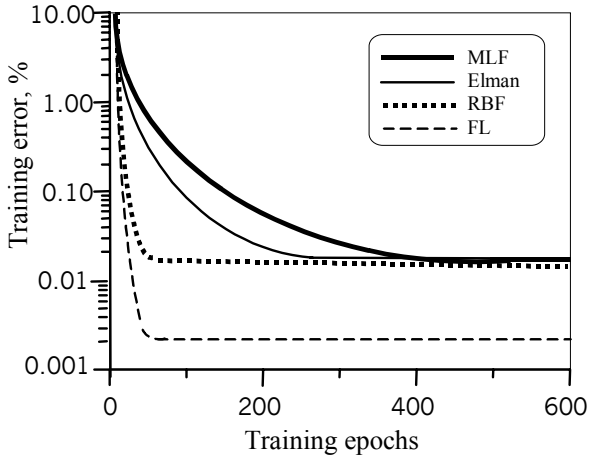

Fig 6.5 Comparison of FL and ANN training

Finally, the FL-based tuner was trained via ANFIS in the MATLAB environment through the same training set. The training converged to 0.002% in 2.5 minutes through only 50 epochs. Fig. 6.5 shows the convergence profile of the ANFIS training as compared with the convergence of LM algorithm for both MLF and Elman networks in addition to RBF network with 25% reduced training set.

6.4.2 Expanded multi-loading training set

The collected training data set was extended covering (0, 20, 40 ..... 100) % of the full-load with 483 training cases for each load. Then, the adopted intelligent tuners were constructed and trained again through the new training data. The input vector contains the aforementioned three

inputs in addition to the Load Correction Factor (LCF) for both FL and ANN tuners. LCF describes the loading condition of the system just prior to the fault inception. It can be calculated as the percentage of the actual load current I_L to the nominal load current I_N as

$$LCF = \frac{I_L}{I_N} \tag{6.2}$$

Table 6.4 Multi-loading testing evaluation

Adopted ILT	Training algorithm	Training error (%)	Training time (min)	Training epochs
MLF-network	BP&M	0.037	108	5000
	ABP	0.034	62	2700
	CG	0.03	34	1800
	LM	0.026	31.5	650
RBF-network (25% training set)	OLS	0.019	27	84
Elman-network	BP&M	0.036	86.5	2650
	ABP	0.032	54.5	1800
	CG	0.028	33.5	1100
	LM	0.024	24	320
FL-network	ANFIS	0.0058	17.5	60

Table 6.4 summarizes the performances for all adopted tuners considering the multi-loading training condition. All AI-based tuners have significantly increased convergence errors. This is mainly due to the extra complexity of the associated dimensional space of the different loading conditions. For the RBF network, only a 25% reduced training set is only considered since the full training set including all loading conditions is impractical due to the huge required number of hidden neurons. As seen from the results, the FL tuner still has a better convergence (a convergence error of 0.0058 %) than other ANN tuners. This reveals the effectiveness of FL system for function approximation purposes.

6.5 Fault Location Accuracy Evaluation

The second viewpoint is to evaluate the developed ILTs from the protection function

prospective. The accuracy of each tuner type was found out for both single and multi-loading cases in order to evaluate the overall performance of the developed tuners. Fig. 6.6(a) and (b) show the overall accuracy of the FL-based tuner as compared with MLF and Elman ANN-based tuners using the selected four training algorithms. On the other hand, the RBF network failed to provide a comparable accuracy as compared with FL or other ANN tuners. Thus, it was excluded from the shown results.

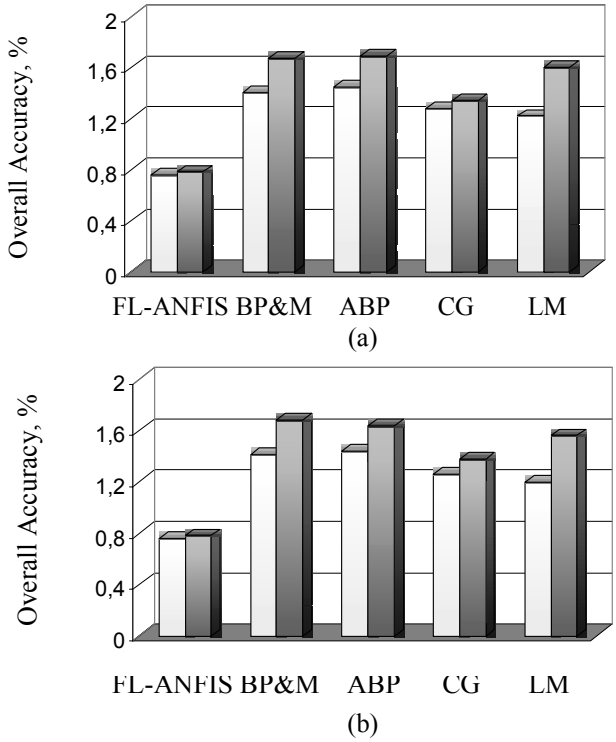

Fig. 6.6 FL-tuner accuracy as compared with ANN tuner accuracy

6.6 Concluding Remarks

FL and ANN are considered as powerful tools for nonlinear mapping and function approximation. Inspite of the systematic design and training of ANN, they suffer from non-explanatory structure and limited applicability. On the other hand, FL systems are characterized by the ease of explanation with understood rules. Also, the ability to deal with a natural language, tolerance of imprecise data and ambiguity data is another advantage. Moreover, adding the training feature supports FL as an ideal AI tool. Generally speaking, FL-based tuner has a faster training and a better accuracy. However, the major problem arises when designing FL-based systems with ANFIS modeling concerning the network stability. This mainly resulted

from the complicated structure of the adopted ANN for ANFIS model (five layers network). Thus, increasing either the selected number of inputs or the adopted memberships for each input may significantly affect the resulting stability of the overall network. This requires using the most suitable inputs in addition to the minimum requirement of the adopted memberships. Also, increasing the collected training data remarkably helps to keep a sufficient stability. Finally, the deep investigations during the testing phase help to compromise between both the accuracy and the stability definitions. In spite of the usually fast training ability of RBF networks, those heavily nonlinear problems that need larger training sets may be a challenge for these networks. MLF ANN may present a better candidate for those cases. Also, there is no further advance in performance with employing Elman network over the normal feedforward networks for this specific application. The superiority of recurrent networks such as Elman ones is, however, expected for other applications that are more sensitive with time such as fast transient-based equipment or control devices.

7 FL-Based Overall Fault Location Tuner With Universal Characteristics

In the last chapter, both FL and ANN tools were extensively examined in order to compensate the errors that affect the performance of the fault location calculation. The presented results revealed that FL has much distinctive capabilities for mapping the resulting estimation error as a function of the available information at the locator position. Moreover, FL shows a better performance regarding complex mapping tasks such as incorporating multi-loading training conditions. This chapter introduces a further step of realizing a practical FL tuner with universal characteristics. This is achieved by extending the capabilities of the developed simple FL tuner to fit a wide variety of system parameters and operating conditions.

7.1 Concept of Universality and FL-Tuning

The development of practical AI-based systems in power system purposes is extremely limited, in spite of the huge amount of the proposed intelligent applications in the literatures. This is mainly due to the lack of the universality essence resulting from developing these schemes for definite system parameters in certain situations. As known, each power system has its own characteristics such as power and voltage ratings, line length and operating conditions. For those schemes basing on FL or ANNs, the constructed networks are usually adapted for certain system parameters and configuration. Thus, the coverage of the resulting AI schemes for all systems and operating conditions is doubtful. Moreover, incorporating all these conditions in the training sets is quite impossible. However, the conventional schemes are generally characterized by a universal performance depending on their general operation theories. These schemes can be,

therefore, adapted to work normally with all system configurations by modifying the setting parameters only. This discourages the industry to accept the AI solutions as a practical solution for their problems. Hence, developing a practical and trustful AI product is considered a basic challenge.

In order to improve the FL-based tuning scheme for realizing the aimed universal behavior, the following sequential steps should be incorporated during the designing process of the aimed intelligent scheme:

- The set of the input features should be carefully selected so that they vary along the defined dimensional space independently of the varying arguments such as the system parameters and the operating conditions. This can be carried out by investigating the behavior of the available information at the locator position to find out the most suitable ones.
- The FL-system core, including the adopted rules in the Rule Base and their describing data in the Data Base, should be designed to suit all system configuration possibilities.
- Finally, the overall scheme should be evaluated extensively by simulation tests to investigate its universality.

7.2 Overall FL Tuner Outline

The Overall FL Tuner, OFLT, is given in Fig. 7.1 as an extension of the same developed ILT in the last chapter. The proceeding is comprised of two basic parts. The basic fault distance L_E is first estimated using the basic fault location algorithm. Then, the OFLT is employed to adapt the basic fault distance based on the available single end data. As the basic fault location algorithm is characterized by a high accuracy during phase faults, the OFLT is utilized for ground faults only. The performance of the overall fault location scheme is consequently improved covering all fault situations effectively. The required tuning is performed by finding the required correction factor C_f, in which the final fault distance L_F can be found according to Equation 6.1. The OFLT is generally characterized by two extra features over the foregoing basic one. Firstly, six different parallel fuzzy networks are adopted. Each FL network is dedicated for a certain fault type on certain phase(s). The first three networks are for single line to ground faults including A-G, B-G and C-G faults respectively. The other three networks are for A-B, A-C and B-C to ground faults. Also the Load Correction Factor, LCF, is introduced here to adapt the

approach reaction according to the line loading condition just before the fault inception. This finally results in a practical tuning scheme dealing with all fault types and all loading conditions.

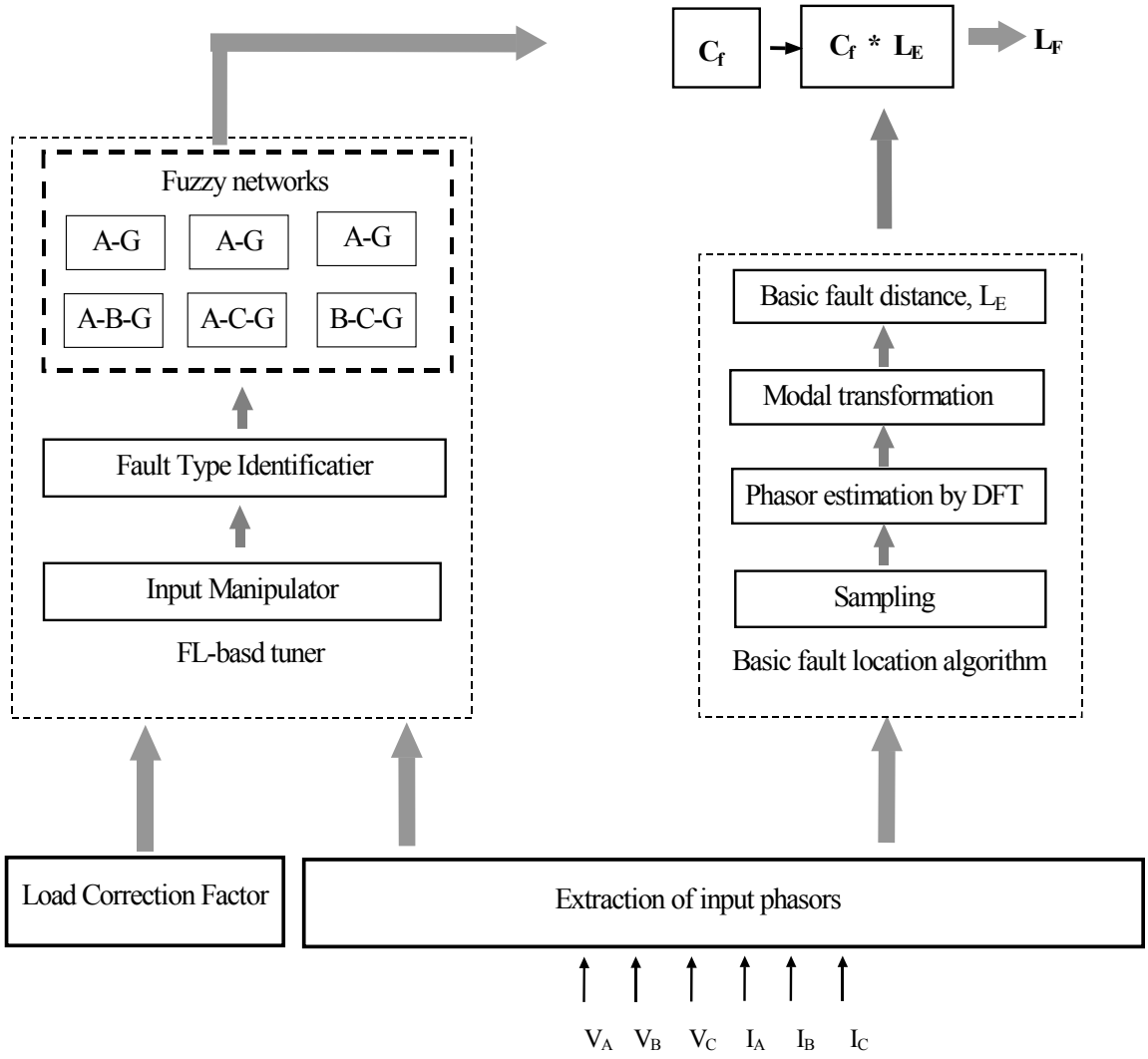

Fig. 7.1 Schematic diagram of the proposed locator

7.3 OFLT Development

7.3.1 Selection of input features

The basic aim of this step was extensively described in Sec. 6.3.1. In the last chapter, the selected features were realized owing to their distinguishable behavior along the defined dimensional space only. This is, however, not sufficient. The more distinguishable and universal features should be realized. For this purpose, the performance of all possible distinguishable quantities at the locator position was investigated to select those with a universal

manner along the dimensional space. A universal manner means that the behavior of these quantities is still acceptable during the applied changes to the system parameters and operating conditions. A line to ground fault on phase A is considered for explanation, where other ground faults (other phases or double line to ground faults) are considered similarly.

In order to facilitate the universal behavior, all used modal voltage and current quantities are normalized by their corresponding rated values. This strongly supports to introduce general characteristics rather than specific ones for a certain configuration. Then, the deduced quantities were tested by varying the operating parameters including the rated voltage, transferred power and line length. For this purpose, a test set of fault cases was prepared covering the entire length of the line and the selected ranges of fault resistance. Three different rated voltages (110, 220 and 380 kV), two different values of transferred power (single and double circuit line) and three different line lengths (100, 200 and 300 km) were covered considering Al/St 185/30 conductors. The configurations of these transmission systems are given in the appendix B. Among these quantities, four quantities were found suitably to perform the required mapping task with an acceptable universal behavior as shown in Fig. 7.2. The variation of both first and second modal voltages to their relevant modal currents proportionally increases with the fault distance and fault resistance as shown in Fig. 7.2(a) and (b) respectively. Also, the multiplication of both modal voltages to their relevant modal currents decreases proportionally with the variation of fault distance and fault resistance as shown in Fig. 7.2(c) and (d).

Fig. 7.3 investigates the behavior of the first input quantity for different conditions in order to illustrate the scheme universality. The normalized first quantity has a universal characteristic against the fault resistance for a fault at 50% of the line for the three selected voltage levels as shown in Fig. 7.3(a). The same result is shown in Fig. 7.3(b) for the same quantity varying the fault point with a fixed fault resistance of 800Ω. Fig. 7.3(c), (d) , (e) and (f) show the same results considering the variation of transferred power (considering single and double circuit lines) and line length (100, 200 and 300 km) respectively. Thus, the validity of the same quantities for all selected configurations is obvious. Similar results were obtained for the other input quantities well revealing the universal behavior of all selected inputs. Based on the distinguishable configuration of these quantities, the required set of rules can be accurately developed. Different tests were applied for other ground faults on other phases. From these tests, it can be concluded that the selected four inputs are suitable for these faults as well. All the adopted six fuzzy networks share, therefore, the same selected features.

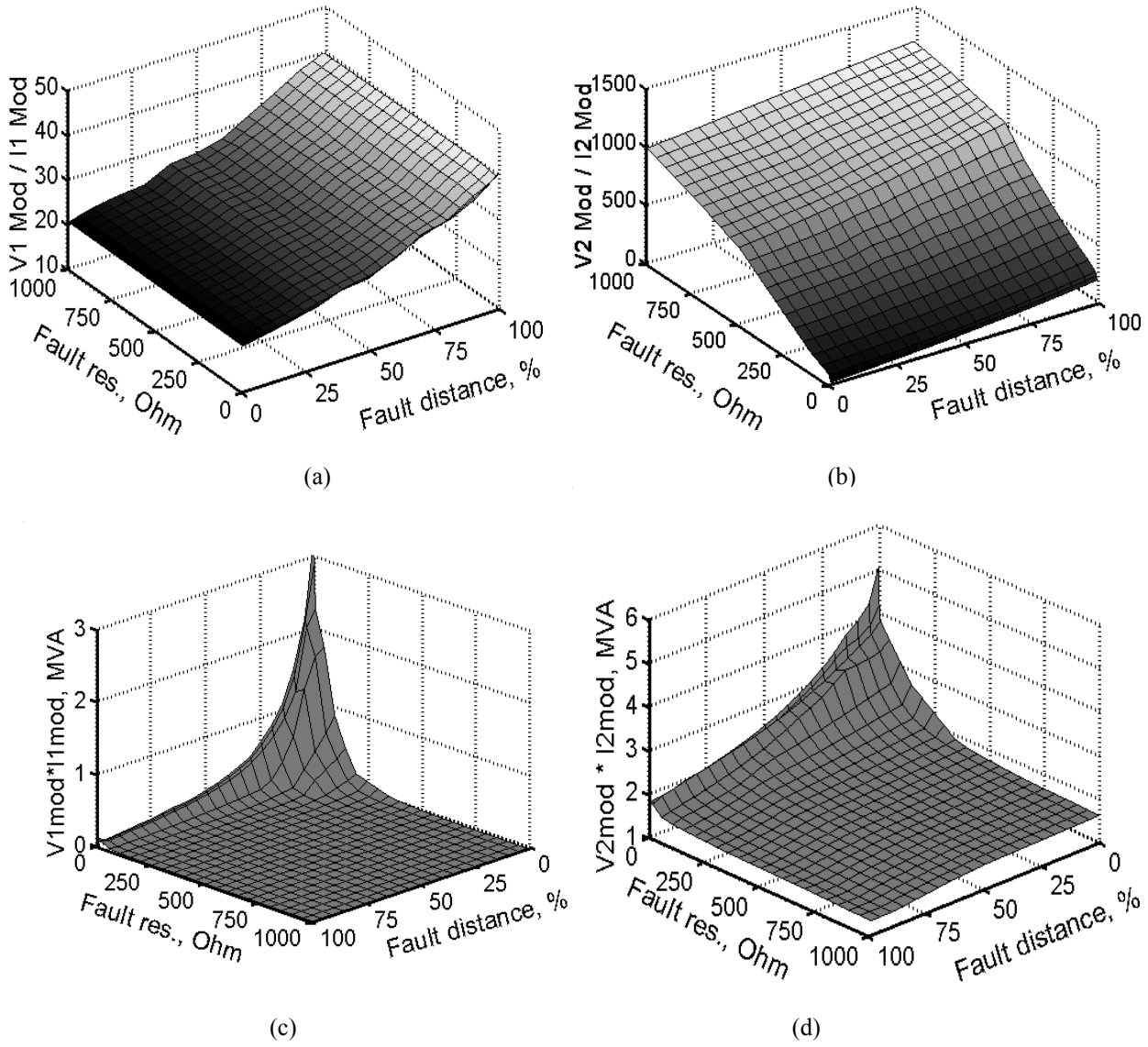

Fig. 7.2 Selected four input quantities

7.3.2 OFLT initial design

Similar to the used FL system designing method in the last chapter, the associated fuzzy networks with the OFLT were initialized. For each adopted fuzzy network, the initial configuration is arbitrary selected and optimized later employing the training paradigm using the (ANFIS) routine. As shown in Fig. 7.1, a separate fuzzy network is adopted with a single output for each fault type. Each of these networks shares the same input vector. The input vector contains the aforementioned selected four quantities in addition to the Load Correction Factor (LCF). LCF is an additional input describing the loading condition of the system just before the fault inception. It can be calculated as the percentage of the actual load current to the nominal load current as seen in Equation (6.2).

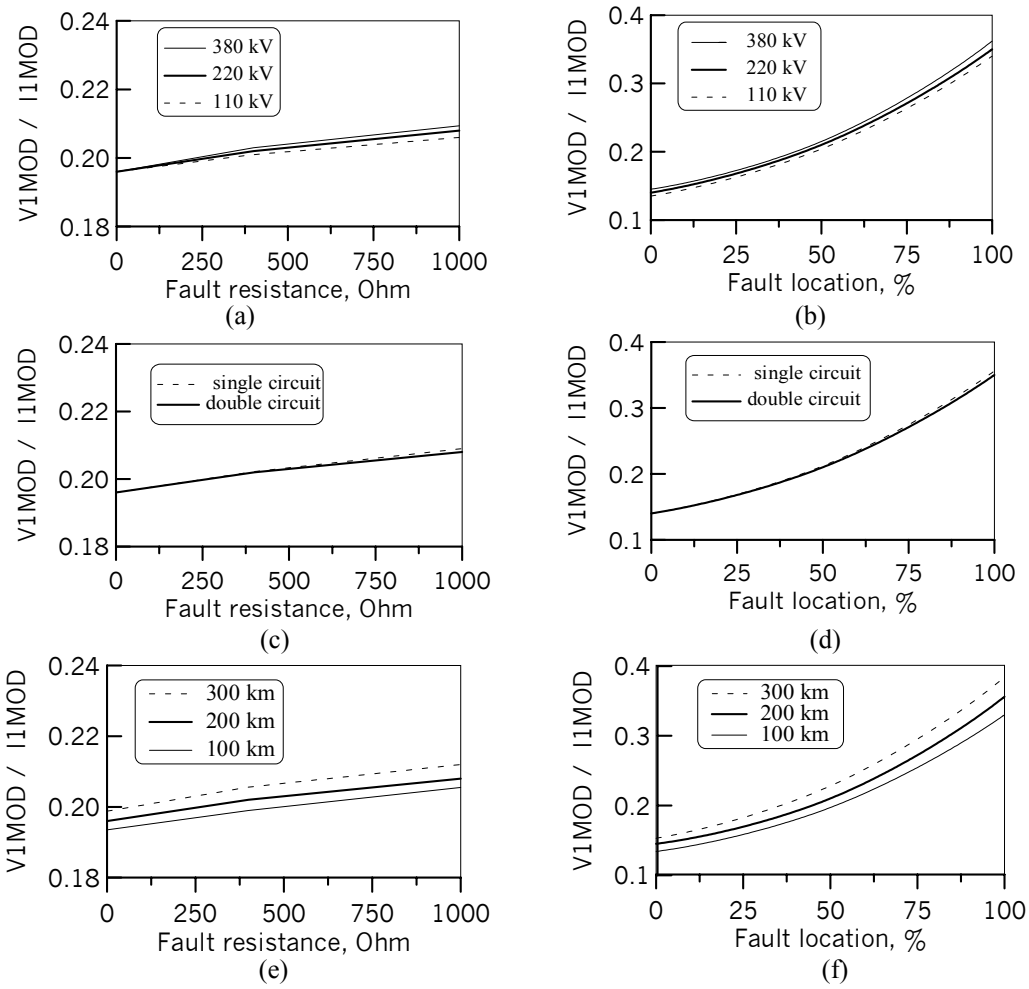

Fig. 7.3 Universality check of the first input quantity

(a)&(b) Rated voltage (c)&(d) Rated power (e)&(f) Line length

All inputs are described with a set of selected overlapping membership functions, while the outputs are described as a linear function of the inputs. An arbitrary set of membership functions is adopted for each input variable. Each of these sets is initialized with a grid of equally spaced overlapping memberships. The rules were adopted for each network depending on the behavior of the adopted five inputs versus the fault position and the added fault resistance value. All available membership shapes in the FL Toolbox in MATALAB were tested to find out the most appropriate ones.

7.3.3 Training process

All required training cases were developed via ATP using a double circuit, double infeed distributed parameter line model. Among the different listed line configurations in Appendix B, the 220 kV, 200 km line is selected as a prime line model for training purposes. Then, other line configurations are considered later in the testing stage. For each FL network, a complete training

set of 6329 fault cases were prepared covering all loading possibilities from no load to 120% of the full load with an increasing step of 10% of the full load current. At each percentage of load, 483 cases were collected covering the entire range of the fault location at (1, 5, 10, 15, 20, 25 ..... 100) % of the line and the selected range of added fault resistance of (1, 5, 10, 50, 100, 150 ..... 1000) Ω. For each case, the required five inputs as well as the required correction factor were prepared. The adopted correction factor is calculated as a percentage of the actual fault location to the estimated fault location at this point. Then, the full training set was processed via the ANFIS training paradigm to optimize the initial designed fuzzy network with hybrid learning.

7.4 OFLT Performance Evaluation

To evaluate the performance of the proposed OFLT, a separate test set was prepared covering the ranges of fault distance, fault resistance and loading condition for each fault case. A line to ground fault on phase A was considered here, where other fault types can be tested similarly. For each case, the overall accuracy expressed by the deviation between the estimated fault distance and the actual fault distance is considered. These test cases were prepared using ATP-EMTP, while the locator equations, phasor estimation and OFLT algorithm were performed via MATLAB. All these cases were prepared considering double infeed, double circuit and untransposed line situations. The resulting estimation error is, therefore, the maximum accumulative error for each loading condition. The sequence of the applied tests has been carried out by taking the sampled data from the ATP-EMTP to be fed into the MATLAB environment.

7.4.1 Protection function efficiency

Firstly, the performance of the overall scheme was investigated considering the prime line model of 220 kV and 200km. Different test cases were carried out considering a wide variety of fault locations, fault resistance values and loading conditions. As an example for these test cases, Fig. 7.4 shows a line to ground fault on phase A at a distance of 52% of the line length. The fault occurred through a fault resistance of 820 Ω under no-load condition. The locator estimated the fault location with 52.58 % of the total line length revealing the significant high accuracy of the overall scheme. The delay time T_d is assigned for the required time for normal relaying operation.

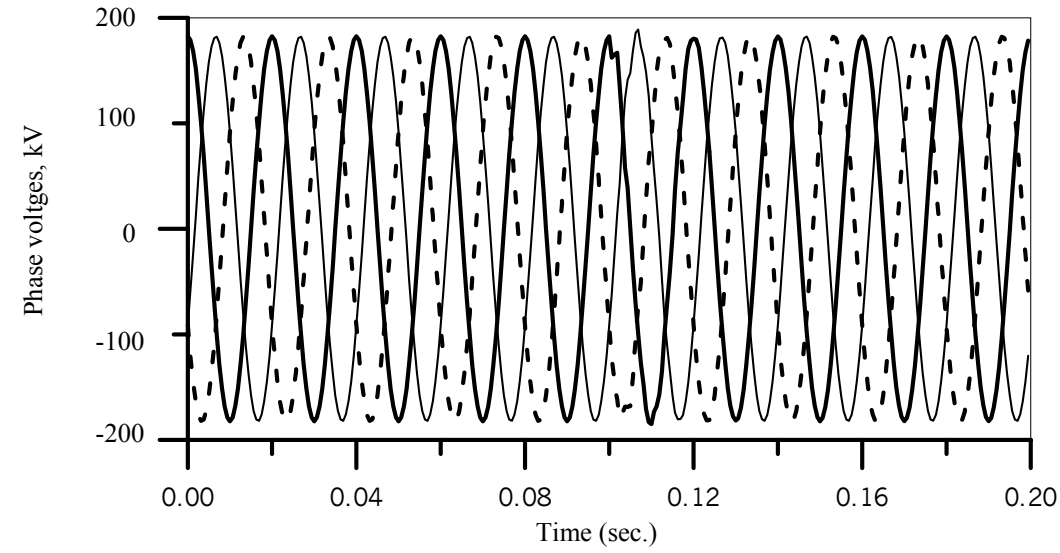

(a)

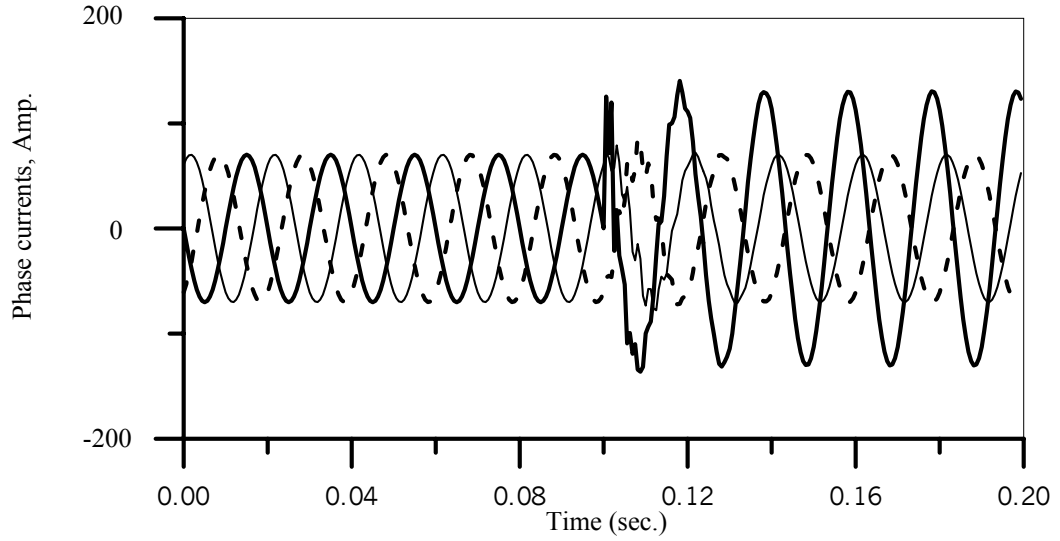

(b)

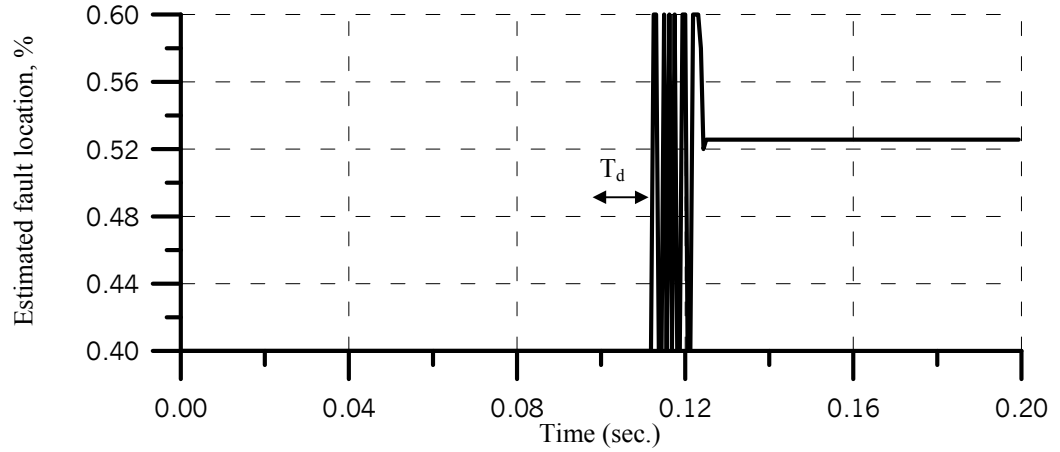

(c)

Fig. 7.4 Overall scheme response to ground fault on phase A at 52 % of the line length through a 820 Ω fault resistance at no-loading

(a) Phase voltages (b) Phase currents (c) Estimated fault location

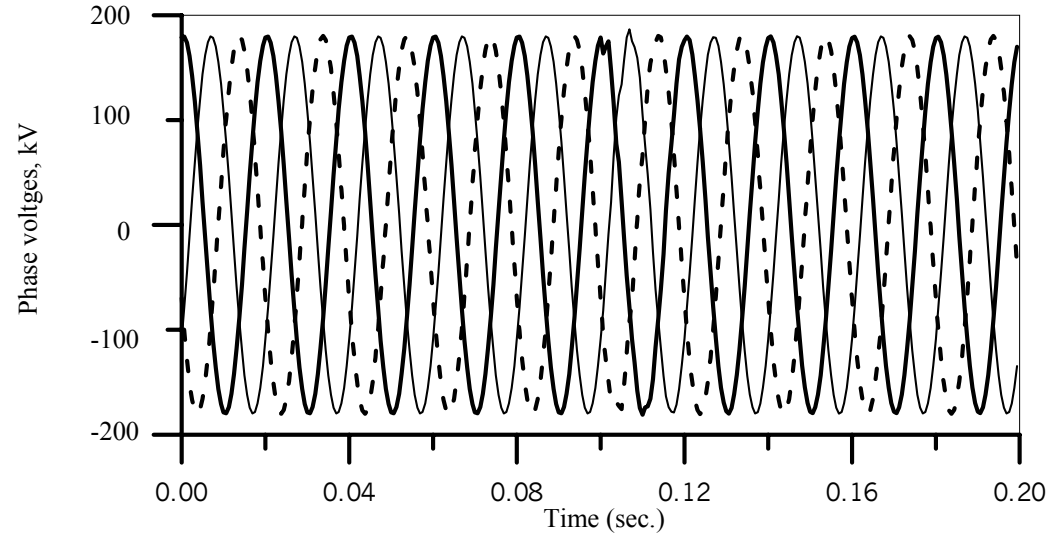

(a)

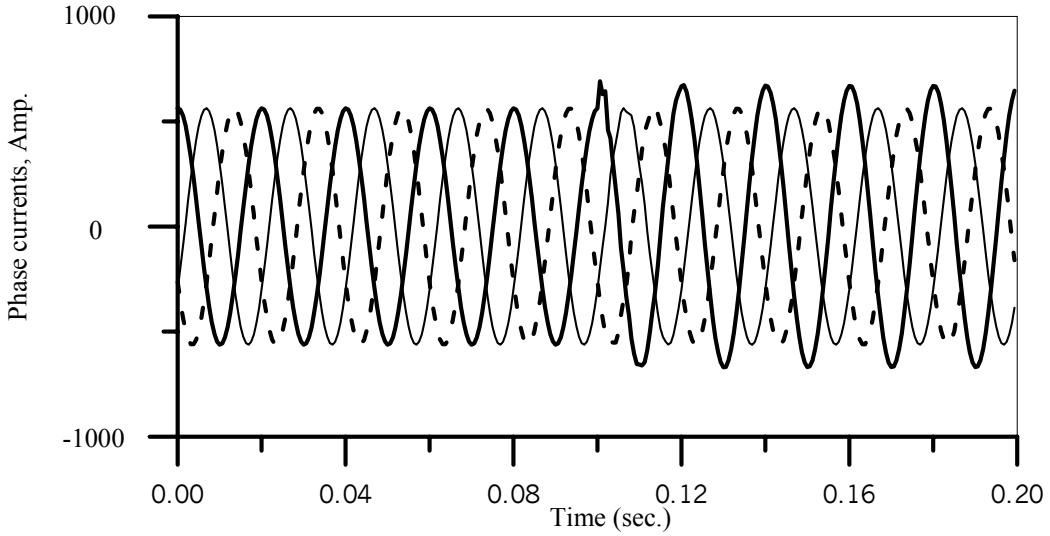

(b)

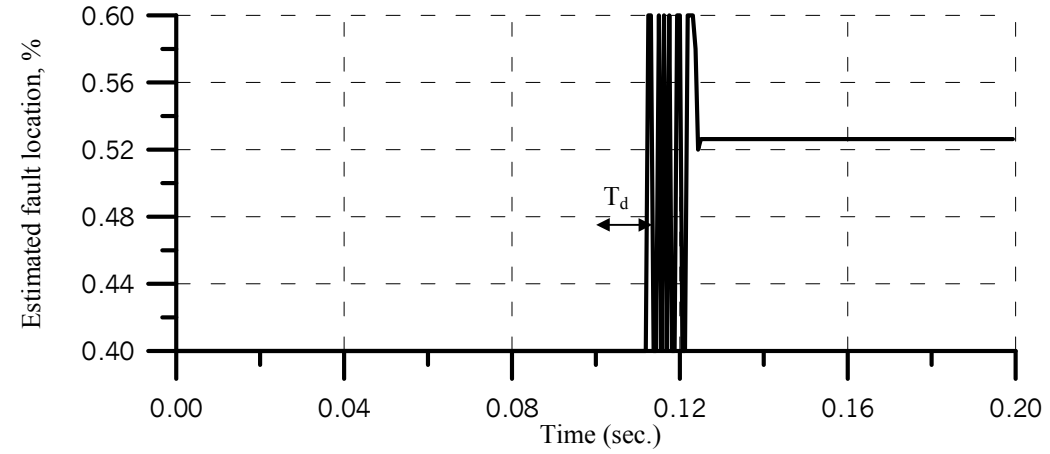

(c)

Fig. 7.5 Overall scheme response to ground fault on phase A at 52 % of the line length through a 820 Ω fault resistance at 50% loading

(a) Phase voltages (b) Phase currents (c) Estimated fault location

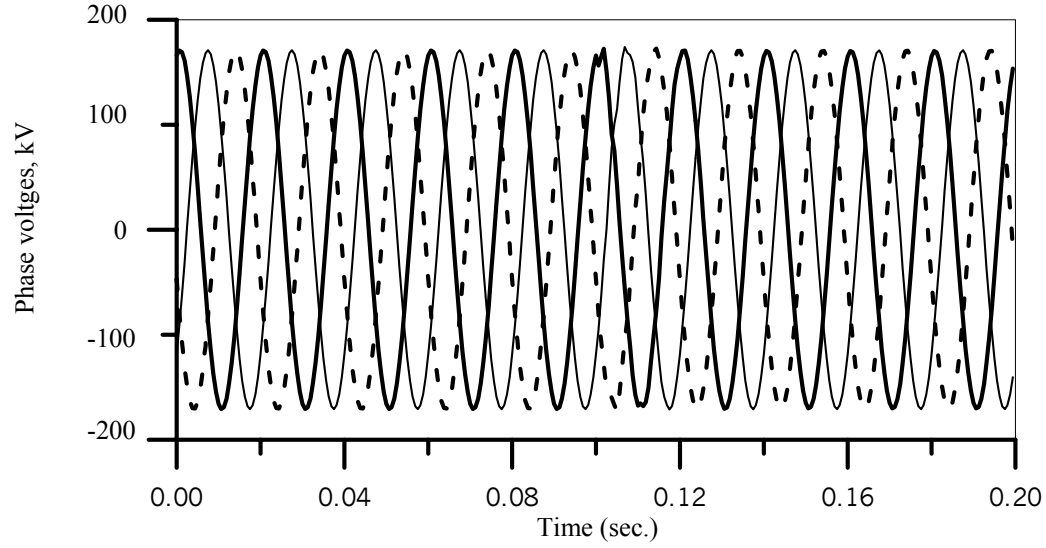

(a)

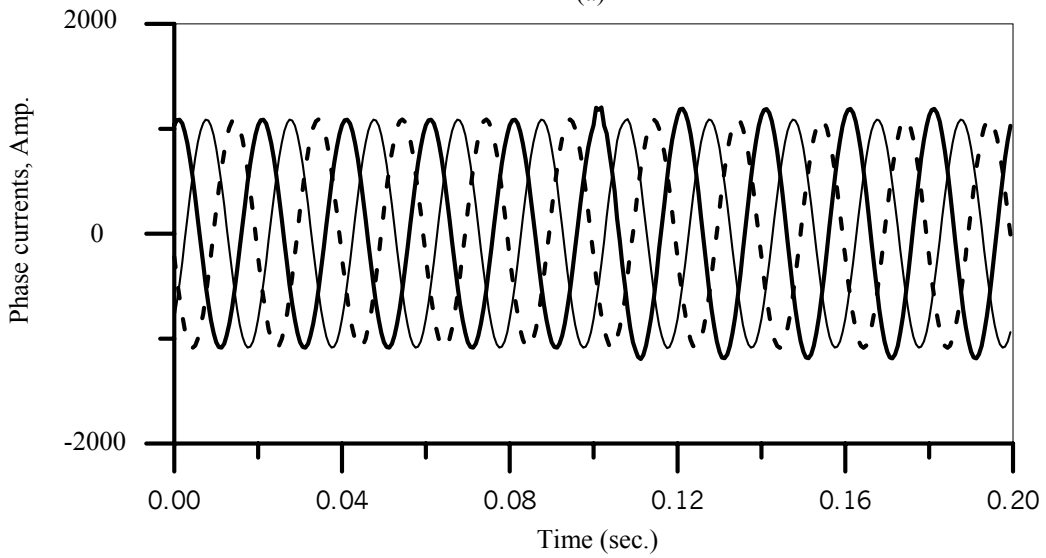

(b)

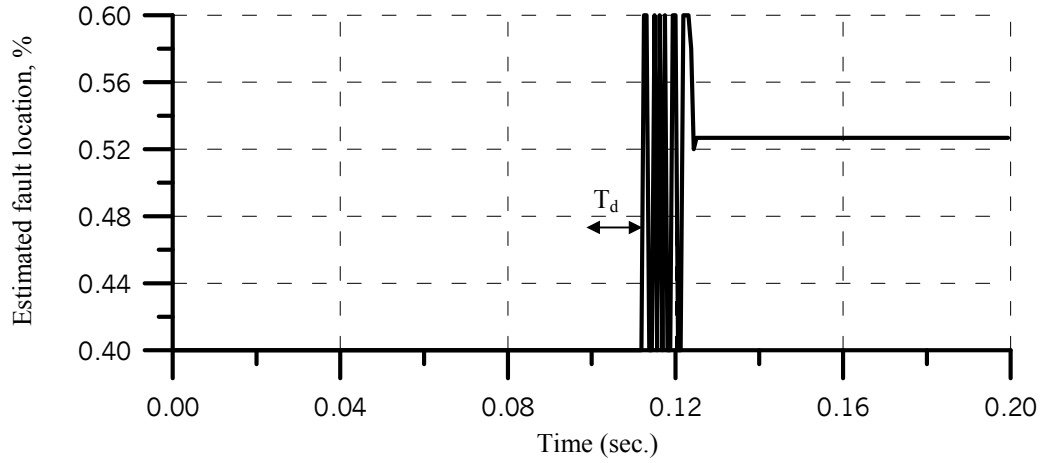

(c)

Fig. 7.6 Overall scheme response to ground fault on phase A at 52 % of the line length through a 820 Ω fault resistance at full-loading

(a) Phase voltages (b) Phase currents (c) Estimated fault location

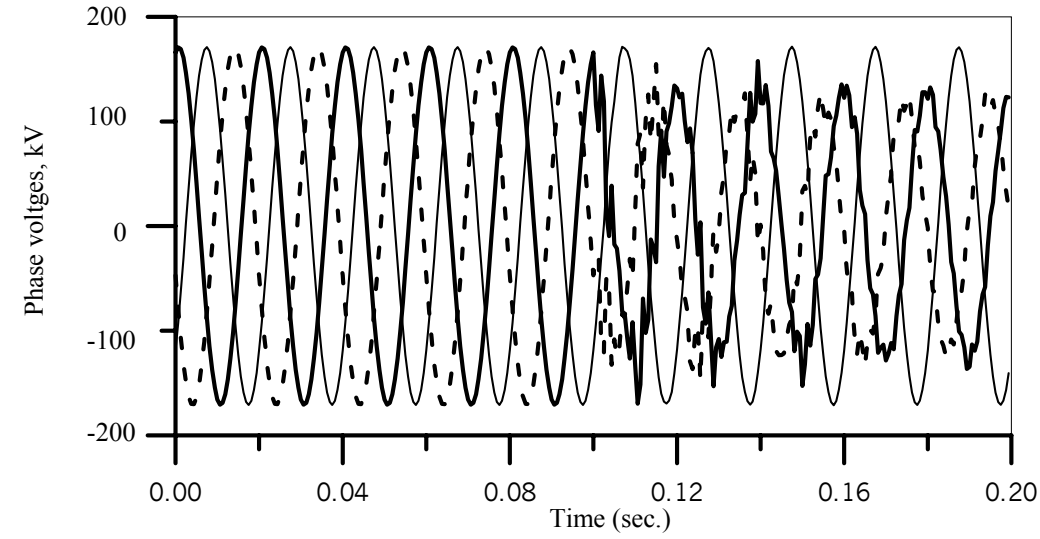

(a)

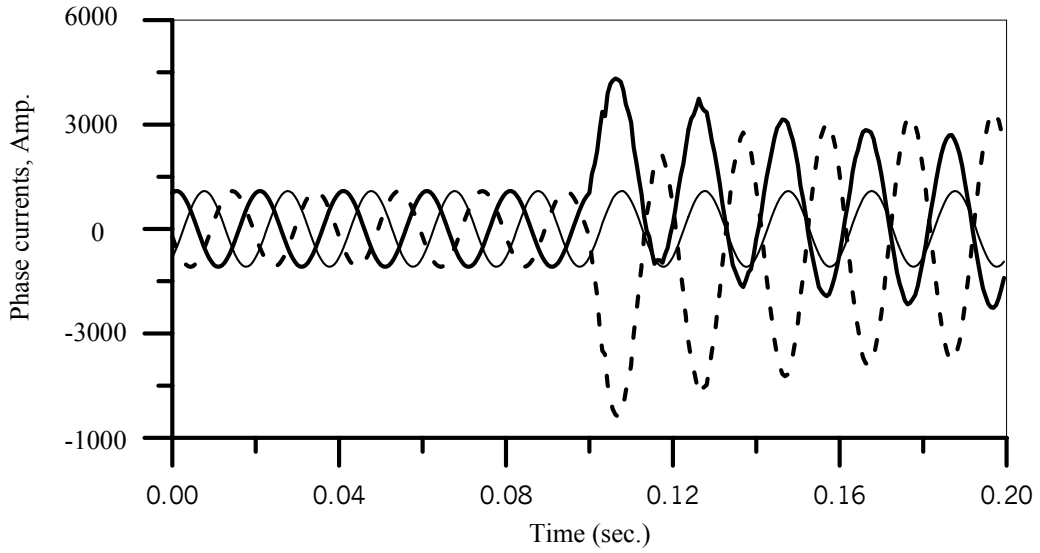

(b)

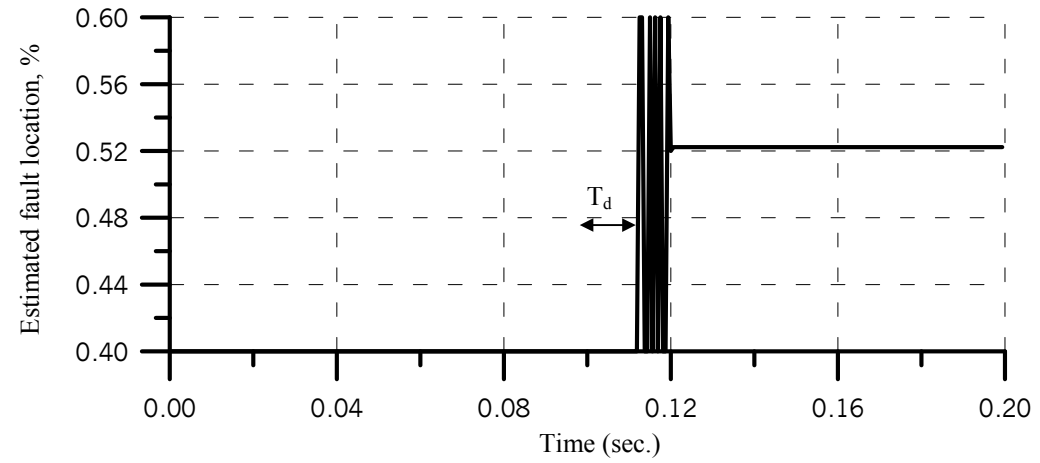

(c)

Fig. 7.7 Overall scheme response to double phase ground fault on phases A and B at 52 % of the line length through a 820 Ω fault resistance at full-loading

(a) Phase voltages (b) Phase currents (c) Estimated fault location

Also, both Fig. 7.5 and 7.6 show the results for the same fault case occurring at 50 % of loading and full loading conditions. The resulted fault location estimated values were 52.62 and 52.68 % for both loading conditions respectively. The same test was also repeated for a double phase to ground fault on phases A and B resulting in a fault estimation of 52.23 % of the whole line as shown in Fig 7.7.The collected test results were expanded to cover the entire range of the fault distance and the whole selected range of the added fault resistance in order to plot the boundaries of the maximum estimation error that can occur. The histogram in Fig. 7.8 shows this boundary, in which the maximum estimation error does not exceed 0.8% of the total line length revealing the efficacy of the overall scheme. This maximum percentage of estimation error can be considered as the overall accuracy of the OFLT for 220 kV line case.

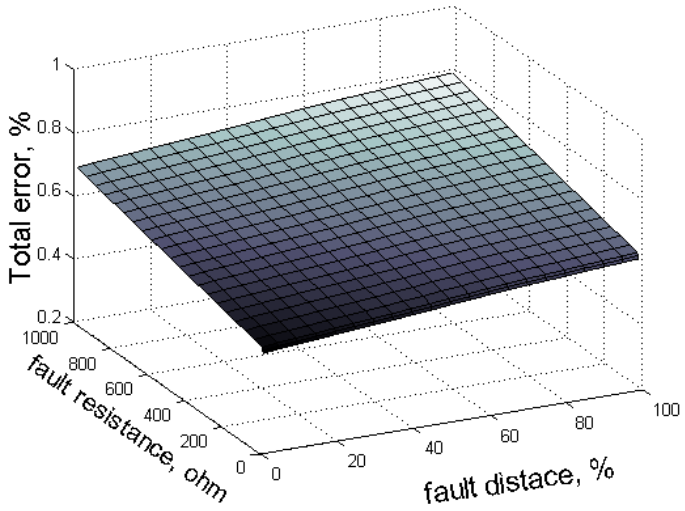

Fig. 7.8 Overall scheme accuracy boundary

7.4.2 Universality evaluation

The aforementioned procedure regarding the general accuracy of the overall scheme is repeated considering 110 and 380 kV lines as well in addition to the prime line model of 220 kV considering 100, 200, 300 km line lengths using the same conductor size. Table 7.1 summarizes these results showing the general accuracy of all these situations considering the selected conductor configurations for each rated voltage level. Only the 300 km line length was not considered for 110 kV, since this does not happen in reality. The above results reveal the high performance of the proposed approach covering a wide variety of system configurations. However, all these results were obtained considering Al/St 180/35 conductors. Thus, the need to investigate the influence of changing the conductor type is obvious. For this purpose, the accuracy of the 220 kV 200 km line is checked for Al/St 240/40 and Al/St 300/50 conductor

types. An accuracy of 2.166% and 2.892% has been got for both types respectively. As compared with the accuracy of the Al/St 180/35, it can be concluded that the proposed approach is capable of dealing with all configuration of rated voltage, transferred power or line length in case of using the same conductor type. A separate training set is needed for each certain conductor type to solve this challenge.

Table 7.1 Accuracy of all selected line configurations using Al/St 180/35 conductors

Rated Voltage	Selected configuration	Overall accuracy %		
		100 km	200 km	300 km
110 kV	(a)	0.7975	0.7854	-
	(b)	0.8012	0.7906	-
220 kV	(a)	0.7936	0.7802	0.8023
	(b)	0.7987	0.7867	0.8109
380 kV	(a)	0.7968	07488	0.8091
	(c)	0.8004	0.7898	0.8141

8 Advanced Testing and Solutions

The overall proposed fault location scheme was introduced in the last chapter comprising the modal transformation-based fault location calculation and the FL-based fault location tuning. All applied tests revealed clearly the efficacy of the proposed locator, in which the resulting estimation error is always limited to an acceptable value even for high impedance faults. Also, the effects of mutual coupling, remote infeed, pre-fault loading and line imbalance are eliminated. In this chapter, more sophisticated cases will be covered in order to emphasize the applicability of the proposed scheme. The chapter investigates these situations and, if needed, gives some suggestions that may collaborate with the overall proposed scheme without extra algorithms or complexities.

8.1 Non-Linear Arcing Faults

It is known that most faults on overhead transmission lines are ground faults including both arcing and non-arcing types. Most of these faults are arcing ones occurring as a result of a flashover of the insulation due to the lightning or the insulation failures. As the current path for these faults includes the arc resistance, tower impedance and tower footing resistance, all these factors impact the related fault impedance as explained in Chapter 2. This effectively affects the performances of all protection equipment, especially those that depend only on single end data. Usually, considering the arc existence for protection purposes is disregarded due to its modeling complexities. It was, however, considered for transmission line protection in [92]. The approach presented an acceptable performance during relatively low impedance fault cases. On the other

hand, it was strongly affected in the cases with high fault impedance values. It is, therefore, more convenient to investigate the effects of these situations on the accuracy of the proposed overall scheme.

8.1.1 Arc fault modelling aspects

From the modeling point of view, the arc fault can be divided into two phases, primary and secondary arcs. A primary arc exists during the fault duration (before the breakers opening), whereas the secondary arc exists after the breakers opening. When the modeling of fast transients of power systems is concerned, both arc periods should be considered such as fast fault detection equipment and autoreclosures. However, for fault location purposes, in particular, considering only the primary arc period is quit sufficient. As far as the primary arc is only considered for this application, neglecting the arc length elongation is acceptable. Also, it is considered that the arc column has a relatively large cross section area and almost all the arc voltage appears across the main arc column [93]. Among the various developed approaches for arc fault modeling, square voltage model and time dependent arc resistance model are known and usually used in the literatures. The first approach assumes the arc voltage to be modeled simply as a square wave shape in phase with the arc fault current [94]. Then, the non-linear arc resistance is calculated as a percentage of the arc voltage to the arc current. The second approach describes the dynamic behavior of the non-linear arc using non-linear differential equations with the facilities of the Transient Analysis of Control Systems (TACS) in the EMTP software [95, 96]. The model was developed basically depending on the dynamic behavior equation expressing the time varying arc conductance (g_{arc}) as a function of the stationary arc conductance G and the exhausted time constant τ as written as [97]

$$\frac{dg_{arc}}{dt} = \frac{1}{\tau}(G - g_{arc}) \tag{8.1}$$

The stationary arc conductance can be expressed as a function of the arc resistive component per unit length (R_{arc}), the selected voltage per arc length parameter (u), the arc current (i) and the arc length (l_{arc}) as

$$G = \frac{|i|}{(u_{arc} + R_{arc}|i|)l_{arc}} \tag{8.2}$$

It yields the time varying arc resistance R_i as follows:

$$R_i = \frac{1}{g_{arc}} \tag{8.3}$$

Fig. 8.1 shows a schematic diagram of the adopted arc modeling in ATP. Further descriptions were reported in the relevant references.

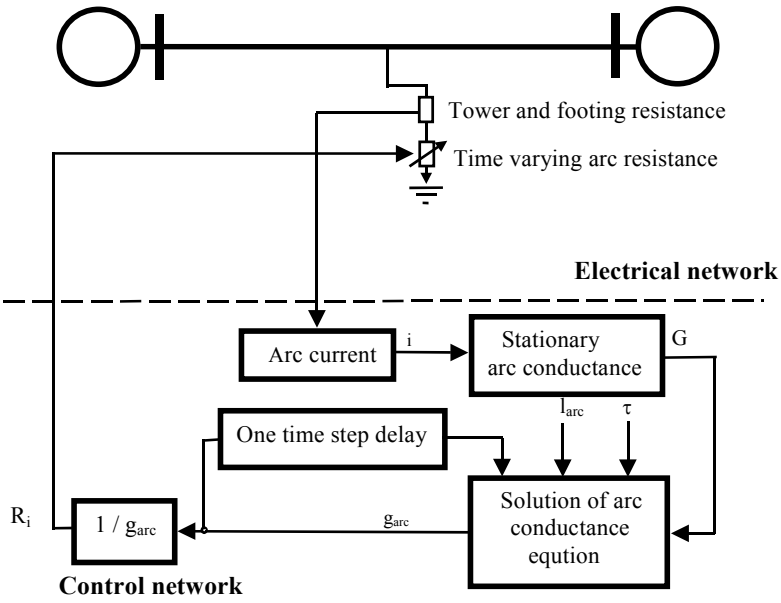

Fig. 8.1 Fault arc modeling in ATP

Various investigations have been carried out for the performance of both approaches. The simplicity and direct employment in power system simulation are main advantages of the first approach. The more accurate performance, especially with detailed power system models, is the advantage of the second one. However, selecting the needed arc parameters is a basic problem. Real field tests and field experience effectively help to get the accurate required parameters [97]. The second approach is considered here for arcing fault simulation purposes using the interactive simulation of control elements with MODELS in ATP. The MODELS paradigm in the ATP facilitates great abilities for embedding the control elements simultaneously during the simulation running.

8.1.2 Test results

Different test cases were carried out to investigate the effect of non-linear arc existence on the accuracy of the proposed fault location scheme. Arc fault and tower footing resistance collaborate together affecting the fault location estimation accuracy. A wide range of the added

fault resistance up to 1 kΩ was considered in these tests. The line imbalance may significant increase the total resulted errors as well. Thus, both transposed and untransposed cases were considered.

As an example for these tests, Fig. 8.2(a) and (b) show the approach response for a line to ground arcing fault occurring at 50 % of the line including 20 Ω and 720 Ω tower footing resistance respectively. The line is considered to be fully loaded and fed from both ends with transposed parameters. The figure shows the related sending end voltage, sending end current, resulting arcing voltage as well as the approach response. After the successful detection of the fault, the fault location algorithm is executed. The percentage of the final estimation error is limited to 0.48% and 0.60% for both selected cases respectively. Repeating the same cases for untransposed line resulted in an increase of the final estimation error to 0.64% and 0.73% for both cases respectively. All tests reveal the stable performance of the proposed scheme during the existence of the non-linear arcing faults and show a similar efficacy as those with permanent fault cases.

The arc parameters were selected according to the applied simulation and experimental investigations [96, 97]. To investigate the impact of these parameters on the performance, each of these parameters was deviated from its selected value with an error of ±10%, ±20% and ±30% of its original value. Then, the behavior was checked in case of an arcing ground fault on phase A through a tower footing resistance of 20 Ω at 50 % of the line with untransposed parameters. The results are listed in Table 8.1. As revealed from the shown results, the scheme is highly immune to the variations in arc parameters. Similar results were obtained for the case of 720 Ω tower footing resistance.

Table 8.1 Investigation of the arc parameter variations

Pa.	**Basic selected value**	**Resulting estimation error, %**					
		-10%	**+10%**	**-20%**	**+20%**	**-30%**	**+30%**
τ	0.9 ms.	0.6397	0.6414	0.6397	0.6413	0.6398	0.6414
u	15 v/cm	0.6398	0.6411	0.6397	0.6413	0.6397	0.6413
R_{arc}	110 mΩ/cm	0.6410	0.6408	0.6409	0.6408	0.6409	0.6409
l_{arc}	200 cm	0.6409	0.6408	0.6410	.6410	0.6410	0.6410

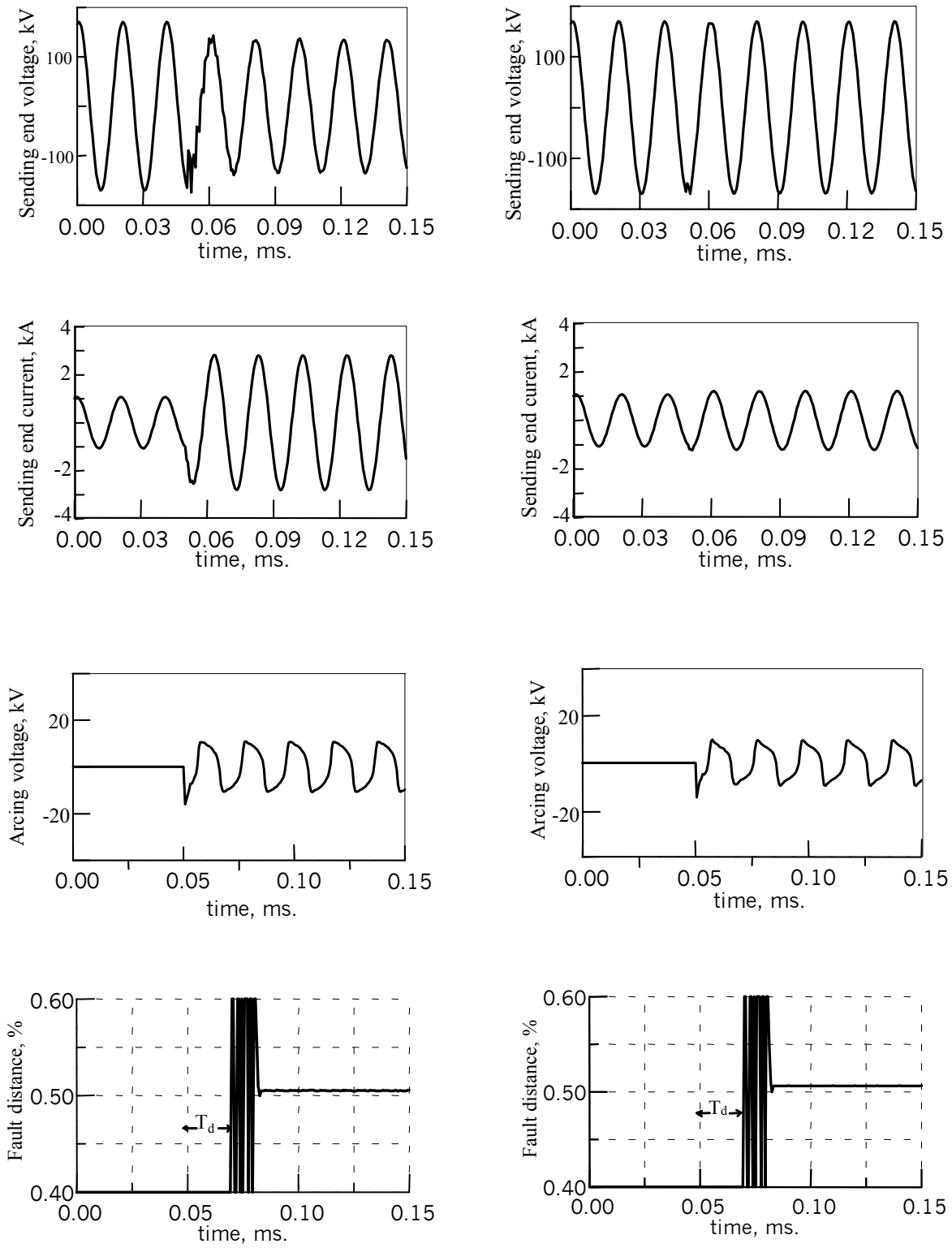

(a) (b)

Fig. 8.2 Approach response to an arcing A-G fault at 50% of the line.
(a) Tower footing resistance: 20Ω (b) Tower footing resistance: 720Ω

8.2 Grounding Means and Fault Location

Ground faults are the most frequent faults in transmission nets (about 80 %). The grounding method and the ground element value influence the performance of all protection equipment requiring, in some cases, special treatments to realize the proper protection. This is mainly due to the direct relation between the grounding method and the fault current quantity during the fault. This is clear in Fig. 8.3, in which the current flows from the fault point F through the fault resistance R_F and returns through the transformer grounding impedance on both line sides. The quantity of the current depends mainly on the value of the fault resistance as well as the fault impedance (the current passed through the capacitance C_o is small). Hence, the efficacy of the fault location estimation strongly depends on the combination of both impedance parts (fault and ground ones).

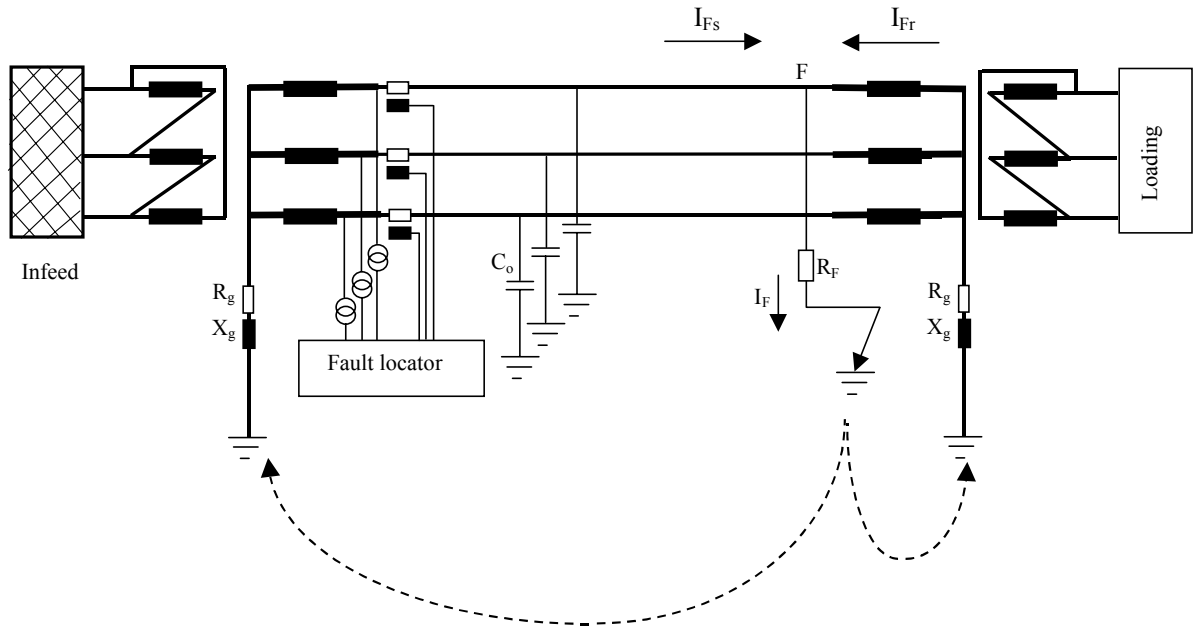

Fig. 8.3 Ground fault current path including the ground impedance

The grounding impedance is practically set according to the selected means of grounding which depends on the rated voltage and the protection philosophy. Different grounding strategies were established varying from solid (or effective) grounding methods to isolated grounding. The usage of the aforementioned grounding means differs from one country to another depending on the considered standards as well as the priority between the equipment protection and human safety. According to the VDEW-statistic in 1998, Table 8.2 shows the used grounding description in Germany.

Table 8.2 Neutral grounding in Germany according to VDEW-statistics 1998

Types of grounding	***Percentage of usage according to the nominal voltage***			
	10 kV	**20 kV**	**110 kV**	**380 kV**
Solidly grounding	13.6	2.2	19.1	99.3
Resonant grounding	77.8	92.8	80.9	0.7
Isolated grounding	8.6	< 0.1	0.0	0.0

Different tests have been carried out to investigate the effect of the grounding type on the accuracy of the proposed scheme. Fig. 8.4(a), (b) and (c) show the estimated fault distance in three different cases considering different grounding means and grounding element values. For all cases, the fault was considered to occur at 85 % of the total line length on a 220 kV, 200 km, double circuit and double infeed untransposed line.

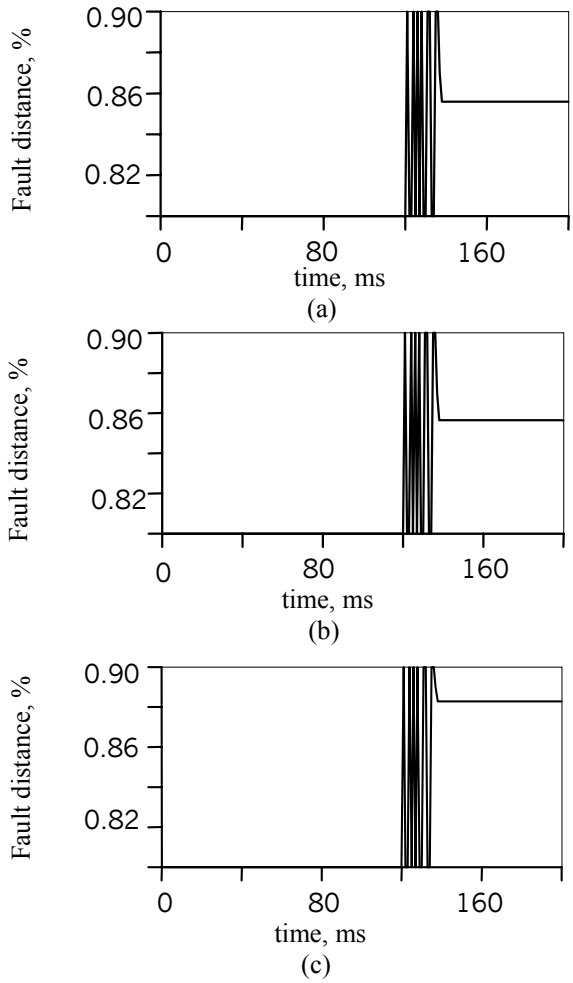

Fig. 8.4 Grounding effect on fault location calculation.

(a) Low resistive grounding (30 Ω) and 200 Ω fault resistance (b) High resistive grounding (400 Ω) and 200 Ω fault resistance (c) Low inductance grounding (80 mH) and 200 Ω fault resistance

From the results, the scheme shows a stable performance with resistive grounding as revealed from Fig. 8.4(a) and (b). However, the effect of low inductance grounding on the scheme accuracy is remarkable even with the small values as shown in Fig. 8.4(c). This is due to the assumption of the main algorithm considering the fault impedance to be a pure resistance. Thus, the scheme is unfortunately not able to work efficiently with inductance grounded systems. Also, the scheme fails to recognize the faults on resonant or isolated grounding systems due to the extremely small fault currents in these cases. It can be concluded that the scheme is generally characterized by a high accuracy for solidly or resistively grounding systems. This is only possible as long as the summation of the fault resistance value and the grounding resistance is limited through the scheme resistance coverage (1 kΩ).

8.3 Multiple Loading/Infeeding Lines

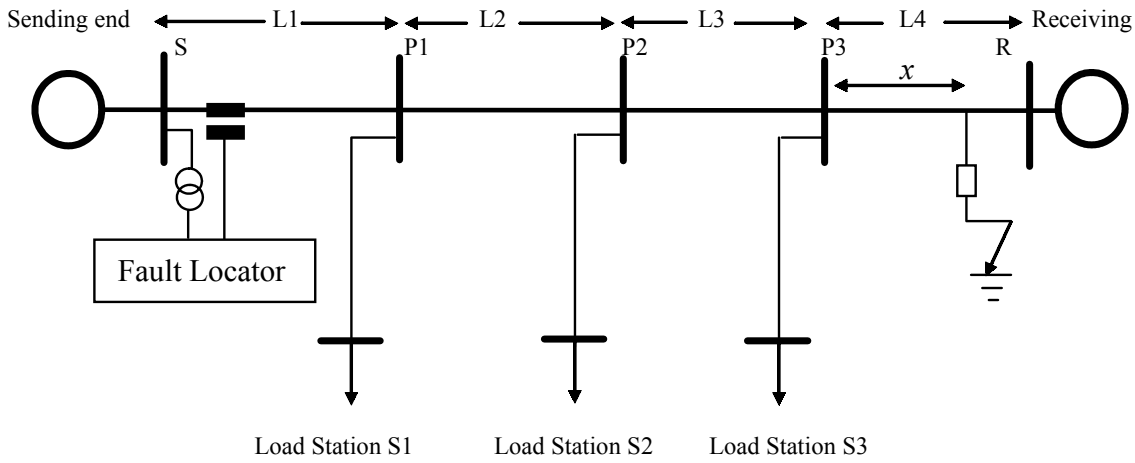

Fig. 8.5 Selected multiple loaded line

The problem of multiple-loading lines for fault location calculation is the change of the network states along the line with every tapped load point. Moreover, the locator at its fixed point at the sending end has a misleading operation since it follows only the available states at its position. Thus, it is more worthy to investigate the effect of these situations on the accuracy of the proposed scheme. For this purpose, a transmission system with three intermediate tapped loads is considered as shown in Fig. 8.5. If the fault occurs at the adjacent line part L1, the locator can recognize that fault well. However, the scheme response to the faults behind the tapped loads is remarkably affected. The same double circuit 220 kV, 200 km line is simulated where the whole length is divided into four equal parts of 50 km of each one. Three tapped load are

inserted at the intermediate points P1, P2 and P3 with loading percentage of 5, 10, and 15 % of the main load at the receiving end.

As an example, a line to ground fault occurred at a distance *x* of 36 km from the tapped point S3 (72% of the line part L4 measured from P3) through a fault resistance of 100 Ω. Four different situations were considered. The ideal case for fault location calculation is when all the required states at all loading stations S1, 2, 3 and 4 are known at the locator position. Then, the information of the last station S3 is missing, while the data of other stations (S1 and S2) are available. The third case concerned with the missing of the information at both S3 and S2 stations. The forth situation considered the missing of all information from the three loading stations. The estimated fault distance as well as the corresponding scheme overall accuracy are shown in Fig.8.6(a) and (b).

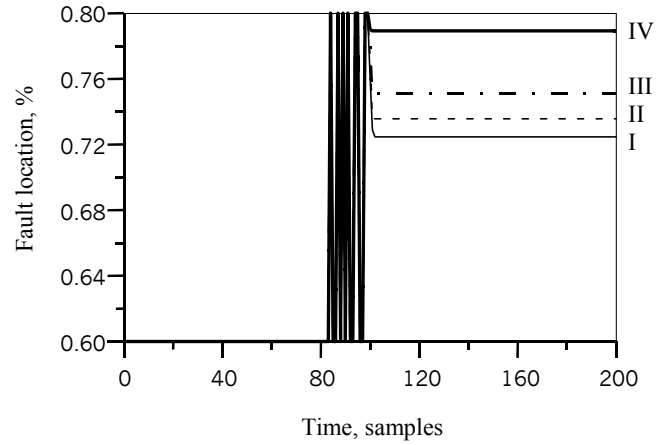

(a)

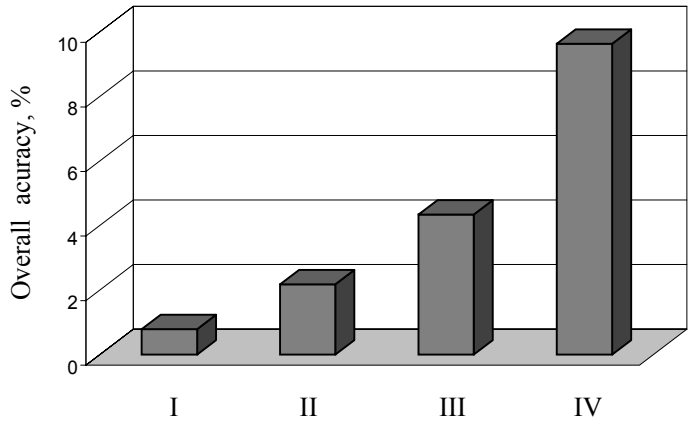

(b)

Fig. 8.6 Multiple-loading case investigation

(a) Estimated fault distance (b) Resulted overall accuracy

Case	I	II	III	IV
Missing data	-	S3	S3 and S2	S1, S3 and S2

Similarly, the case with multiple infeeding lines was considered with changing the loading stations in Fig. 8.5 with infeed stations. The stations share the sending end for delivering the load to the receiving end. Then, the effects of these intermediate infeeding can be investigated. Fig. 8.7 shows the evaluation of the scheme overall accuracy including the same four different situations considering the data availability from the remote infeed stations.

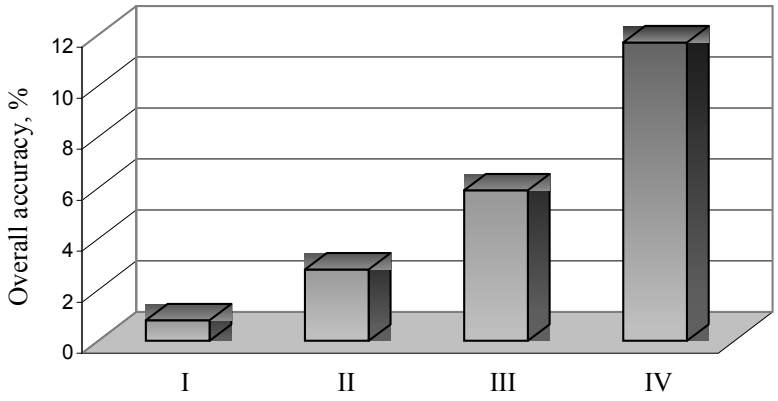

Fig. 8.7 Overall accuracy evaluation for multiple infeed line

Case	I	II	III	IV
Missing data	-	S3	S3 and S2	S1, S3 and S2

As revealed from the results, the scheme still keeps its superior performance for multiple-loading or multiple-infeed lines as long as the required states (voltages, currents, power) at all remote stations are valid. The states of the intermediate points can be calculated using the sending end information, the intermediate currents and the network parameters. Then, the fault distance is estimated starting from the intermediate point prior to the fault position.

8.4 Partially Mutual Coupled Lines

Partially mutual transmission lines are sometimes found in real fields when the mutual coupling between the adjacent circuits exists only on a certain part of the total line length. A common figure of these situations occurred when two different circuits share common double-circuit support lines, or when there is close parallel run of lines for a certain portion of the total length. As shown in Fig. 8.8, two different situations were considered. The partially coupling is either at the beginning or at the end of the line. Locating the fault on these lines accurately, requires the faulted segment to be definitely classified (i.e. classifying accurately if the fault occurs after or before the separate point between the partially and fully mutual line parts). Due to the lack of

measurement instrument at the separation point usually, it is considered a basic challenge for fault location problems.

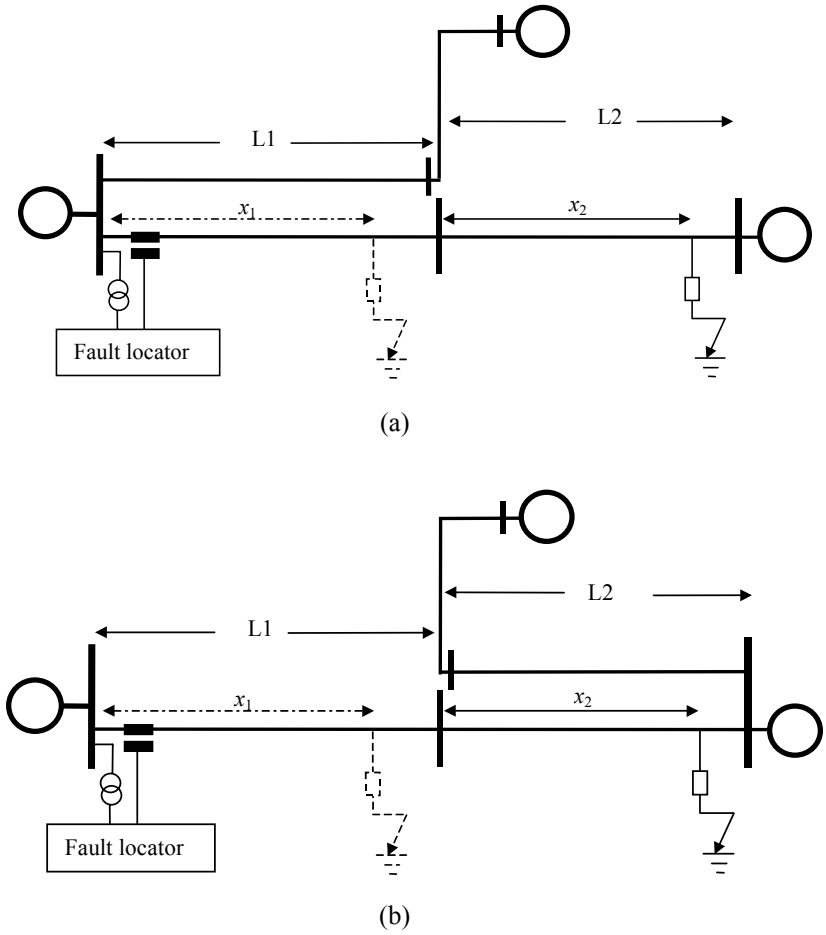

Fig. 8.8 Partially mutual lines

(a) Partially coupled part at the line beginning (b) Partially coupled part at the line end

Due to the handling complexities of these problems, the published efforts for realizing a practical fault location scheme for partially mutual lines are remarkably limited. To overcome this difficulty, a practical algorithm was introduced in [98] adopting two different fault distance calculation routines for both adjacent or remote coupled areas of the line (L1 part of the line in Fig. 8.8(a) or (b)). According to the results of both routines, the faulted part of the line is precisely declared and hence the final distance is realized. The worst case arises when the fault occurs near to the separation point between the partially and non-partially coupled line parts. This results in an expected blind margin (about 5%), in which the selection procedure between both calculation routines is doubtful. The aforementioned fault location method was modified here to fit the proposed scheme. Fig. 8.9 describes the proposed solution. Firstly, the preliminary fault distance is estimated considering a symmetrical line situation. This is calculated by

considering the extra mutual coupling for the full line length for Fig. 8.8(a) and neglecting it for the whole line for Fig. 8.8(b). Then, the faulted line part of the line is detected according to the resulting estimated distance. If the estimated distance is located in the adjacent part of the line to the locator, it is considered as the final estimated fault location. If this measured fault distance is located in the remote part of the line, the states of the separation point is calculated according to the available states at the locator position as well as the related parameters of the adjacent line part. Then, the fault location routine is repeated starting from this point for the remote part of the line.

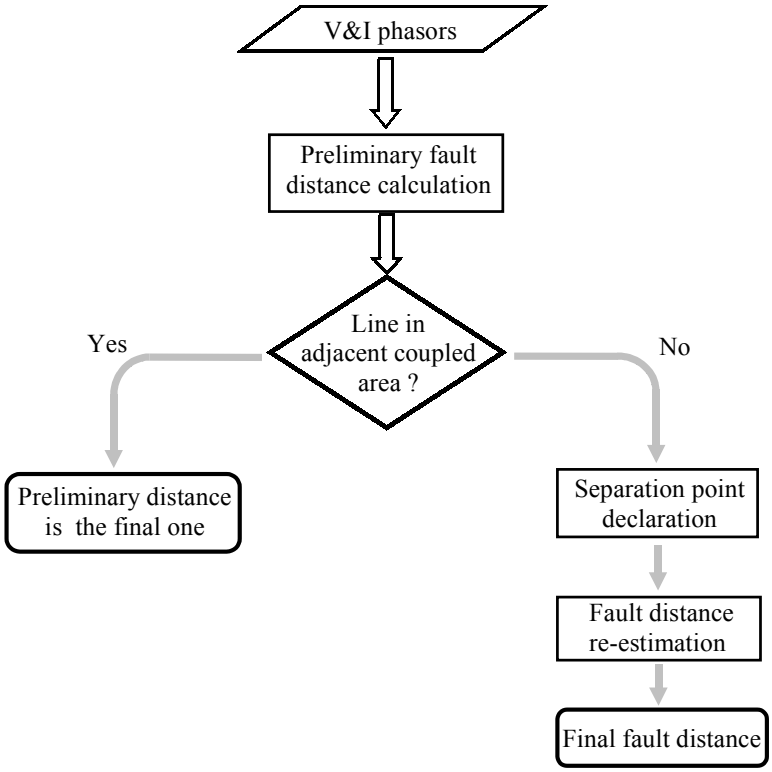

Fig. 8.9 Selection procedure for partially coupled lines

Different investigations have been carried out to emphasize the efficacy of the proposed procedure using the 220 kV, 200 km double infeed and double circuit line. The second circuit is considered to be coupled only for 50 % of the line length. Fig. 8.10 shows both preliminary and final fault distances for two different fault cases occurred 178 and 122 km away from the locator position respectively. In the first case, the adjacent line part is considered to be partially coupled similarly to Fig. 8.8(a), whereas the other case considered the remote line part as the partially coupled part. As shown in Fig. 8.10(a), the preliminary fault distance is 90.62 % of the total line length. Then, the final fault distance is recalculated starting form the separation point to be 78.54% of the remote part line length. The preliminary fault distance is 62.43% of the total line

length, whereas the final fault distance is 22.48% for the second test case as shown in Fig. 8.10(b). Other different investigations were carried out for the faults close to the separation point between the partially coupled and coupled line parts. It has been concluded that the resulting blind margin around the separation point does not exceed 2% of the line length. This resulted in a simple fault location algorithm (with only one calculation routine) and smaller blind area around the separation point in addition to the ability to deal with coupled lines and high resistance faults efficiently.

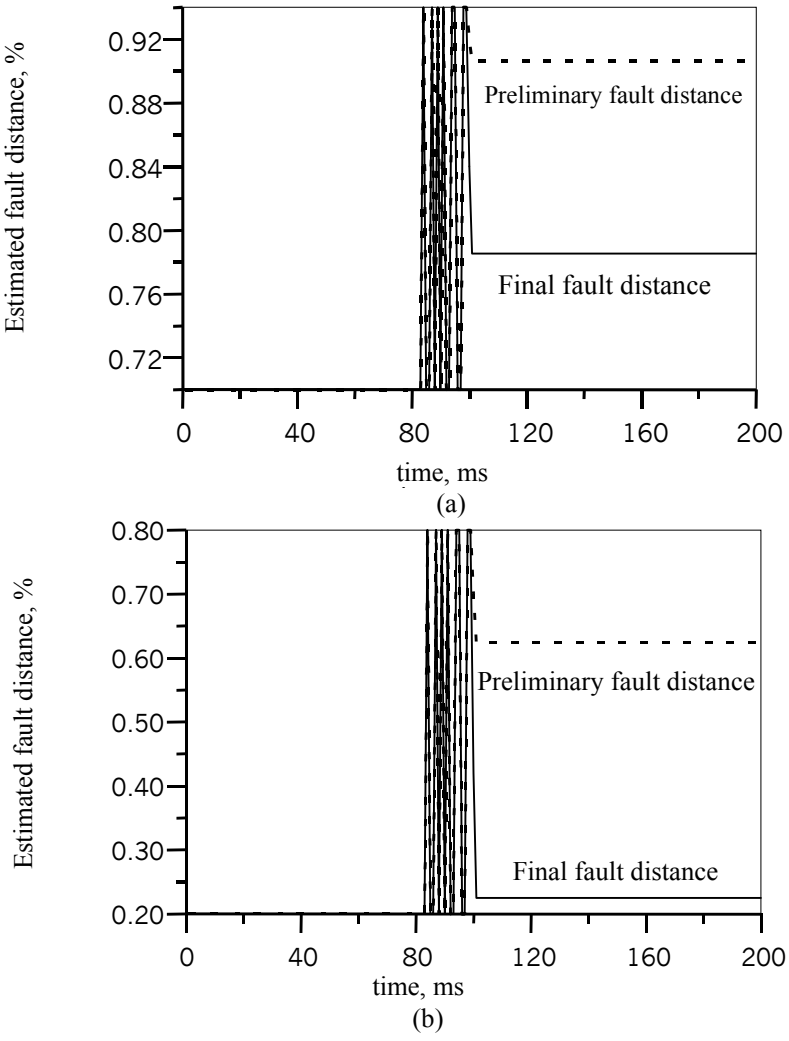

Fig. 8.10 Partially coupled line fault location procedure evaluation
(a) Partially coupled part is the adjacent part (b) Partially coupled part is the remote part

8.5 Multi-Circuit Coupled Lines

All applied tests considered only single or double circuit lines with the same line voltage. Even in the universality check with changing the used rated voltage and the network configuration,

both simulated line circuits have the same voltage and configuration. However, it is common to use more than two circuits at one or more voltage levels due to the economical viewpoint. Thus, it is more convenient to investigate the effects of this situation on the accuracy of the overall proposed scheme. For this purpose, a sophisticated compound of 200 km and 6 circuits with 110, 220 and 380 kV is evaluated. Both circuits of 110 kV line is partially coupled to the other circuits with a length of 50 km. Table 8.3 summarizes the details of the line construction, whereas Fig. 8.11 shows the configuration of the line. The ATP LINE CONSTANT routine is employed to calculate the associated line parameters according to the transmission system dimension in Fig. 8.11. The required parameters for each voltage level are found in Appendix B.

Table 8.3 Selected multi-circuit line configuration

Rated voltage	Line length, km	Line circuits	No. of bundles	Conductor type
110	50	2	2	Al/St 185/30
220	200	2	2	Al/St 185/30
380	200	2	4	Al/St 240/40

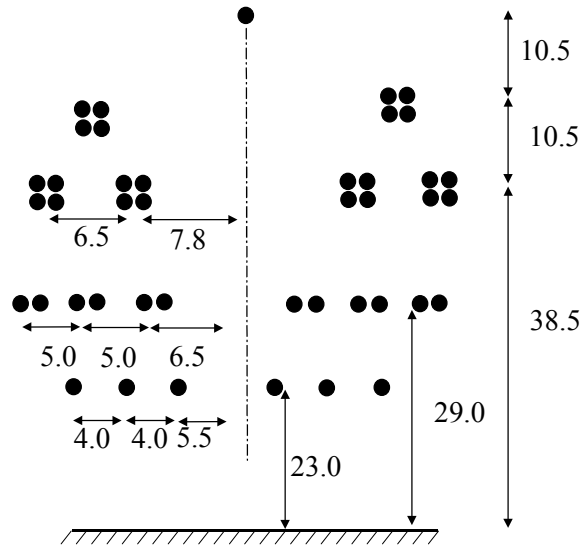

Fig. 8.11 Multi-circuits line configuration

Different test cases have been carried out along the entire range of the line length to investigate the impact of coupled circuits on the overall scheme accuracy. Fig. 8.12 shows the overall accuracy of each voltage level as a percentage of its total line length. In the results, the overall accuracy is still acceptable for both 110 and 220 kV as both voltage level circuits used the same conductor size of (Al/St 185/30), while both 380 kV line circuits have a remarkable lower

accuracy. This is mainly due to the difference in conductor size for the 380 kV line circuits. The shown results reveal the scheme efficacy for all multi circuit lines resulting from the ability of the modal transformation to eliminate the effects of mutual coupling perfectly.

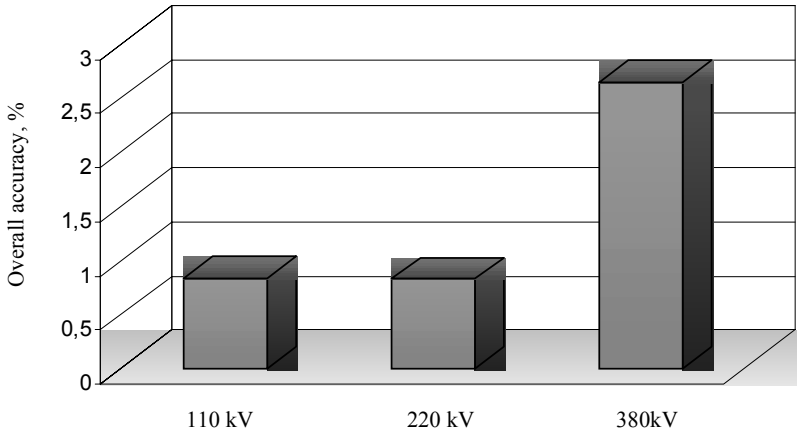

Fig. 8.12 Multi-circuit line accuracy evaluation

9 Conclusions

The general aim of this thesis is to develop an accurate fault location scheme that can solve the problems affecting the accuracy of the existing conventional fault locators. This is mainly due to the great benefits provided by detecting the fault position accurately including the maintenance and restoration time reduction as well as the economical aims. This consequently helps to fit the new deregulation policies and competitive marketing.

This work was proceeded in three sequential steps. Firstly, a thorough investigation of the performance of some known fault location methods was performed aiming to emphasize the basic characteristics of the fault location estimation procedure. This provided a good understanding of the process essence and helped to visualize the following contributions throughout the work successfully. Toward this goal, a group of 12 fault location algorithms covering most of the published algorithms has been introduced in this comparative study. EMTP-ATP has been employed to develop the test set with sophisticated power system models aiming to simulate the actual circumstances in the real field such as the line parameter distribution, mutual effects and line imbalance. More than 1200 simulation cases were developed for this objective. As a general conclusion, a better performance of two terminal algorithms has been emphasized as compared with other one terminal ones. However, the latter has the commercial superiority due to the extra requirements of two terminal methods such as the communication and synchronization equipment. On the other hand, one terminal algorithms with compensation features provide an acceptable performance as compared with the performance of two terminals ones. As concluded from this study, the mutual coupling among

the adjacent conductors is a serious problem, in which the total line impedance significantly changes resulting from the added impedance parts that are reflected mutually from other phases. Thus, it represents a serious problem affecting the accuracy of all protection equipment. Also, the effects of high impedance faults on the accuracy of all fault locators with both single and double terminal methods were emphasized. Both problems represent the major challenges that can remarkably affect the performance of all existing fault locators.

In order to eliminate the effects of both mutual coupling and fault resistance existence, a new fault location algorithm was introduced employing the modal transformation in conjunction with the apparent impedance approach. The essential goal of modal transformation is to transform some coupled equations into decoupled ones resulting in diagonalized equation matrices. Thus, the solution of the multi-phase transmission line equations will be simpler since every decoupled equation will be treated as a single phase line. This decoupling was, therefore, a perfect solution for those problems resulting from mutual coupling effects. On the other hand, the apparent impedance approach provides an effective compensation for remote current infeed and pre-fault loading current. The combination of both tools results in a superior fault location algorithm suitable for both single and two terminal lines depending on single end data. The behavior of the proposed algorithm was evaluated by employing ATP-EMTP and MATLAB. All applied tests revealed a high accuracy and promising performance for all fault situations. However, measurable estimation errors were recorded through the cases that associated with very high fault resistance values in addition to remote infeed and loading currents. Although the proposed algorithm is characterized with a solid improvement over the existed ones, it still suffers from the remarkable errors during high impedance faults. Hence, the need for further enhancements is obvious.

In the third part, AI-based tuning was established tuning the modal transformation-based algorithm to compensate the total errors that can not be eliminated conventionally. The AI-based tuner aims basically to provide the proposed fault location algorithm with a generated correction index. This, in order to adapt the estimated fault distance, reduces the total estimation error. The great capabilities of AI tools of non-linear mapping were successfully employed to perform the aimed tuning which only depends on the available information at the locator position. In order to realize the optimal AI tool, both ANN and FL systems were examined to perform the required mapping. Different ANN structures including MLF, RBF and Elman networks were tested for the ANN-based tuners with a variety of training methods. Whereas the ANFIS training

paradigm for FL system training was employed to optimize the FL-based tuner. MATLAB was selected as the platform for developing all tuning tools with its powerful toolbox for ANN and FL systems. As revealed from the tests of all developed tuners, FL and ANN are considered as powerful tools for nonlinear mapping and function approximation. Unlike conventional mathematical methods, both tools have the potential to approximate any complex function without considering simplifying assumptions. However, FL-based tuner has a faster training speed and a better accuracy from the protection viewpoint. On the other hand, the major problem when designing FL-based systems with ANFIS modeling concerns with the network stability. This mainly results from the complicated structure of the adopted neural network for ANFIS model (five layer feedforward network). Thus, increasing either the selected number of inputs or the adopted memberships for each input affect the resulted stability of the overall network. This requires the employment of the most suitable inputs in addition to the minimum requirement of the adopted memberships. Also, increasing the collected training data remarkably helps to keep a sufficient stability. Finally, the overall FL-based fault location tuner was introduced, which provides a complete coverage of all fault cases even with high resistance values up to 1kΩ. As seen from the simulation investigations, the overall scheme successfully deals with all loading conditions as well as the variation of line configuration including the rated voltage, power and the line length. Thus, the thesis presented a new perspective providing the universality for AI-based tools for power system protection applications. This provides a further enhancement to realize a practical and reliable intelligent fault locator.

The overall scheme, comprising from the modal transformation-based algorithm in conjunction with the FL-based universal tuner, was subjected to a variety of advanced test cases to evaluate its performance. These test cases included some situations that are real challenges not only for fault locator algorithms, but also for all protection equipment of transmission protection. As revealed from these tests, the overall scheme shows a high immunity to the existence of the non-linear arcs that usually occur with temporary faults. Also, the scheme shows a superior performance for multiple-loading (infeed) lines; when all loading (infeeding) stations data are available. Also, the lines with partially coupled parts or with multiple coupled circuits have no significant influence on the scheme accuracy. However, it was found that the existence of an inductive element (as a part of the grounding means of the main transformers) remarkably affects the scheme accuracy. This is a general characteristic of all protection equipment that depends on the apparent impedance approach.

In general, the proposed scheme presents a precise fault location algorithm suitable for both single and multi-circuit lines covering all fault types including permanent and transient fault cases for a wide range of the added fault resistance. However, the scheme performance is only restricted for the systems that are grounded solidly or through a resistive element. Thus, the scheme presents an ideal candidate for all high voltage networks as they are usually solidly or through a low resistance grounded. For medium voltage or distribution networks, the scheme can be efficiently used with only networks that are grounded solidly or through a pure resistance element. Unfortunately, most of medium or lower voltage networks in Germany are grounded through resonant grounding means. Thus, employing the proposed scheme for those networks is not beneficial.

The following recommendations may help the further contributions in this area.

- Modal analysis shows a great ability for eliminating the coupling effects. It results in simplifying the mathematical basis for protection algorithms for multi-terminal lines. Thus, it may be more helpful to develop more protection functions in the future.

- Considering the universal characteristics for intelligent protection functions is a real encouragement to develop a widely used commercial intelligent tool for protection equipment in the future.

- Resonant or inductive grounded systems are still real challenges not only for fault locators, but also for all protection equipment. These cases require further efforts to provide them with extra proper protection functions.

- The importance of the information availability of all line terminals at the line main station is obvious. This requires further efforts to enhance the communication and control equipment for transmission networks.

Throughout the time during the work described in this thesis, it contributed into the following publications:

[1] T. Kawady and J. Stenzel, “Investigation of practical problems for digital fault location algorithms based on EMTP simulation”, IEEE/PES Transmission and Distribution Conference and Exhibition: Asia-Pacific, Yokohama, Japan, 6-10, October, 2002, pp. 118-123.

[2] T. Kawady and J. Stenzel, " A new single end approach for transmission line fault location using modal transformation", 13th International Conference on Power System Protection, Bled, Slovenia, September 25-27, 2002, pp. 98-103.

[3] T. Kawady and J. Stenzel, "A Practical Fault Location Approach for Double Circuit Transmission Lines Using Single End Data", IEEE Transaction on Power Delivery, Vol. 18, No. 4, Oct. 2003, pp. 1166-1173

[4] T. Kawady and J. Stenzel, "A Precise High Impedance Fault Locator Using Single End Data", the 38th Universities Power Engineering Conference, UPEC 2003, Thessaloniki-Greece, Sept. 1-3, 2003, pp. 613-616.

[5] T. Kawady and J. Stenzel, " A new adaptive fault location approach for arcing/non-arcing ground faults", The 9th International Middle East Power Systems Conference, MEPCON 2003, Minoufiya University, Shebin El-Kome, Egypt, 16-18 Dec. 2003.

[6] T. Kawady and J. Stenzel, "Comparison of Adaptive fuzzy Systems and Artificial Neural Networks for Power System Protection Purposes", 14th International Conference on Power System Protection, Bled, Slovenia, 28 Sept. to 1 Oct., 2004, pp. 69-74.

[7] T. Kawady and J. Stenzel, "A Practical Intelligent Fault Location Approach With Universal Characteristics", 14th International Conference on Power System Protection, Bled, Slovenia, 28 Sept. to 1 Oct., 2004, pp. 181-186.

Appendix A:
Digital Fourier Transform Description

Phasor estimation approaches represent the basic core for digital protection schemes. Among the different approaches for this purpose, Discrete Fourier Transform (DFT) is still considered the most dependable and popular one since the 1980s till now. Generally speaking, any periodic function f(t) can be normally represented by a Fourier series of discrete harmonics. Let the continuous function f(t) be represented in the interval (t_0, t_0+T) as a Fourier series as

$$f(t) = \frac{a_0}{2} + \sum_{k=1}^{\infty} (C_k \cos(k\omega_0 t) + S_k \sin(k\omega_0 t)) \qquad (A.1)$$

where ω_0 is the angular fundamental frequency, a_0 is the dc component and S_k , C_k are the sine and cosine components respectively of the Fourier coefficients for the k-th harmonic component. These coefficients can be written as follows:

$$\frac{a_0}{2} = \frac{2}{T} \int_{t_0}^{t_0+T} f(t)dt \qquad (A.2)$$

$$S_k = \frac{2}{T} \int_{t_0}^{t_0+T} f(t)\sin(k\omega_0 t)dt \qquad (A.3)$$

$$C_k = \frac{2}{T} \int_{t_0}^{t_0+T} f(t)\cos(k\omega_0 t)dt \qquad (A.4)$$

If the waveforms are sampled with N samples per cycle with a sampling time of Δt, the integral of equation (A.3) can be rewritten as

$$S_k = \frac{2}{N\Delta t}\left[f(t_0)\sin\omega_0 t_0 + f(t_1)\sin\omega_0 t_1 + \ldots\ldots\ldots + f(t_{N-1})\sin\omega_0 t_{N-1} + f(t_N)\sin\omega_0 t_N\right] \qquad (A.5)$$

Then equation (A.5) can be rewritten as

$$S_k = \frac{2}{N}\sum_{j=1}^{N} f_j \sin\left(\frac{2\pi kj}{N}\right) = \frac{2}{N}\sum_{j=1}^{N} f_j W_{k,j} \qquad (A.6)$$

Where f_j is the j-th sample of the function f and $W_{k,j}$ is the weighting factor for the j-th sample used to calculate the the S_k. Where $W_{k,,j}$ can be represented as

$$W_{k,j} = \sin(k\omega_0 t_j) = \sin\left(\frac{2\pi k}{T} j\Delta t\right) = \sin\left(\frac{2\pi kj}{N}\right) \qquad (A.7)$$

Similarly the cosine coefficient C_k can be represented as

$$C_k = \frac{2}{N}\sum_{j=1}^{N} f_j \cos\left(\frac{2\pi kj}{N}\right) = \frac{2}{N}\sum_{j=1}^{N} f_j V_{k,j} \qquad (A.8)$$

where the related cosine weighting factor $V_{k,j}$ can be represented as

$$V_{k,j} = \cos(\omega_0 t_j) = \cos\left(\frac{2\pi k}{T} j\Delta t\right) = \cos\left(\frac{2\pi kj}{N}\right) \qquad (A.9)$$

Hence, for a sampling rate of 32 samples per cycle, a 32 Fourier coefficients can be rewritten in a matrix form for both sine and cosine coefficients as

$$\mathbf{S} = \begin{bmatrix} S_1 \\ S_2 \\ \cdot \\ \cdot \\ S_{31} \\ S_{32} \end{bmatrix} = \begin{bmatrix} \sin\left(\frac{2\pi*1*1}{32}\right) & \sin\left(\frac{2\pi*1*2}{32}\right) & \ldots & \sin\left(\frac{2\pi*1*31}{32}\right) & \sin\left(\frac{2\pi*1*32}{32}\right) \\ \sin\left(\frac{2\pi*2*1}{32}\right) & \sin\left(\frac{2\pi*2*2}{32}\right) & \ldots & \sin\left(\frac{2\pi*2*31}{32}\right) & \sin\left(\frac{2\pi*2*32}{32}\right) \\ \cdot & \cdot & \ldots & \cdot & \cdot \\ \cdot & \cdot & \ldots & \cdot & \cdot \\ \sin\left(\frac{2\pi*31*1}{32}\right) & \sin\left(\frac{2\pi*31*2}{32}\right) & \ldots & \sin\left(\frac{2\pi*31*31}{32}\right) & \sin\left(\frac{2\pi*31*32}{32}\right) \\ \sin\left(\frac{2\pi*31*1}{32}\right) & \sin\left(\frac{2\pi*31*2}{32}\right) & \ldots & \sin\left(\frac{2\pi*32*31}{32}\right) & \sin\left(\frac{2\pi*32*32}{32}\right) \end{bmatrix} \begin{bmatrix} F_1 \\ F_2 \\ \cdot \\ \cdot \\ F_{31} \\ F_{32} \end{bmatrix}$$

(A.10)

$$\mathbf{C}=\begin{bmatrix} C_1 \\ C_2 \\ . \\ . \\ C_{31} \\ C_{32} \end{bmatrix}=\begin{bmatrix} \cos(\frac{2\pi*1*1}{32}) & \cos(\frac{2\pi*1*2}{32}) & . & . & \cos(\frac{2\pi*1*31}{32}) & \cos(\frac{2\pi*1*32}{32}) \\ \cos(\frac{2\pi*2*1}{32}) & \cos(\frac{2\pi*2*2}{32}) & . & . & \cos(\frac{2\pi*2*31}{32}) & \cos(\frac{2\pi*2*32}{32}) \\ . & . & . & . & . & . \\ . & . & . & . & . & . \\ \cos(\frac{2\pi*31*1}{32}) & \cos(\frac{2\pi*31*2}{32}) & . & . & \cos(\frac{2\pi*31*31}{32}) & \cos(\frac{2\pi*31*32}{32}) \\ \cos(\frac{2\pi*32*1}{32}) & \cos(\frac{2\pi*32*2}{32}) & . & . & \cos(\frac{2\pi*32*31}{32}) & \cos(\frac{2\pi*32*32}{32}) \end{bmatrix}\begin{bmatrix} F_1 \\ F_2 \\ . \\ . \\ F_{31} \\ F_{32} \end{bmatrix} \tag{A.11}$$

For the k_{th} harmonic, the complete phasor can be defined using the resulting sine and cosine coefficients as follows:

$$F_k = \sqrt{S_k^2 + C_k^2} \tag{A.12}$$

$$\theta_k = \tan^{-1}\frac{S_k}{C_k} \tag{A.13}$$

Fig. A.1 summarizes the DFT calculation procedure as shown below as

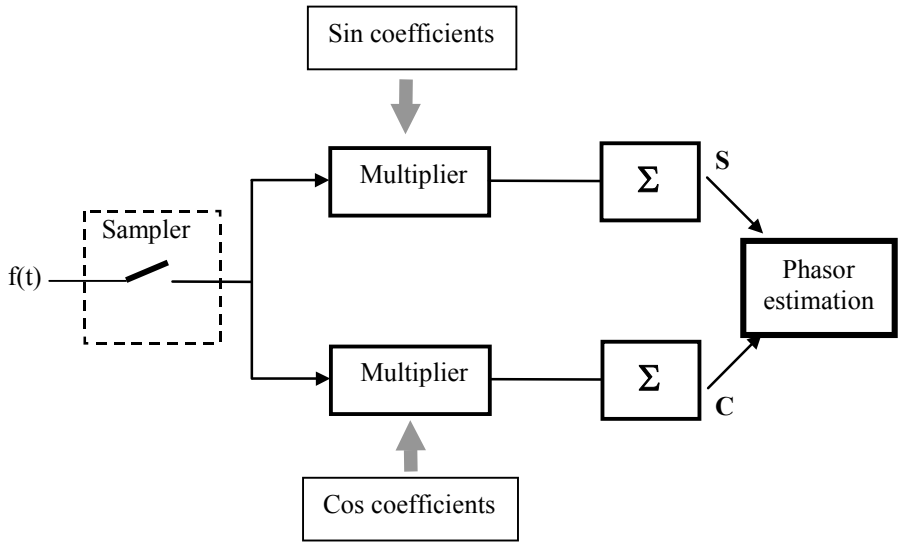

Fig. A.1 DFT routine schematic

Appendix B:
Power System Simulation Data for ATP

During the work through this thesis, different line parameters were considered for 110, 220 and 380 kV transmission systems. Three different conductors were selected: Al/St 185/30, Al/St240/40 and Al/St 300/50. Table B.1 summarizes the main specifications for each conductor type according to DIN 48204.

Table B.1 Selected conductor parameters

Cond. Type	R Ω/km(20°)	r (mm)	A (mm^2)	Bundle spacing (cm)
Al/St 185/30	0.157	9.5	183.8	40.0
Al/St 240/40	0.119	10.95	243.0	40.0
Al/St 300/50	0.096	12.25	304.3	40.0

For each voltage level, two different tower configuration systems were selected. Table B.2 presents the tower configuration for each system describing the conductor spacing, number of bundles and the dimensions according to the configurations in Fig. B.1.

Table B.2 Selected tower configuration dimensions

Rated voltage	Conf.	No. of bundles	Tower dimensions, m						
			h_1	h_2	h_3	H_g	d_1	d_2	d_3
110 kV	(a)	1	23.0	23.0	23	8.5	5.5	9.5	13.5
	(b)	1	19.0	23.5	28.0	4.5	4.0	5.5	4.0
220 kV	(a)	2	29.0	29.0	29.0	10.5	6.5	11.5	16.5
	(b)	2	22.0	27.5	33.0	5.5	5.5	6.75	5.5
380 kV	(a)	4	39.5	39.5	39.5	10.5	7.8	14.3	20.8
	(c)	4	28.0	28.0	38.5	10.5	7.8	14.3	10.8

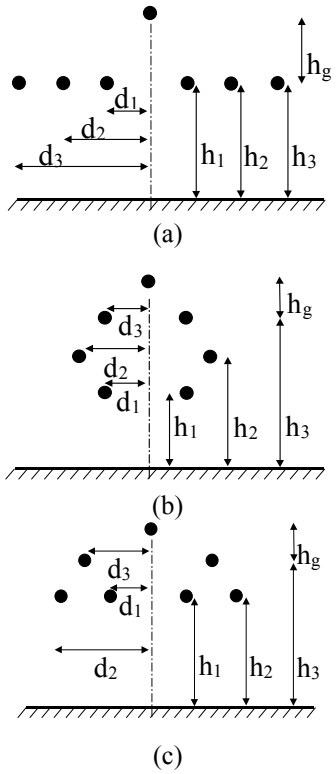

Fig. B.1 Selected tower configuration description

The subroutine LINE CONSTANT in the EMTP-ATP is employed for each system to calculate the associated parameters based on the above conductor configurations using the distributed parameter line model for each transmission system.

Appendix C:
Foundations of Modal Theory for Matrix Solution for Polyphase Systems

In 1963, Wedepohl established the basic fundamentals of matrix methods for solving polyphase systems using the phenomena of modal theory [99]. The aim of this appendix is to emphasize the basic outlines of the modal theory. For this purpose, the basic equations for a single conductor are described first. Then the introduced analysis is expanded to cover the two conductor lines and finally the polyphase lines.

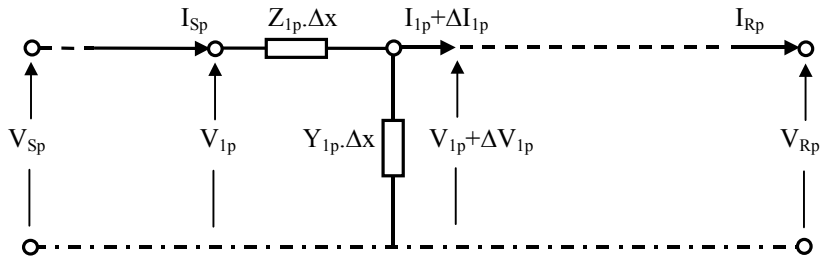

Fig. C.1 Single conductor with earth return

Fig. C.1 shows the circuit diagram of a single conductor line with earth return, where the indices S, R, and p refer to the sending, receiving and phase quantities. For a specific small element of the line Δx, the fundamental equations relating to this element as functions of the conductor impedance Z_{1p} and admittance Y_{1p} are described as

$$\frac{dV_{1p}}{dx} = -Z_{1p}I_{1p} \qquad (C.1)$$

$$\frac{dI_{1p}}{dx} = -Y_{1p}V_{1p} \tag{C.2}$$

Writing the second derivative for both equations (C.1) and (C.2) yields,

$$\frac{d^2V_{1p}}{dx^2} = -Z_{1p}Y_{1p}I_{1p} \tag{C.3}$$

$$\frac{d^2I_{1p}}{dx^2} = -Y_{1p}Z_{1p}V_{1p} \tag{C.4}$$

These differential equations can be then solved for V_{1p} as

$$V_{1p} = Ae^{-\lambda_1 x} + Be^{\lambda_1 x} \tag{C.5}$$

where A and B are arbitrary constants and $\lambda_1 = \sqrt{Z_{1p}Y_{1p}}$ is the propagation constant.

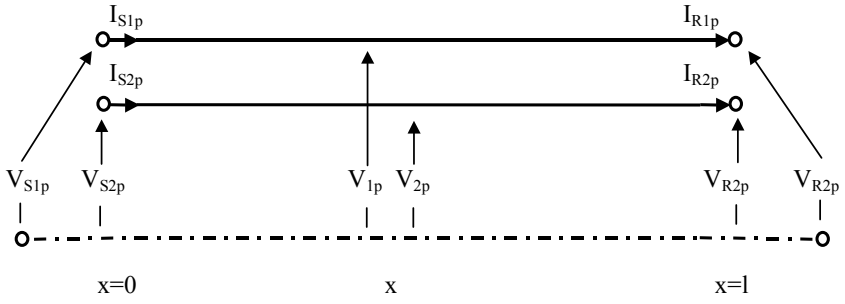

Fig. C.2 Two conductor line with earth return

The above mathematical formalization can be modified to fit the two conductor line with earth return shown in Fig. C.2. through the following equations:

$$\frac{dV_{1p}}{dx} = -Z_{11p}I_{1p} - Z_{12p}I_{2p} \tag{C.6}$$

$$\frac{dV_{2p}}{dx} = -Z_{21p}I_{1p} - Z_{22p}I_{2p} \tag{C.7}$$

$$\frac{dI_{1p}}{dx} = -Y_{11p}V_{1p} + Y_{12p}V_{2p} \tag{C.8}$$

$$\frac{dI_{2p}}{dx} = Y_{21p}V_{1p} - Y_{22p}V_{2p} \tag{C.9}$$

Z_{11} and Z_{12} (or Z_{21}) are the self and mutual impedance parts respectively. Also, Y_{11}, Y_{12} (or Y_{21}) are the self and mutual admittance parts respectively. These equations can be rewritten in matrix notation as

$$\frac{d}{dx}\mathbf{V}_p = -\mathbf{Z}_p\ \mathbf{I}_p \tag{C.10}$$

$$\frac{d}{dx}\mathbf{I}_p = -\mathbf{Y}_p\ \mathbf{V}_p \tag{C.11}$$

where $\mathbf{V}_p$ and $\mathbf{I}_p$ are the column matrices corresponding to the voltage and current values. $\mathbf{Z}_p$ and $\mathbf{Y}_p$ are the square matrices for impedance and admittance values respectively. The corresponding diagonal elements refer to the self values, whereas the others refer to the mutual parts for both impedance and admittance matrices. Then the following equation can be derived as

$$\frac{d^2}{dx^2}\mathbf{V}_p = -\mathbf{P}\ \mathbf{V}_p \tag{C.12}$$

$$\frac{d^2}{dx^2}\mathbf{I}_p = -\mathbf{P}\ \mathbf{I}_p \tag{C.13}$$

$$\text{where } \mathbf{P} = \begin{bmatrix} Z_{11p}Y_{11p} - Z_{12p}Y_{12p} & Z_{11p}Y_{12p} - Z_{12p}Y_{22p} \\ -(Z_{11p}Y_{12p} - Z_{12p}Y_{22p}) & -(Z_{12p}Y_{12p} - Z_{22p}Y_{22p}) \end{bmatrix} \tag{C.14}$$

The modal quantity matrices $\mathbf{V}_m$ and $\mathbf{I}_m$ can be derived through the selected proper transformation $\mathbf{T}_v$ and $\mathbf{T}_i$ as

$$\mathbf{V}_p = \mathbf{T}_v\ \mathbf{V}_m \tag{C.15}$$

$$\mathbf{I}_p = \mathbf{T}_i\ \mathbf{I}_m \tag{C.16}$$

Substituting in equations (C.12) and (C.13) yields,

$$\frac{d^2}{dx^2}\mathbf{V}_m = \mathbf{T}_v^{-1}\mathbf{P}\ \mathbf{T}_v\mathbf{V}_m = \lambda_V^2\mathbf{V}_m \tag{C.17}$$

$$\frac{d^2}{dx^2}\mathbf{I}_m = \mathbf{T}_i^{-1}\mathbf{P}\ \mathbf{T}_i\mathbf{I}_m = \lambda_i^2\mathbf{I}_m \tag{C.18}$$

The transformation matrices should be selected in such a way that $\boldsymbol{\lambda}_v^2$ and $\boldsymbol{\lambda}_{\hat{i}}^2$ are diagonal matrices of the forms as

$$\boldsymbol{\lambda}_v^2 = \begin{bmatrix} \lambda_{v1}^2 & 0 \\ 0 & \lambda_{v2}^2 \end{bmatrix} \tag{C.19}$$

$$\boldsymbol{\lambda}_i^2 = \begin{bmatrix} \lambda_{i1}^2 & 0 \\ 0 & \lambda_{i2}^2 \end{bmatrix} \tag{C.20}$$

The mutual parts in both equations (C.17) and (C.18) are canceled resulting in a direct solution of the equation groups. In order to be mathematically possible, $\mathbf{PT}_v$ should be equal to $\mathbf{T}_v\boldsymbol{\lambda}_v^2$. This condition ca be rewritten as

$$\mathbf{P}\,\mathbf{T}_v - \mathbf{T}_v\,\boldsymbol{\lambda}_v^2 = 0 \quad \text{or} \quad \det(\mathbf{P} - \boldsymbol{\lambda}_v^2) = 0 \tag{C.21}$$

Then Equation (C.21) can be rewritten as

$$\begin{bmatrix} (P_{11} - \lambda_{v1}^2)T_{v11} + P_{12}T_{v21} & (P_{11} - \lambda_{v2}^2)T_{v12} + P_{12}T_{v22} \\ P_{21}T_{V11} + (P_{22} - \lambda_{v1}^2)T_{v21} & P_{21}T_{V12} + (P_{22} - \lambda_{v2}^2)T_{v22} \end{bmatrix} = 0 \tag{C.22}$$

The corresponding condition for the current equation is similarly, where

$$\mathbf{P}\,\mathbf{T}_i - \mathbf{T}_i\,\boldsymbol{\lambda}_{\hat{i}}^2 = 0 \quad \text{or} \quad \det(\mathbf{P} - \boldsymbol{\lambda}_{\hat{i}}^2) = 0 \tag{C.23}$$

The same group of equations from (C.10) to (C.23) in their matrix representation can be directly applied on polyphase systems by expanding the matrix orders to fit the related system order. For a three phase coupled balanced system, the impedance and admittance matrices can be written as follows:

$$\mathbf{Z}_p = \begin{bmatrix} Z_{11p} & Z_{12p} & Z_{13p} \\ Z_{21p} & Z_{22p} & Z_{23p} \\ Z_{31p} & Z_{32p} & Z_{33p} \end{bmatrix} \tag{C.24}$$

$$\mathbf{Y}_p = \begin{bmatrix} Y_{11p} & -Y_{12p} & -Y_{13p} \\ -Y_{21p} & Y_{22p} & -Y_{23p} \\ -Y_{31p} & -Y_{32p} & Y_{33p} \end{bmatrix} \tag{C.25}$$

Owing to the line balance,

$$\mathbf{T}_v = \mathbf{T}_i = \mathbf{T} \tag{C.26}$$

$$\boldsymbol{\lambda}_v^2 = \boldsymbol{\lambda}_i^2 = \boldsymbol{\lambda}^2 \tag{C.27}$$

From the condition raised in equations (C.21) or (C.23), the sufficient condition to fulfill the decoupling requirement is as

$$\det(\mathbf{P} - \boldsymbol{\lambda}) = \det \begin{bmatrix} (P_{11} - \lambda_{11}^2) & P_{12} & P_{13} \\ P_{21} & (P_{22} - \lambda_{22}^2) & P_{23} \\ P_{31} & P_{32} & (P_{33} - \lambda_{33}^2) \end{bmatrix} = 0 \tag{C.28}$$

Solving the above equation for the unknowns λ_{11}^2, λ_{22}^2 and λ_{33}^2 as follows:

$$\lambda_{11}^2 = \frac{1}{2}\left(P_{11} + P_{22} + P_{12} + \sqrt{(P_{11} - P_{22} + P_{13})^2 + 8P_{13}P_{31}})\right) \tag{C.29}$$

$$\lambda_{22}^2 = \frac{1}{2}\left(P_{11} + P_{22} + P_{12} - \sqrt{(P_{11} - P_{22} + P_{13})^2 + 8P_{13}P_{31}})\right) \tag{C.30}$$

$$\lambda_{33}^2 = P_{11} - P_{12} \tag{C.31}$$

The corresponding transformation matrix [T] can be then forwardly found. Different values can be assigned for this matrix. As a common practice, the Clarke transformation matrix can be employed for the required transformation as

$$\mathbf{T}_V = \mathbf{T}_i = \mathbf{T} = \frac{1}{\sqrt{3}} \begin{pmatrix} 1 & \sqrt{2} & 0 \\ 1 & \frac{-1}{\sqrt{2}} & \frac{\sqrt{3}}{\sqrt{2}} \\ 1 & \frac{-1}{\sqrt{2}} & \frac{-\sqrt{3}}{\sqrt{2}} \end{pmatrix} \tag{C.32}$$

Finally, the corresponding modal impedance and admittance matrices can be found as

$$\mathbf{Z}_m = \mathbf{T}_v^{-1} * \mathbf{Z} * \mathbf{T}_v \tag{C.33}$$

$$\mathbf{Y}_m = \mathbf{T}_i^{-1} * \mathbf{Y} * \mathbf{T}_i \tag{C.34}$$

Appendix D:
ANNs Training Outlines

D.1 MLF Training Procedures

D.1.1 Basic BP training algorithm

Fig. D.1 Summarizes a general schematic of the Backpropagation (BP) supervised incremental training. It is generally considered as the workhorse in the area of training neural networks. It was invented independently by several authors since the 1960s. In 1986, Rumelhart, Hinlton and McClelland rediscovered and modified it to suit neural network training techniques. Now, it is the most widely used method for training (MLF) networks, in spite of the other several implemented algorithms.

For the simple construction of a MLF network having n inputs, the sum of inputs to the j-th hidden neuron for each training example can be written as

$$u_j = \sum_{i=1}^{n} IN_i . W_{ij} + W_j \qquad (D.1)$$

where the IN_i is the i-th input signal, n is the number of inputs and u_j is the signal giving the weighted sum of all inputs. The W_{ij} and W_j refers to the connections weights and neuron bias respectively. Applying the activation function F yielding,

$$i_j = F_j(u_j) \qquad (D.2)$$

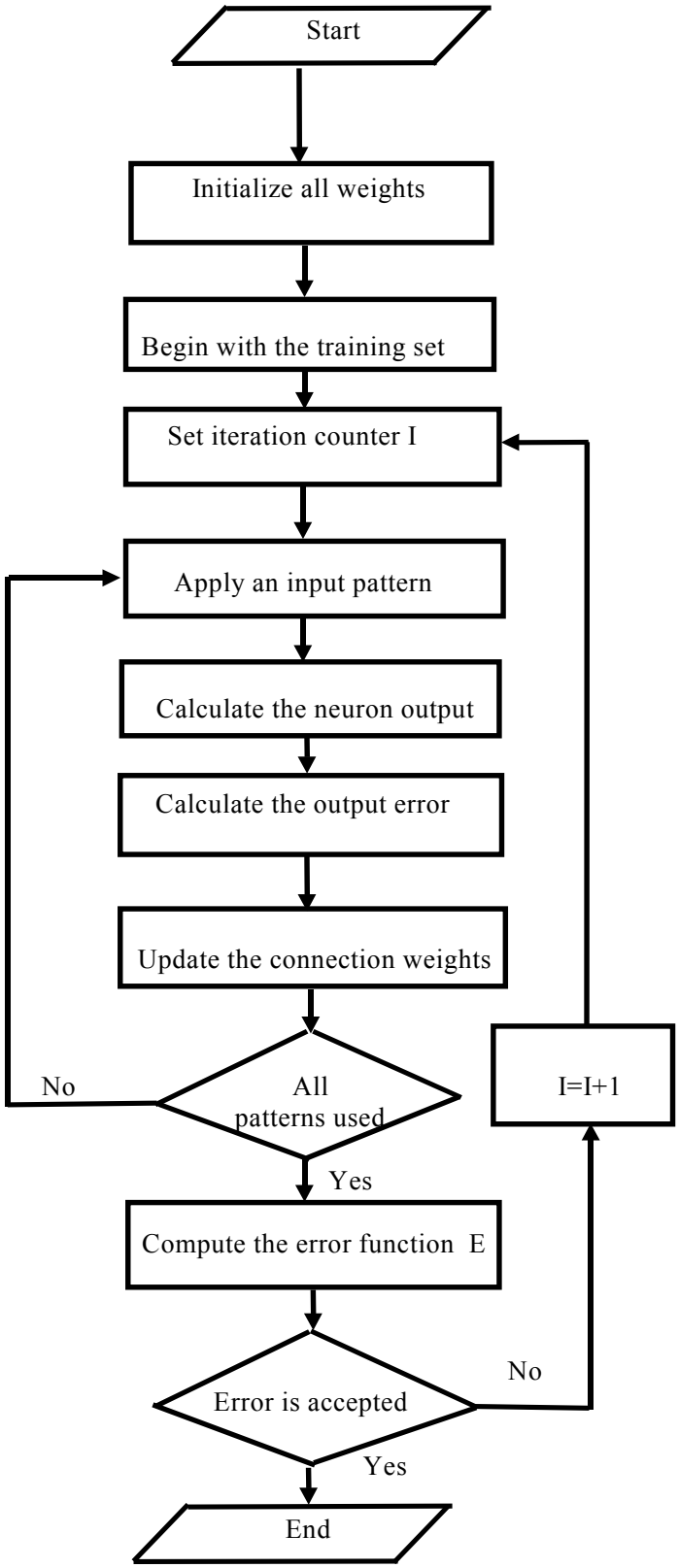

Fig. D.1 Supervised BP incremental training

where i_j is the output of the j-th hidden neuron. Similarly, the sum of inputs to the k-th output neuron can be obtained as

$$s_k = \sum_{j=1}^{h} W_{kj}.i_j + W_k \tag{D.3}$$

where s_k is the signal giving the weighted sum of all hidden neuron outputs and h is the number of hidden neurons. Then, the output of the k-th output neuron can be expressed as

$$y_k = F_k(s_k) \tag{D.4}$$

The aim of learning algorithm is to minimize the instantaneous squared error E of the output signal which is computed as

$$E = \frac{1}{2}(d_k - y_k)^2 = \frac{1}{2}e^2 \tag{D.5}$$

where e is the instantaneous error between the computed output y_k and the desired one d_k. In order to minimize the error for a given set of weights, the gradient rule can be applied to equation (D.5) which yields,

$$\frac{\partial E}{\partial W_{kj}} = -(d_k - y_k).\frac{\partial}{\partial W_{kj}}(F(s_k)) \tag{D.6}$$

Applying the differentiation chain rule yields,

$$\frac{\partial E}{\partial W_{kj}} = -(d_k - y_k).\frac{\partial F_k}{\partial s_k}.\frac{\partial s_k}{\partial W_{kj}} \tag{D.7}$$

where

$$\frac{\partial s_k}{\partial W_{kj}} = \frac{\partial}{\partial W_{kj}}(\sum_{1}^{h} W_{kj}.i_j + W_k) = i_j \tag{D.8}$$

Substituting from equation (D.8) into equation (D.7) yields,

$$\frac{\partial E}{\partial W_{kj}} = -(d_k - y_k).F_k'(s_k).i_j \tag{D.9}$$

As far as the magnitude of the weight change is concerned, it is taken to be proportional to the negative gradient obtained in equation (D.9). Thus, the weights of the output neurons in terms of the previous iteration t are updated according to

$$W_{kj}(t+1) = W_{kj}(t) + \Delta\ W_{kj}(t) \tag{D.10}$$

where

$$\Delta W_{kj}(t) = -\mu(d_k - y_k)F'_k.(s_k).i_j \tag{D.11}$$

and μ is the learning rate parameter determining the speed of convergence to the minimum. Its value is usually positive and less than 1. Similarly, the weights of hidden neurons are updated. This procedure is continuously repeated until an acceptable total error was reached. If the training set is prepared containing p pairs of input/output learning examples. The global error can be found as

$$E = \sum_p E_p = \frac{1}{2}\sum_P \sum_k \left(d_{kp} - y_{kp}\right)^2 \tag{D.12}$$

where d_{kP} and y_{kP} are the desired and actual outputs of the k-th output neuron for the p-th learning example.

The above explanation shows briefly the basic incremental mode of BP training, in which the list of weights is incrementally updated at each training case. Another mode of BP is possible by batch training, in which all inputs are applied to the network before the weights updating. Thus the weights are updated according to the overall sum of the resulted errors for all training cases rather than the individual training error for each case.

D.1.2 BP with adaptive learning rate

As shown from equation (D.11), the learning rate (μ) controls the convergence speed during training. With standard BP training, the learning rate is kept constant throughout the training procedure. On the other hand, the training performance is sensitive to the selected learning rate. If learning rate is selected to be high, the training may oscillate and become unstable. If it is selected to be small, the training consumes a long time to converge. Although, setting the optimal learning rate before starting the training process may improve the process, it does not get the optimum setting of the learning rate as the required optimum values actually changes

during the learning process. The essential aim of the variable learning rate is attempting to keep the learning step size as large as possible while keeping the learning stability. Further details are available in [86].

D.1.3 BP with momentum terms

The momentum terms allow the network to respond not only to the local gradient, but also to the recent trends in the error surface. Acting like a low pass filter, momentum allows the network to ignore small features in the error surface. Thus the network may get stuck into a shallow local minimum without the momentum terms. To include the momentum term, equation (D.10) for updating the weights is improved by introducing the momentum term α as

$$W_{kj}(t+1) = W_{kj}(t) + \Delta\ W_{kj}(t) + \alpha\ W_{kj}(t-1) \qquad \text{(D.13)}$$

As seen in the above equation, the weights are updated equally to the sum of a fraction of the last weight change in addition to the new resulting recent weight change from the BP [66, 86].

D.1.4 Numerical optimization training for MLF networks

In spite of the wide applicability of the BP and other further enhancements over the standard form, it suffers from, in most cases, the slow convergence. It may therefore not be the optimum tool for large scale training sets or complex tasks. To solve these problems, research efforts have been directed to employ numerical optimization techniques to perform the training procedure. Among these efforts, Levenberg-Marquardt (LM) and Conjugate Gradient (CG) training algorithms arise as powerful tools for training purposes [100, 101].

While BP is a steepest descent algorithm, the LM algorithm is an approximation to Newton's methods. As seen in the BP equations, the error function E, derived in equation (D.5), is minimized using the gradient optimization as shown in the equations from (D.6) to (D.12). While the weight update in LM optimization is performed through the Newton's method. Also the CG is a class of methods for unconstrained optimization employed for optimization purposes. It is therefore expected to optimize efficiently the ANN parameters. The mathematical basis for both algorithms is beyond the scope of this thesis, whereas the details are fully described in their relevant references. The MATLAB provides a powerful, direct and friendly-using platform to employ these algorithms for training purposes.

D.2 Training of Elman Networks

Elman networks are considered to a special constructed multi-layers network by enabling special feedback extracted from the hidden neurons to be added to the inputs. It can be therefore trained forwardly similar to the normal MLF network. The training procedures should modified to include the output of the hidden elements of the last training case into the present training running. The same MATLAB training routines can be directly employed as well.

D.3 RBF network Training

A classical RBF network perform a mapping from the n inputs to the scalar output according to the relation,

$$Y(x) = W_0 + \sum_{i=1}^{n} (W_i \phi(x, c_i) \tag{D.14}$$

where W_0 and W_i denote the bias and the connection weights respectively. ϕ denotes the non-linear transformation of each input x around each fixed center c_i. Thus the core of the RBF training is to choose the proper non-linear transformation and the centers that can enable the RBF network to perform the required mapping. For this purpose the Orthogonal Least Square (OLS) optimization can be employed to find out the adequate network construction. Thus RBF network can be considered as a special case of the linear regression model expressed as

$$d(t) = \sum_{i=1}^{n} p_i(t)\theta_i + \varepsilon(t) \tag{D.15}$$

where d(t) is the desired output, the elements of θ_i are the network parameters and $p_i(t)$ are considered as the regressors and assumed to be fixed functions of the inputs $x_i(t)$. The error signal $\varepsilon(t)$ is assumed to be uncorrelated with the regressors $p_i(t)$. As clear from equation (D.15), the fixed centers c_i with the given non-linearity ϕ correspond to the regressor $p_i(t)$. Then the training procedure essentially aims to set the proper RBF centers from the training data as well as the associated connection weights. Thus the OLS optimization procedure can be considered as an optimum tool for this purpose. The exact solution of this optimization problem is set via a total number of centers equal to the number of the vectors in the training set. However, this situation may be not the best solution in those cases having huge training sets [102].

Appendix E:
FL-ANFIS Structure and Training

The basic challenge for developing a fuzzy-based systems is how to set the parameters of the fuzzy system. The "Adaptive Network-based Fuzzy Inference System (ANFIS)" architecture for fuzzy network structure optimization is employed for this purpose. ANFIS simulates the fuzzy structure using the feedforward neural network to make use of the training ability of the ANN so that the FL system parameters can be optimized using the same adopted algorithms used for ANNs. Once the FL system parameters are optimized, the FL can be used independently based on the resulted parameter. Generally speaking, a fuzzy inference system performs the fuzzy reasoning through the following steps,

- Firstly the network inputs are extracted. These inputs are then compared with the adjusted membership functions associated with the antecedent part of the rules to get the membership values of each linguistic quantity.
- Combine through a specific T-norm operator (multiplication or minimum usually) the weight (firing strength) of each rule.
- Depending on the weights of the rules, the consequent of each rule is generated.
- Finally the produced consequents are aggregated to produce the crisp output.

Among the different types of fuzzy reasoning methods, Sugeno inference type is the most suitable for ANFIS structure. In Sugeno-based fuzzy systems all inputs are described with a set of selected overlapping membership functions, while the outputs are described as a linear function of the inputs. Fig. E.1 shows a simple FL system with only two inputs x and y and two rules using Sugeno inference model. The adopted two rules can be described as follows:

Rule1: if x is A1 and y is B1, then $f_1=p_1x_1+q_1y_1+c_1$

Rule2: if x is A2 and y is B2, then $f_2=p_2x_2+q_2y_2+c_2$

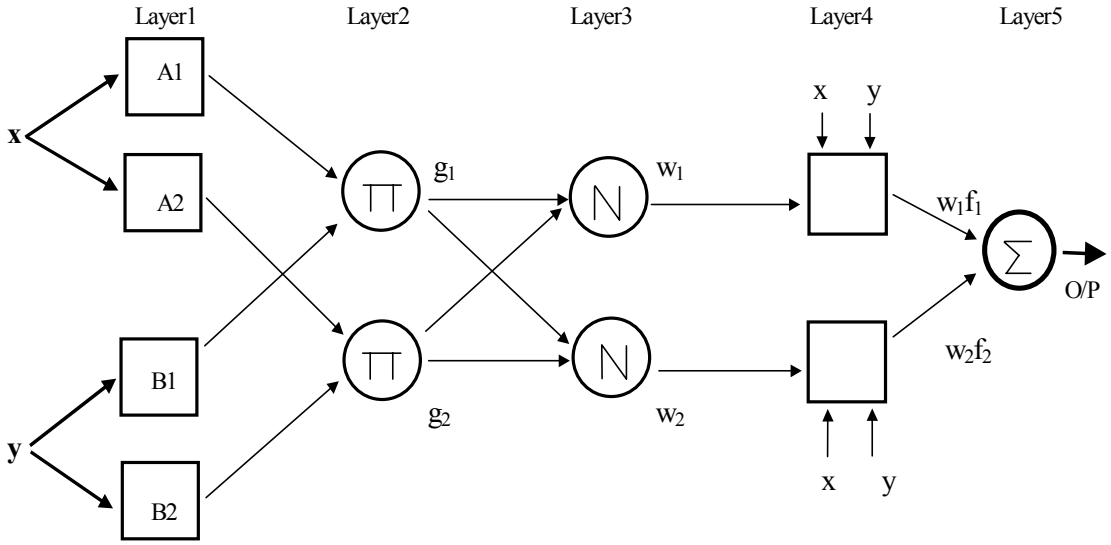

Fig. E.1 Two inputs simple ANFIS network

Then the output of each of the network layers can be described as follows:

Layer1: The basic objective of this layer is to assign the related membership function value to each input to specify the degree to which the given input (x or y here) satisfies the linguistic quantities (A_i or B_i and i=1, 2) . Thus the output O for both inputs x and y out of this layer can be described as

$$O_{A,i} = \mu_{Ai}(x), \quad i=1,2 \tag{E.1}$$

$$O_{B,i} = \mu_{Bi}(y), \quad i=1,2 \tag{E.2}$$

Where μ_{A1}, μ_{A2}, μ_{B1} and μ_{B2} are the assigned four memberships for both x and y inputs respectively. As an example, the μ_{A1} is described with the Bell-shape membership as

$$\mu_{A1}(x) = \frac{1}{1+\left[\left(\frac{x-c_1}{a_1}\right)^2\right]^{b1}} \tag{E.3}$$

where a_1, b_1, c_1 are the parameters of this membership owing to the the first linguistic quantity A1.

Layer2: Every node in this layer is a fixed node whose output is the product of all incoming inputs to find out the weight of each rule (the firing strength) as seen below as

$$g_1 = \mu_{A1}(x) \times \mu_{B1}(y) \quad \text{(E.4)}$$

$$g_2 = \mu_{A1}(x) \times \mu_{B1}(y) \quad \text{(E.5)}$$

Layer 3: The output of every node in this layer is the ratio of the firing strength of this nod to the sum of all firing strengths of all rules. This output is the normalized firing strength and can be described as

$$w_i = \frac{g_i}{g_1 + g_2}, \; i=1,2 \quad \text{(E.6)}$$

Layer 4: Each node of this layer is connected to all network inputs (here x and y) and a node in the foregoing layer. The objective of this layer is to calculate consequent parameter of each rule as

$$w_1 f_1 = w_1(p_1 x_1 + q_1 y_1 + c_1) \quad \text{(E.7)}$$

$$w_2 f_2 = w_2(p_2 x_2 + q_2 y_2 + c_2) \quad \text{(E.8)}$$

Layer 5: This layer is the output layer so that it computes the final network output by summing all the outputs from the previous layers as

$$O/P = \sum w_i f_i \;, \; i=1,2 \quad \text{(E.9)}$$

The core of the ANFIS structure is the ability to adjust both the antecedent and consequent parameters of the constructed network using BP or Least Square algorithms (or both algorithms in a hybrid manner). However, the rules should be previously prepared. MATLAB provides a special routine for ANFIS training, providing also a preliminary construction of the rule base using matrix partitioning. The weight of each preliminary rule is evaluated through the training procedure. Further details are available in the MATLAB FL-Toolbox manual [87].

Appendix F:
Deutsche Zusammenfassung

Fehlerortungssysteme dienen dazu, bei Auftreten eines Kurzschlusses auf einer Freileitung, die Fehlerstelle möglichst genau zu bestimmen. Damit wird es möglich, Reparaturarbeiten zur Wiederinstandsetzung der Leitung unmittelbar einzuleiten, um die Leitung wieder in Betrieb zu nehmen. Neben technischen Vorteilen durch verkürzte Ausfallzeiten hat das schnelle Erkennen der Fehlerstelle auch ökonomische Vorteile, da die Menge nicht zeitgerecht gelieferter Energie vermindert wird. Das Ziel dieser Arbeit war, ein genaues Fehlerortungssystem zu entwickeln, das die bekannten Nachteile von vorhandenen konventionellen Systemen vermeidet..

Die vorliegende Arbeit wurde in drei Schritten durchgeführt. Zum Beginn wurde eine gründliche Analyse der Leistungsfähigkeit der aus der Literatur bekannten Fehlerortungsmethoden durchgeführt. Es war möglich 12 unterschiedliche Gruppen zu bilden, denen die verschiedenen benutzten Algorithmen zugeordnet werden konnten. Damit konnten die Vor- und Nachteile der verschiedenen Verfahren herausgearbeitet werden. Es wurden weiterhin mit Hilfe des Programmsystems EMTP-ATP Testreihen entwickelt, die eine Beurteilung der verschiedenen Methoden erlaubte. Dazu wurden Netzmodelle aufgestellt, die es ermöglichten die Parameter, die die größten Einflüsse auf die Ungenauigkeit der Fehlerortung haben, in weiten Bereichen zu variieren. Mehr als 1200 Simulationsrechnungen wurden schließlich durchgeführt. Grundsätzlich kann gesagt werden, dass die Methoden zur Fehlerortung, die Daten von beiden Enden einer Leitung benutzen bessere Resultate liefern, als Methoden, die allein auf die Messdaten eines Leitungsendes angewiesen sind. Der Nachteil für die zweiseitigen Verfahren liegt jedoch darin, dass zusätzliche Kommunikationsverbindungen zwischen den

beiden Messstellen vorhanden sein müssen - ein nicht zu vernachlässigender Kostenfaktor. Bei diesen vergleichenden Untersuchungen wurde herausgefunden, dass einige Methoden, die mit den Daten eines Leitungsendes auskommen, durchaus akzeptable Ergebnisse liefern. Weiterhin konnte festgestellt werden, dass die größten Einflüsse auf die Genauigkeit zur Fehlerortbestimmung von den gegenseitigen Kopplungen der Leitungen und den unbekannten Fehlerwiderständen, z.B. durch den Lichtbogen, ausgehen. Diese beiden Einflussgrößen soweit möglich zu eliminieren oder zu kompensieren bildete die Aufgabenstellung für das weitere Vorgehen.

Im zweiten Schritt wurde ein Algorithmus zur Fehlerortbestimmung entwickelt, der darauf basiert, das die Leitungsdaten einer Transformation unterzogen werden, die es erlaubt auf entkoppelte Moden zurückzugreifen. Das Prinzip der modalen Transformation ist die Umwandlung einer voll besetzten Matrix in eine Diagonalform. Weiterhin wurde eine Scheinimpedanz eingeführt, die es ermöglichte die Belastung der Leitung vor Eintritt des Fehlers zu berücksichtigen. Das Verhalten des vorgeschlagenen Algorithmus wurde durch Simulationsrechnungen mit den Programmsystemen ATP-EMTP und MATLAB beurteilt. Alle angewandten Tests zeigten, dass der neu entwickelte Algorithmus eine hohe Genauigkeit bei der Bestimmung der Fehlerentfernung aufweist. Dabei wurden unterschiedliche Fehlersituationen betrachtet.

Im dritten Schritt wurde eine auf AI-Methoden basierende Optimierung eingeführt, um die Leistung des modalen transformationsbasierten Algorithmus weiter zu verbessern. Es wurden dazu die Tools ANN (Artificial Neural Networks) und FL (Fuzzy Logic) vom Programmsystem MATLAB eingesetzt um eine weitere Verminderung der Ungenauigkeiten bei der Fehlerortbestimmung zu erreichen. Dabei hat sich gezeigt, dass FL-Methoden zu besseren und schnelleren Ergebnissen führen als ANN-Methoden. Es konnten praktisch alle Fehlerfälle, selbst mit hohen Lichtbogenwiderständen, mit hoher Genauigkeit identifiziert und die Fehlerentfernung bestimmt werden. Alle Tests wurden an unterschiedlichen Leitungsanordnungen und unterschiedlichen Belastungsfällen durchgeführt.

Die vorliegende Arbeit liefert damit ein neues Instrument zum Schutz und der Fehlerortbestimmung in Hochspannungsnetzen. Die Kombination eines auf der Modaltransformation und einem Scheinwiderstand basierenden Algorithmus mit Fuzzy Logic Instrumenten zur Feinabstimmung liefert ein Fehlerortungssystem, das bei komplizierten Fällen

von Kurzschlüssen auf Leitungen sehr genaue Ergebnisse liefert. Die vielen unterschiedlichen Testfälle haben gezeigt, dass die Einflussparameter in weiten Bereichen variiert werden können ohne dass es zu unzulässig hohen Ungenauigkeiten bei der Fehlerortbestimmung kommt.

List of Symbols and Abbreviations

Symbols

A_I	Individual accuracy
A_L	Local accuracy
A_O	Overall accuracy
$\mathbf{C}$	Fourier cosine component matrix
C_s	Lumped line self capacitance
C_m	Lumped line mutual capacitance
f_i^k	Corresponding i-th antecedent membership for the k-th rule
F_k	Phasor magnitude for the k-th harmonic
G	Stationary arc conductance
g_{arc}	time varying arc conductance
g_i^k	Corresponding i-th consequent membership for the k-th rule
I_{Cm}	Lumped mutual capacitance equivalent current
I_{Cs}	Lumped self capacitance equivalent current
I_F	Fault current
I_{Fs}	Fault current contribution from the sending end
I_{Fr}	Fault current contribution from the receiving end
$\mathbf{I}_L$	Pre-fault loading currents
$\mathbf{I}_{LM}$	Pre-fault modal loading currents
$\mathbf{I}_m$	Modal current matrix
$\mathbf{I}_p$	Phase current matrix
I_R	Receiving end current

I_S	Sending end current
I_{sel}	Selected current quantity for apparent impedance
k(x)	Current distribution factor
L_A	Actual fault distance
l_{arc}	arc length
L_E	Estimated fault distance
LF	Final estimated fault distance
L_L	Total line length
R_{arc}	arc resistance per unit length
R_F	Fault resistance
R_{Fs}	Apparent fault resistance from the sending end
R_i	Time varying arc resistance
S	Fourier sine component matrix
T	Clarke transformation matrix
T_d	Allowable delay time for fault detection and classification
$\mathbf{T}_i$	Modal current transformation matrix
$\mathbf{T}_v$	Modal voltage transformation matrix
u_{arc}	voltage per arc length parameter
$\mathbf{V}_m$	Modal voltage matrix
$\mathbf{V}_p$	Phase voltage matrix
V_R	Receiving end Voltage
V_S	Sending end Voltage
V_{sel}	Selected voltage quantity for apparent impedance
Wi	ANN i-th connection weight
x	Fault distance
Y	Line admittance matrix
$\mathbf{Y}_m$	Modal admittance matrix
Z	Line impedance matrix
Z_0	Line characteristic impedance
Z_{app}	Apparent impedance
Z_L	Total line impedance
$\mathbf{Z}_m$	Modal impedance matrix
γ	Line propagation constant

μ	Adopted membership function
ω_0	Angular fundamental frequency
θ_k	Phasor angle for the k-th harmonic
τ	arc time constant

Abbreviations

ABP	Adaptive Backprobagation training for ANN
AI	Artificial Intelligence
ANFIS	Adaptive Network Fuzzy Inference System
ANN	Artificial Neural Network
ATP	Alternative Transient Program
BP	Backprobagation training for ANN
BP&M	Backprobagation training with momentumfor ANN
CG	Conjugate Gradient for ANN training
DFT	Digital Fourier Transform
DFR	Digital Fault Recorder
EMTP	Electro-Magnetic Transient Program
ES	Expert System
FL	Fuzzy Logic
FTI	Fault Type Identifier
GA	Genetic Algorithms
GPS	Global Position System
ILT	Intelligent Location Tuner
IM	Input Manipulator
LCF	Load Correction Factor
LM	Levenberg Marquardt for ANN training
MLF	Multi-Layer Feedforward ANN
OVLT	Overall Fuzzy Logic Tuner
PMU	Phase Measurement Unit
RBF	Radial Basis Function ANN
WT	Wavelet Transform
TACS	Transient Analysis of Control Systems in EMTP
TC	Tuning Calculator

Bibliography

[1] P. Gale, P. Taylor, P. Naidoo, C. Hitchin and D. Clowes, "Travelling Wave Fault Locator Experience on Eskom Transmission Network", Developments in Power System Protection, Seventh International Conf. On IEE, 9-12, April 2001, pp. 327-331.

[2] Dubbaghchi, R. Christie, G Rosenwald and L. Chen-Ching, "AI Applications Areas in Power Systems", Expert, IEEE, Vol. 12: Issue 1, Jan.-Feb. 1997, pp. 58-66.

[3] K.P. Wong, "Artificial Intelligence and Neural Networks Applications in Power Systems", IEE 2nd International Conference on Advances in Power System Control, Operation and Management, 7-10 1993, Hong Kong, pp. 37-46.

[4] M. Kezunovic, "Intelligent Systems in Protection Engineering", Power System Technology, Proceedings of PowerCon 2000, 4-7 Dec. 2000, Vol. 2, pp. 801-806.

[5] D. Waikar and F Rahman, "Assessment of Artificial Intelligence Techniques for Power System Protection", Energy Management and Power Delivery, Proceedings of EMPD '98, 3-5 March 1998, Vol. 2, pp. 436 – 441.

[6] S. Rahman, "Artificial intelligence in electric power systems: a survey of the Japanese industry", IEEE Trans. on Power Systems, Vol. 8 , No. 3 , Aug. 1993, pp. 1211– 2218.

[7] C. Liu and D. Pierce, "Verification and Validation of artificial Intelligent Systems with Applications to Power Systems", Artificial Intelligence Techniques in Power Systems (Digest No: 1997/354), IEE Colloquium on, 3 Nov. 1997. Pp. 2/1-2/4.

[8] T. Stringfield et. al., "Fault Location for Overhead Lines", AIEE Transactions, August 1957, pp. 518-526.

[9] L. Lewis, "Travelling Wave Relations Applicable to Power System Fault Locators", AIEE Transactions, 1951, pp. 1671-1680.

[10] M. Sneddom and ,P. Gale**, "**Fault Location on Transmission Lines", Distribution and Transmission Systems (Digest No. 1997/050), IEE Colloquium on Operational Monitoring, 28 Jan. 1997 , pp. 2/1 - 2/3.

[11] F. Gale et. al., "Fault location based on travelling waves", Developments in Power System Protection, 5th International Conference on , 1993, pp. 54 – 59.

[12] F. Gale, J. Stokoe and P. Crossley, "Practical experience with travelling wave fault locators on Scottish Power's 275 & 400 kV transmission system", Developments in Power System Protection, 6th International Conference on, 25-27 March 1997, pp. 192 – 196.

[13] Z. Bo et. al. “Application of GPS based fault location scheme for distribution system”, Power System Technology, Proceedings. POWERCON '98. International Conference on , 18-21 Aug. 1998, Vol. 1, pp. 53 – 57.

[14] Z. Q. Bo, A. T. Johns, R. K. Aggarwal, “A novel fault locator based on the detection of fault generated high frequency transients“, Developments in Power System Protection, Sixth International Conference on (Conf. Publ. No. 434) , 1997, pp. 197-200.

[15] G. Rockefeller, “Fault Protection with a Digital Computer”, PAS-88 IEEE Trans., 1969, pp. 438-461.

[16] B. Mann and I. Marrison, “Digital Calculation of Impedance for Transmission Line Protection”, PAS-90 IEEE Trans., 1971, pp. 270-279.

[17] G. Gilchrist, G. Rochefeller and E. Udren, “High Speed Distance Relaying using a digital computer, Part I: System Description”, PAS-91 IEEE Trans., 1972, pp. 1235-1243.

[18] G. Gilchrist, G. Rochefeller and E. Udren, “High Speed Distance Relaying using a digital computer, Part II”, PAS-91 IEEE Trans., 1972, pp. 1244-1258.

[19] P. McLaren and M. Redfern, “Fourier series Techniques Applied to Distance Protection”, Proceedings of IEE, 1975, Vol. 122, pp. 1295-1300.

[20] A. Johns and M. Martin, “Fundamental Digital Approach to the distance Protection of EHV Transmission Lines”, Proceedings of IEE, 1978, Vol. 125, pp. 377-384.

[21] A. Phadke, J. Thorp and M. Adamiak, “A New Measurement Technique for TrackingVoltage Phsors, Local System Frequency and rate of Change of Frequency”, PAS-102 IEEE Trans., may 1983, pp. 1025-1038.

[22] A. Phadke and J. S. Thorp, “Computer Relaying for Power Systems”, John welly & sons,1988.

[23] A. Johns and S. Salman, “Digital Protection for Power Systems”, IEE Power Series 15, The Institution of Electrical engineering, 1995.

[24] IEEE-Power System relaying Committee (PSRC), “IEEE Guide for Protective Relay Applications to Transmission Lines”, IEEE Std C37.113-1999.

[25] J. L. Blackburn, “Protective Relaying: Principles and Applications”, Marcel Dekker, Inc, New York, 1987.

[26] T. Funabashi, H. Otoguro, Y. Mizuma, L. Dube, M. Kizilcay and A. Ametani, “Influence of Fault Arc Characteristics on the Accuracy of digital Fault Locators”, IEEE Trans. On Power Delivery, Vol. 16, No. 2, April 2001, pp. 195-199.

[27] J. Rohrig, “Location of Faulty places by measuring with cathode ray oscilloscope”, Elekticität Zeitschrift, 19th Feb. 1931, 241-242.

[28] G.B.Ancell, N.C. Pahalawaththa, **“**Effects of frequency dependence and line parameters on single ended travelling wave based fault location schemes**“,** IEE Proceedings C, Vol. 139, 1992 , pp. 332-342.

[29] B. Jeyasura and M. A. Rahman, “Accurate fault location of transmission lines using microprocessors“, developments in power system protection, 1988, Forth International Conference, pp. 13-17.

[30] A. Johns, S. Jamali, “Accurate fault location technique for power transmission lines“, IEE Proceedings, Vol. 137 Pt. C, NO. 6 1990, pp. 395-402.

[31] D. Novosel, D. Hart, E. Udren and J. Garitty, “Unsynchronized two-terminal fault location estimation“, IEEE Trans. on Power Delivery, Vol. 11. No. 1, Jan. 1996, pp. 130-138.

[32] Girgis, d. Hart, W. Peterson, “A new fault location technique for two and three terminal lines“, IEEE Trans. on Power Delivery, Vol. 7, No. 1, Jan. 1992, pp. 98-107.

[33] J. Jiang, J. Yang, Y. Lin, C. Liu and J. Ma, "An adaptive PMU based fault detection/location technique for transmission lines. P. I: Theory and algorithms", IEEE Trans. on Power Delivery, Vol. 15, No. 2, Jan. 2000, pp.486-493.

[34] J. Jiang, J. Yang, Y. Lin, C. Liu and J. Ma, "An adaptive PMU based fault detection/location technique for transmission lines. P. I: Theory and algorithms", IEEE Trans. on Power Delivery, Vol. 15, No. 4, Oct. 2000, pp. 1136-146.

[35] V. Cook, "Fundamental aspects of fault location algorithms used in distance protection", IEE Proceedings, Vol. 133 Pt. C, 1986, pp.359-366.

[36] M. S. Sachdev and R. Agarwal, "A technique for estimating line fault locations from digital impedance relay measurements", IEEE Trans. on Power Delivery, Vol. 3, No. 1, Jan. 1988, pp. 121-129.

[37] T. Adu, "A new Transmission Line Fault Locating System", IEEE Trans. on Power 7Delivery, Vol. 16, No. 4, Oct. 2001, pp. 498-503.

[38] T. Takagi, Y. Yamakoshi, J. Baba, K. Uemura and T. Sakaguchi, "a new algorithm for EHV/UHV transmission lines: Part I-Fourier transform method", IEEE Trans. on Power Apparatus and Systems, Vol. PAS-100, 1981, pp. 1316 1323.

[39] T. Takagi, Y. Yamakoshi, J. Baba, K. Uemura and T. Sakaguchi, "a new algorithm for EHV/UHV transmission lines: Part-II Laplace transform method", IEEE PES Summer Meeting 81, SM 411-8.

[40] T. Takagi, Y. Yamakoshi, M. Yamaura, R. Kondow and T. Matsushima, "Development of a new type fault locator using the one-terminal voltage and current data", IEEE Trans. on Power Apparatus and Systems, Vol. PAS-101, 1982, pp. 2892-2898.

[41] A. Wiszniewski, "Acuurate fault impedance locating algorithm", IEE Proceedings, Vol. 130, Pt. C, 1993, pp.331-314.

[42] M. T. Sant, M. Tech and Y. G. Paithankar, "On line digital fault locator for overhead transmission line", IEE proceedings, Vol. 126, 1979, pp. 1181-1185.

[43] L. Eriksson, M. Saha and G. D. Rockefeller, "An accurate fault locator with compensation for apparent reactance in the fault resistance resulting from remote end infeed", IEEE Trans. on Power Apparatus and Systems, Vol. PAS-104, NO. 2, Feb. 1985, pp. 424-436.

[44] A. Girgis and E. Makram, "Application of adaptive Kalman filtering in fault classification, distance protection and fault location using microprocessors", IEEE Trans. on Power Systems, Vol. 3, No. 1, Feb. 1988, pp. 301-309.

[45] M. Tawfik anf M. Morcos, "ANN-based techniques for estimating fault location on transmission lines using Prony method", IEEE Transactions on Power Delivery, Vol. 16, No. 2, April 2001, pp. 219 – 224.

[46] M. Joorabian, "Artificial neural network based fault locator for EHV transmission system", 10th Mediterranean Electromechanical Conference, MELECON 2000, Vol. 3, 29-31 May 2000, pp. 1003 – 1006.

[47] Zamora et. al., "Fault location system on double circuit two-terminal transmission lines based on ANNs", PowerTech ´2001, 10-13 Sept. 2001, Porto, Portugal.

[48] F. Magnago and A. Abur, "Fault location using wavelets", IEEE Transactions on Power Delivery, Vol. 13 , No. 4 , Oct. 1998, pp. 1475 – 1480

[49] K. Gi-Taek, K. Hyuck-Soo and C. Hmg-Yong, "Wavelet transform based power transmission line fault location using GPS for accurate time synchronization", IEEE Industrial electronics Society, IECON '01, The 27th Annual Conference of the IEEE , 29 Nov.-2 Dec. 2001, Vol. 1, pp. 495 - 499.

[50] J. Qin, X. Chen and J. Zheng, "Travelling wave fault location of transmission line using wavelet transform", Power System Technology Proceedings, POWERCON '98 International Conference , 18-21 Aug. 1998, Vol. 1, pp. 533 – 537.

[51] K. El-Naggar "A genetic based fault location algorithm for transmission lines", Electricity Distribution, CIRED, 16th International Conference and Exhibition on IEE, 18-21 June 2001, vol.3.

[52] M. Kezunovic and Y. Liao, "Fault location estimation based on matching the simulated and recorded waveforms using genetic algorithms", Developments in Power System Protection, 2001, Seventh International Conference on (IEE) , 9-12 April 2001, pp. 399 – 402.

[53] G. John Webster, Editor, "Wiley Encyclopedia of Electrical and Electronics Engineering", John Wiley & Sons, Inc., 1999.

[54] D. Novosel et. al., "Fault Location Using Digital Relay Data", Computer Application in Power, IEEE, Vol. 8, No. 3, July 1995, pp. 45-50.

[55] Leuven EMTP Center (LEC), Alternative Transient Program, ATP, Rule Book, 1987.

[56] Mathworks, Inc., MATLAB, Ver. 6.5.

[57] D. Lawrence, L. Cabeza and L. Hochberg, "Development of an advanced transmission line fault location system, Part II-Algorithm development and simulation", IEEE Trans. on Power Delivery, Vol. 7, No. 4, Oct. 1992, pp. 1972-1983.

[58] Siemens, "Distance protection relay for Transmission lines, 7SA522: User Catalog", Catalog SIP 4.2, Siemens AG 1999.

[59] GE Power Management, "Advanced Line Protection System, ALPS: Instruction Manual", GE-2001.

[60] ABB, "Line Protection, REL 100, User Manual", June, ABB-1999.

[61] D. Waikar, "Mathematical Basis for Modal Transformation Based Improved digital Distance Relaying Algorithm", IEE International Conference on Advances in Power System Control, Operation and Management, Nov. 1991, Hong Kong, pp. 101-106.

[62] M. Sachdev and S. Kolla, "A Polyphase Digital Distance Relay", Trans. of Canadian Electrical Association Engineering and Operatinf division, Vol. 26, 1987, pp. 1-19.

[63] S. Kolla, "Application of Block Pulse Functions in a Polyphase Digital Distance relay", Industry applications Conf., IAS '95, 13th IAS Annual Meeting, Vol. 2, pp. 1841-1946.

[64] J. Pinto and L. Pedro, "Modal Kalman Foltering Based Impedance Relay", IEEE Trans. on Power Delivery, Vol. 6, No. 1, Jan. 1991, pp. 78-84.

[65] Leuven EMTP Center (LEC), Alternative Transient Program, ATP, Theory Book, 1995.

[66] M. Hagan et. al., "Neural Network Design", Brooks Cole, 1996.

[67] Rob Callan, "Artificial Intelligence", Papgrave Macmillan Ltd., USA, 2003.

[68] Earal Cox, "The Fuzzy Systems Handbook: a Practitioner's Guide to Building, Using and Maintaining Fuzzy Systems", AP Professional, USA, 999.

[69] K. F. Man, K. S. Tang and S. Kwong, "Genetic Algorithms, Concepts and Applications", IEEE Trans. on Industrial Electronics, Vol. 43, No. 5, Oct. 1996.

[70] K. Junglas and J. Stenzel, "Prüfung eines Expertensystems zur Störungsanalyse", Elektrizitätswirtschaft, Vol. 92, No. 22, 19 Oct. 1992, pp. 1435-1443.

[71] K. Junglas and J. Stenzel, "Knowledge Base Evaluation of an Expert System to Diagnose Network Faults", ESAP'93 Conference, pp. 315-320.

[72] K. Junglas and J. Stenzel, "Generic Knowledge Base Improving Acquisition of Declarative Knowledge", ESAP'93 Conference, pp. 351-354.

[73] K. Junglas, "Entwicklung und Prüfung eines Expertensystems zur Störungsanalyse in Elektrischen Energieversorgung", Ph.D. Thesis, TU-Darmstadt, 1993, Darmstadt, Germany.

[74] Girgis and M. Johns, "A hybrid expert system for faulted section identification, fault type classification and selection of fault location algorithms", IEEE Trans. on Power delivery, Vol. 4, No. 2, April 1989, pp.978 – 985.

[75] L. Lay, "Development of an expert system for power system protection coordination", Developments in Power Protection, 4th International Conference, 11-13 Apr 1989, pp. 310 – 314

[76] R. Broadwater et. al., "An expert system for integrated protection design with configurable distribution circuits: Part I", IEEE Trans. on Power Delivery, Vol. 9 , No. 2 , April 1994, pp. 1115 – 1121.

[77] R. Broadwater et. al., "An expert system for integrated protection design with configurable distribution circuits: Part II", IEEE Trans. on Power Delivery, Vol. 9 , No. 2 , April 1994, pp. 1122 – 1128.

[78] H. Hong, et. al., "Protective Device Coordination Expert System", IEEE Trans. on Power Delivery, Vol. 6 , No. 1, Jan. 1991, pp. 359 – 365.

[79] C. Benner and B. Russell, "Practical high-impedance fault detection on distribution feeders", IEEE Trans on Industry Applications, Vol. 33 , No. 3, May-June 1997, pp. 635-640.

[80] S. Chen, C. Cowan and M. Grant, "Orthogonal Least Squares Learning Algorithm for Radial Basis Function Networks", IEEE Transactions on Neural Networks, Vol. 6, No. 2, March 1191, pp. 302-309.

[81] Lu Yingwei et. al., "Performance Evaluation of a sequentional minimal Radial Basis Function (RBF) Neural Network Learning Algorithm", IEEE Transactions on Neural Networks, Vol. 9, No. 2, March 1998.

[82] J. Elman, "Finding Structure in Time", Cognitive Science, Vol. 14, 1990, pp. 179-211.

[83] E. Haselsteiner, "What Elman Networks Can not Do", IEEE World Congress Intelligence, the 1998 IEEE International joint Conference, 4-9 May, 1998, Vol. 2, pp. 1245-1249

[84] J. A. Freeman and D. M. Skapura, "Neural Networks: Algorithms, Applications, and Programming Techniques", Addison-Wesely Publishing Company, 1992.

[85] Timothy Masters, "Practical neural network recipes in C++", Academic press, Inc,1995.

[86] Mathworks, Inc., "Neural Network Toolbox for use with MATLAB: user guide", Ver. 4

[87] Mathworks, Inc., "Fuzzy Logic Toolbox for use with MATLAB: user guide", Ver. 2.

[88] J. Mendel and G. Mouzouris, "Designing Fuzzy Logic Systems", IEEE Transactions on Circuits and Systems-II: Analog and Digital Signal Processing, Vol. 44, No. 11, Nov. 1997, pp. 885-895.

[89] J. Jang, "ANFIS: Adaptive-Network-Based Fuzzy Inference System", IEEE Transactions on Systems, Man, and Cybernetics, Vol. 23, No. 3. May/June 1993, pp. 665-685

[90] J. Jang, C. Sun and E. Mizutani, "Neuro-Fuzzy and soft computing: a computational approach to learning and machine intelligence", Prentice Hall International, Inc., 1997.

[91] Detlef Nauck, Frank Klawonn and Rudolf Kruse, "Foundations on Neuro-Fuzzy Systems", Wiley, 1997.

[92] Z. Radojevic, V Terzija and M. Djuric, "Numerical Algorithm for Overhead Lines Arcing Faults Detection and Distance and Directional Protection", IEEE Trans. On Power Delivery, Vol. 15, No. 1, Jan. 2000, pp. 31-37.

[93] A. T. Johns, R. K. Aggarwal and Y. H. Song, “Improved techniques for modelling fault arcs on faulted EHV transmission systems”, IEE Proc.-Gener. Transm. Distrib., Vol. 141, No. 2, March 1994, pp. 148-154.

[94] M. B. Djuric and V. V. Terzija, “A new approach to the arcing Faults Detection for Fast Autoreclosure in transmission systems”, IEEE Trans. on Power Delivery, Vol. 10, No. 4, Oct. 1995, pp. 1793-1798.

[95] M. Kizilcay, T. Pniok, “Digital Simulation of fault Arcs in Power System”, ETEP Vol. 1, No. 1, Jan./Feb. 1991, pp. 55-60.

[96] M. Kizilcay and K. H. Koch, “Numerical Fault Arc simulation Based on Power Arc Test”, ETEP Vol. 4, No. 3, May./june 1994, pp. 177-185.

[97] A. Grütz and A. Hochrainer, “Rechnerische Untersuchung von Leistungsschaltern mit Hilfe einer verallgemeinerten Lichtbogentheorie”, Elektrotech. Z. (ETZ), 1972, No. 4, pp. 185-191.

[98] J. Izkowski and R. Kawecki, “Location of Faults in Partially Parallel Transmission Networks”, Power Tech Conf., Porto, Portugal, 10-13 Sept. 2001.

[99] L.M.Wedepohl, “Application of matrix methods to the solution of travelling-wave phenomena in polyphase systems”, IEE Proceedings, Vol. 110, No. 112, Dec. 1963. Pp. 2200-2212.

[100] C. Charalambous, “Conjugate Gradient Algorithm for Efficient Training of Artificial Neural Networks”, IEE Proceedings G, Vol. 139, No. 3, June 1992, pp. 301-310.

[101] T. Hagan and Mohamed Menhaj, “Training Feedforward Networks with the Marquardt Algorithm”, IEEE Trans. on Neural Networks, Vol. 5, No. 6, Nov. 1994, pp. 989-993.

[102] S. Chen, F. Cowan and P. Grant, “Orthogonal Least Squares Learning Algorithm for Radial Basis Function Networks”, IEEE Trans. on Neural Networks, Vol. 2, No. 2, March. 1991, pp. 302-309.

Lebenslauf

Persönliche Daten

Name	Tamer Amin Said Kawady
Geburtsdatum	30. September 1972
Geburtsort	El.Menoufia, Ägypten
Staatsangehörigkeit	Ägypter
Familienstand	Verheiratet

Schulbildung

1978–1987	Hurimla Grundschule, Saudi Arabian
1987-1990	Abdelmonem Reyadh Gymnasium, Shebin El-Kome, Ägypten
	Abschluß: Abitur

Hochschulstudium

1990-1995	Minufiya Universität, Shebin El-Kome, Ägypten
	Abschluß: B.Sc. in Elektrotechnik
1995-1999	Minufiya Universität, Shebin El-Kome, Ägypten
	Abschluß: M.Sc. in Elektrotechnik
	M.Sc. arbeit „Generator Protection Using Advanced Techniques“

Akademische Berufserfahrung

1995-2001	Wissenschaftlicher Mitarbeiter, Elektrotechnik Departement,
	Minoufiya Universität, Shebin El-Kome, Ägypten
Seit Juli 2001	Wissenschaftliche Mitarbeiter, Institut für Elektrische
	Energieversorgung, Technische Universität,
	Darmstadt, Deutschland